JOINT INSTITUTE FOR AERONAUTICS AND ACOUSTICS

NASA
National Aeronautics and
Space Administration
Ames Research Center

NASA-CR-168661
19820012273

Stanford University

JIAA TR - 40

AN EXPERIMENTAL INVESTIGATION OF THE FLOW PAST A FINITE CIRCULAR CYLINDER AT A LOW SUBCRITICAL REYNOLDS NUMBER

M. Budair, A. Ayoub, and K. Karamcheti

STANFORD UNIVERSITY
Department of Aeronautics and Astronautics
Stanford, California 94305

JUNE 1981

JIAA TR - 40

AN EXPERIMENTAL INVESTIGATION OF THE FLOW PAST A FINITE CIRCULAR CYLINDER AT A LOW SUBCRITICAL REYNOLDS NUMBER

M. BUDAIR, A. AYOUB, AND K. KARAMCHETI

Department of Aeronautics and Astronautics

JUNE 1981

SUMMARY

Results of hot-wire measurements made in the near-wake of a finite circular cylinder of fixed aspect ratio ($\ell/D = 37$) at a Reynolds number of 9955 are reported. The measurements included the mean velocity profiles, root-mean-square values of the velocity fluctuations, frequency spectra, and velocity cross-correlations.

The mean velocity and root-mean-square values measurements extended over a downstream distance of 12 diameters, and a spanwise distance of 15 diameters from the free end. The frequency spectra and the cross-correlation measurements extended over a downstream distance of 13 diameters and a spanwise distance of 26 diameters.

The mean velocity profiles were used to determine the wake width, whose variation in the downstream and spanwise directions was examined. It is observed that close to the cylinder, the wake is narrower toward the free end than it is away from it, while further downstream the wake is wider toward the tip than it is away from it.

Based on the spectral study it was found that the flow over the span can be characterized by four regions:

1 - A tip region where vortex shedding occurs at a lower frequency than that prevalent far away from the tip.

2 - An intermediate region adjacent to the first one where a frequency component of a nonshedding character is present.

3 - A third region characterized by a gradually increasing shedding frequency with increasing distance from the tip.

4 - A "two-dimensional" region where the shedding frequency is constant.

In addition, the propagating character of the frequency component present in region 2 was studied.

ACKNOWLEDGEMENTS

We wish to express our gratitude to Professor I-Dee Chang and Professor Sotiris Koutsoyannis for reading the manuscript. Special thanks go to Mr. Warren Ahtye and Mr. David Hickey of NASA Ames Research Center for their interest in the problem and kind help.

In modifying the wind tunnel test section the job was done expertly by Jerry DeWerk, Vadim Matte, and Al Armes. Mr. William Janeway assisted in operating the electronics. To all of them we extend our thanks.

To Ms. Carolyn Edwards who ably typed the final draft we express our sincere appreciation.

Particular gratitude is expressed to the University of Petroleum and Minerals in Saudi Arabia for supporting one of us (Muhammad Budair) during his stay at Stanford.

This research was carried out as part of the program of the Joint Institute for Aeronautics and Acoustics, Department of Aeronautics and Astronautics, at Stanford University and was sponsored by NASA Ames Research Center under grant NASA NCC 2-75.

NOMENCLATURE

As	Cross-sectional area of best section
b	Half wake width
C_D	Drag Coefficient; drag force/($\frac{1}{2} \rho_o U_o^2$)
D	Diameter of circular cylinder
d_f	Wakewidth at the end of formation region
f	Frequency of vortex shedding
K_B	Pressure correction factor
K_T	Temperature correction factor
ℓ	Length of circular cylinder
L	Width of test section
ℓ_f	Length of formation region (i.e. parallel to free stream direction)
Mo	Mach number of uniform free stream
p	Barometric pressure
q	Dynamic Pressure, $\frac{1}{2} \rho_o U_o^2$
Re	Reynolds number in the free stream, $\rho_o U_o D/\mu$
S	Frontal area of model
S_b	Universal Strouhal number; fd_f/U_s
T	Time
T_f	Temperature
$\overline{U}$	Local speed of fluid
U_o	Free stream speed

U_s	Seperation speed
u'_{rms}	Root-mean-square of velocity fluctuations
x	Coordinate dimension parallel to free stream direction
y	Coordinate dimension perpendicular to cylinder axis
z	Coordinate dimension parallel to cylinder axis
δ	Boundary layer thickness
Δ	Incremental change
ε	Model blockage factor
μ	Viscosity of fluid
ϕ	Phase change between two periodic frequency components
ρ_o	Density in free stream

TABLE OF CONTENTS

LIST OF FIGURES

CHAPTER 1

INTRODUCTION

Consider a long circular cylinder placed normal to a uniform stream. As a result of the no-slip condition on the surface of the cylinder, vorticity is generated in the shear layers leaving the body. At sufficiently high Reynolds numbers, the interaction between the two shear layers leads to the formation of two rows of alternating vortices in the wake. The region at the back of the cylinder is characterized by its low pressure (base pressure). Such low pressure is responsible for the so-called form drag which constitutes most of the total drag on the cylinder. The alternate shedding of vortices causes fluctuations in the drag and lift forces acting on the body.

Strouhal in 1878 showed that a non-dimensional frequency parameter for the circular cylinder, defined as $\frac{fD}{U_o}$ (where f is the frequency of vortex shedding, D is the diameter of the cylinder, and U_o is the mean speed of the free stream) stays constant over a wide range of conditions (McCroskey 1977). Later in 1879, Rayleigh performed similar experiments to those of Strouhal and showed, through dimensional analysis, that the non-dimensional frequency parameter $\frac{fD}{U_o}$, later known as the Strouhal number, is only a function of Reynolds number (see Bishop & Hassan 1963). Since then a number of investigators (see for instance Goldberg et al (1965), Goldberg & Florsheim (1966), Roshko (1954a)) tried to formulate a non-dimensional frequency parameter, similar to that of Strouhal, that holds constant for various bluff cylindrical contours and for a wide range of Reynolds numbers. Such parameter, referred to as a universal

Strouhal number, is very relevant to the problem of the flow past a bluff body since the proper choice of the elements of this number reveals a great deal of information about the basic mechanism of vortex shedding.

In an effort to explain the process of formation of vortices, Gerrard (1966) proposed a hypothesis which suggested the following process. When the boundary layer is separated from one side of the cylinder, a free shear layer results which continues to be fed by circulation from the separated boundary layer. The free shear layer continues to grow in this manner until it becomes strong enough to draw vorticity of opposite sign from the opposite shear layer. The addition of the drawn fluid in sufficient amounts finally stops the growth in the vortex. The shedding process, then, is considered to have started. Gerrard defined a formation length ℓ_f within which the vortices form before the shedding is started. He also defined a wake width d_f at the end of the formation region. His argument on determining the frequency of vortex shedding was based on relating the two characteristic lengths.

Bearman (1967) introduced a new universal Strouhal number (S_b) in which the characteristic length was based on d_f and the characteristic speed was based on the flow speed at separation. Such number, when plotted against the base-pressure parameters, was found to remain constant for a variety of bluff body contours including bodies with fitted splitter plates and base bleed.

The many aspects of the flow past two-dimensional bluff bodies in general and circular cylinders in particular caused a widely varied type of research effort. Hence, the knowledge which has accumulated

over the past century, since 1878, is quite considerable. Therefore, review papers on this topic appeared over time in the literature. Among the authors who reviewed the subject in the past two decades, one may cite, Morkovin (1964), Marris (1964), Berger & Wille (1972) and more recently King (1977) and McCroskey (1977).

The flow past a finite cylinder has not received extensive investigations as that past the infinite cylinder. Part of the reason for such attitude was the apparently accepted assumption that for cylinders of large aspect ratios (defined as length/diameter) the gross features of the flow away from the finite end are similar to those found in the case of an infinite cylinder (Ayoub & Karamcheti). That resulted in few published papers on the flow past a finite cylinder. Until recently, the objective of addressing the flow past the finite cylinder was limited to furnishing data in order to help designers estimate mean drag forces on finite cylindrical shapes such as telegraph poles, smoke stacks, buildings, etc. The results of Wieselsberger's experiments (in 1922) on mean drag coefficients for a finite circular cylinder, for instance, were used to estimate air drag forces on telegraph poles and smoke stacks for a long time (Okamoto & Yagita 1973). Dryden and Hill (1930), Gould, Raymer and Ponsford (1968) measured local drag distributions on the surface of chimney structures.

1-1 THE UNSTEADY LOADING ON A FINITE CYLINDER

The unsteady loading on finite cylinders, as well as infinite cylinders, is important because of its relation to the structural vibrations which pose one of the important engineering problems that the design engineer has to concern himself with. As was mentioned

earlier, the primary source of fluctuating forces on the cylinder's surface is the vortex shedding process.

In talking about the vortex shedding phenomenon in the case of a finite cylinder, one would find it reasonable to address the following two questions, 1) how does the vortex structure look in the wake of the finite cylinder, 2) how does the presence of a finite end alter the frequency of vortex shedding.

1-2 VORTEX STRUCTURE IN THE WAKE OF A FINITE CYLINDER

The vortex structure of the flow past a finite cylinder was addressed for the first time by Taneda (1952). His model for the vortex structure, which took into account the presence of the finite end, was based on flow visualization at a low Reynolds number (less than 100). He concluded that each vortex in one row connects to the two facing vortices in the opposite row, since a spanwise vortex filament cannot end in the fluid (See Figure 1-1). Taneda's picture stresses the three-dimensional character of the vortex structure as well as the flow, near the tip of the cylinder.

At higher Reynolds numbers several attempts to model the vortex structure proposed a different flow structure near the tip. The experiments conducted by Gould et al (1968) and Etzold & Fiedler (1976) who used circular cylinders as their models and smoke as the visualization agent suggested the existence of two vortices, emanating from the tip region and springing in the downstream direction. Furthermore, the experiment conducted by Maull & Young (1972) who used a finite model with a different contour configuration suggested

the same structure. Although the above experiments seem to agree on the nature of the phenomenon in the tip region one particularly finds the suggestion made by Etzold & Fiedler (1976), about the symmetric pair of vortices around the tip to be unrealistic since, the maximum fluctuating lift near the tip, reported by the same paper seems to rule out such characterization.

Confusing as it may seem, we have two proposed vortex models for the flow around the tip of a finite cylinder. If those models represent the actual flow phenomenon, then it is logical to say that the flow parameters as well as goemetric conditions must have a great influence on the manner in which the flow behaves, especially around the finite end. With this in mind one would expect that the following parameters are quite pertinent to the flow features in the wake of a finite cylinder.

Re	Reynolds number of free stream.
Mo	Mach number of free stream.
$\frac{u'_{rms}}{U_o}$	Root-mean-square value of free stream velocity fluctuations, normalized by the mean speed of the free stream (turbulence level).
$\frac{\ell}{D}$	Length of cylinder, normalized by cylinder's diameter.
$\frac{L-\ell}{D}$	Separation distance between the tip of cylinder and wall of wind tunnel. normalized by cylinder's diameter.
$\frac{D}{L}$	Diameter of cylinder, normalized by the width of the test section.

$\frac{\delta}{\ell}$ Boundary layer thickness, normalized by cylinder's length.

$\frac{\delta}{L-\ell}$ Boundary layer thickness, normalized by the separation distance between the tip of cylinder and wall of test section.

Perhaps the question that comes to mind next is how the frequency of vortex shedding is altered if at all by having a finite cylindrical shape instead of the so-called two-dimensional cylinder. Before taking up this subject, the next section talks briefly about the vortex shedding in the case of a two-dimensional cylinder in order to lay the appropriate background for the coming discussions as well as to familiarize the reader with some general concepts.

1-3 VORTEX SHEDDING FOR A TWO-DIMENSIONAL CYLINDER

The fluctuating nature of the flow in the wake of a two-dimensional cylinder placed in a uniform flow can be categorized in terms of Reynolds numbers (based on the cylinder's diameter) into three ranges (Roshko 1954b).

1- A range that extends from a value of Re between 30 to 40 up to a value of Re between 150-200. The vortex shedding in this range is stable in character and could easily be detected experimentally.

2- The next range, referred to as transitional, extends from a value of Re between 150-200 up to a value between 300-400. In this range, as the flow separates from the sides of the cylinder it goes through a laminar - turbulent transition as indicated by irregular hot-wire signals. Such irregularities make the detection

of the vortex shedding frequency rather difficult (Ayoub & Karamcheti 1976).

3- The irregular range which extends from a value of Re between 300-400 up to a value of about 10^7. This range bears a special significance since most of the practical applications fall within this range. Insofar as the shedding is concerned, this range, in terms of Reynolds number, may be divided into three subranges:

a) The subcritical range which extends up to a Reynolds number of about 2.0×10^5. In this range separation on the sides of the cylinder is laminar and as the Reynold's number is increased the region of the laminar-turbulent transition moves upstream toward the separation point. Despite the laminar-turbulent transition in this range, the wake is periodic and thus the vortex shedding phenonon is present and could be detected experimentally.

b) The critical range which lies between $Re \simeq 2.0 \times 10^5$ and $Re \simeq 3.5 \times 10^6$. The separation in this range, which is still laminar, is followed by a transition and a reattachment of the separated shear layer after which a turbulent separation is followed. That process results in a narrower wake and a loss in the periodicity of the wake. This range is particularly determined by the experimental conditions, as was illustrated by Bearman (1969) who, by carefully cleaning the cylinder often, obtained a periodic wake up to a Reynolds number of 5.5×10^5.

c) The transcritical range which starts at Re = 3.5×10^6. In this range the boundary layers on the sides of the cylinder experience a turbulent separation from the start. The wake in this case is surprisingly periodic and thus the vortex shedding phenomenon is present.

The present section dealt breifly with the vortex shedding phenomenon. A more comprehensive account of the above ranges is covered by Ayoub & Karamcheti (1976).

1-4 FREQUENCY OF VORTEX SHEDDING FOR A FINITE CYLINDER

To properly address the question of frequency of vortex shedding in the wake of a finite cylinder, one would have to concern himself with two main aspects. First, the variation of frequency of vortex shedding both in the spanwise and streamwise directions for a given set of flow and geometric conditions. Second, the effect of varying these conditions on the frequency. The latter aspect requires careful systematic and extensive investigations since it involves a number of parametric variables (Section 1-2). However, addressing the former aspect is quite fundamental and should be addressed first.

Up until recently, addressing the frequency of vortex shedding insofar as the finite cylinder is concerned was limited to the component that is pertinent at a relatively far distance from the tip of the cylinder, in a region where the flow was considered two-dimensional. In the few published papers on the flow past a finite cylinder, the variation of such frequency component with Reynolds number and aspect ratio received some attention. In an experiment of the flow past a

finite cylinder of aspect ratio 4, Fiedler & Wille (1970) found that at a critical Reynolds number of about 2.4×10^5, a distinct frequency component appeared in the spectral distribution, and as the Reynolds number was decreased this component got weaker until it was no more discernable at a subcritical Reynolds number of about 5×10^4. This behavior is contrary to what is observed in the case of an infinite cylinder (Section 1-3). In similar experiments, Okamoto & Yagita (1973) observed that, in the range of Reynolds numbers tested ($2 \times 10^3 < Re < 1.2 \times 10^4$), the frequency of voretx shedding, for a fixed ℓ/D increases with increasing Re. Also, for a fixed Re, they observed that the frequency of vortex shedding increases with increasing aspect ratio (for $10 \leq \ell/D \leq 20$). The same observation was noted by Gowda (1975), cited by King (1977), who observed that an increase in the frequency of vortex shedding is accompanied by an increase in the aspect ratio. The experiment by Gowda (1975), however, was limited to Reynolds numbers between 10^3 and 10^4. The paper by Okamoto & Yagita (1973) presents the most comprehensive set of data on the frequency, as well as the surface pressure for the flow past a finite cylinder. It was observed that the frequency assumes different values along the span in the tip region, with a gradual decrease in its value as the tip is approached. Although, they did not observe shedding for a cylinder of aspect ratio less than 7, the ranges of Reynolds number and aspect ratio at which Okamoto & Yagita (1973) conducted their experiments were, however, limited to a low subcritical Re ($2 \times 10^3 < Re < 1.5 \times 10^4$) and an aspect ratio between 7 and 20.

In order to explain those observations, one would attempt to use

the concept of a universal Strouhal number, defined by Bearman (1967), which relates the shedding frequency to the base pressure and the wake width. Okamoto & Yagita (1973) observed that, at a fixed Reynolds number, the base pressure away from the tip increases with a decreasing aspect ratio, in agreement with the observed decrease in the shedding frequency. However, this agreement with the idea of a universal Strouhal number fails in the near-tip region since, the decrease in the base toward the tip, as observed by Okamoto & Yagita (1973), was attended by a decrease in the shedding frequency. The present investigation, as shall be seen later (chapter 3), supports the decrease in the frequency of vortex shedding in the tip region.

Because of these and other unresolved questions the flow near the tip of a finite cylinder, Ayoub & Karamcheti conducted an experimental investigation in which they addressed the question of vortex structure in the tip region. They conducted their experiment on a finite cylinder of aspect ratio 11.96 and at Re $\simeq 0.85\times10^5$, 1.8×10^5, 7.7×10^5. Their investigation included the measurements of surface pressure fluctuations in the tip region of the cylinder, and the velocity fluctuations in the wake. They placed several microphones on the surface of the cylinder over a distance of about 3.5 diameters from the tip and 2 single hot-wire probes, one near the tip as a reference probe and the other, a traversing probe, at 5 diameters downstream which covered a spanwise distance of 7 diameters from the tip. They concluded the following:

1. The vortex shedding process extends up to a short distance from the tip of the cylinder.

2. The shedding in the tip region starts as a coherent process, and at some distance downstream, beyond the formation region, a separate phenomenon causes the gradual decrease in the frequency of vortex shedding toward the tip.

3. The shedding regime toward the tip corresponds to a lower Reynolds number than the nominal one. A subcritical regime of vortex shedding in the tip region as well as a supercritical regime on the main portion of the cylinder may coexist.

4. The shedding regime toward the tip may, under certain circumstances, assume different frequencies at different time intervals. The authors point out that this deserves further study.

The interesting results revealed in the preceeding sections illustrate clearly the peculiar aspects of the flow around the tip of a finite cylinder; they certainly mark the degree of complexity faced in truly describing the details of such a flow. Although the amount of effort needed to conclusively resolve the unanswered questions seem to be considerable, the task, however, could be lessened to a larger degree by appropriately following a systematic methodology in prusuing further investigations. A good example of such methodology is set by the study conducted by Ayoub & Karamcheti on their investigation of the vortex structure of the flow past the finite cylinder.

1-5 NATURE OF THE PRESENT INVESTIGATION

Due to the interesting issues that evolved from the investigation of Ayoub & Karamcheti on one hand and the gaps left in the Reynolds number and the range of velocity and pressure measurements, both in the wake and on the surface of the cylinder, on the other, the present investigation was initiated. The study was conducted on a finite cylinder of a fixed aspect ratio ($\ell/D=37$) at a Reynolds number of 9955. The measurements included the mean velocity profiles, root-mean-square values of the velocity fluctuations, frequency spectra and velocity cross-correlations.

The mean velocity profiles were used to determine the mean wake width whose variation in the downstream and spanwise directions was examined. The frequency spectra helped determine the frequency components that exist in the range of the frequency domain examined. To investigate the nature of the frequency components, a cross-correlation analysis was made in order to determine the shedding nature of those componenets.

Chapter 2 contains description of the experimental apparatus with a detailed description of the type of measurements that were carried out. Chapter 3 discussed the results of this investigation whose conclusions are contained in Chapter 4.

CHAPTER 2

EXPERIMENTAL PROCEDURE

2-1 INTRODUCTION

The experimental study was aimed at gaining some insight into the flow features associated with the wake of a finite cylinder. The work involved measuring the mean wake boundaries in the spanwise and streamwise directions and constructing the frequency spectra of the velocity fluctuations, in a thorough manner, in the near wake region. The following sections describe the experimental set-up and the methodology used during the course of measurements. In addition, the circumstances that led to choosing the experimental arrangement are also discussed.

2-2 WIND TUNNEL

The wind tunnel used in this project was a subsonic closed circuit type. The test section which has square cross-section has the dimensions of 90.2 x 45.7 x 45.7 cm. The flow speed in the test section can be varied between 20 m/sec and 65 m/sec. For more details about the wind tunnel a reference may be made to Smith, Varzaly, and Baganoff (1978) and Smith (1978).

The wind tunnel was run at a nominal speed of 22.8 m/sec. The model was situated at a distance of 53.2 cm from the beginning of the test section. It was located midway between the upper and lower boundaries of the test section. The profiles of the mean velocity and the root-mean-square values of the velocity fluctuations in the empty test section were measured at the location in which the model was placed. The profile measurements were carried out in the spanwise and cross-wise directions.

The measurements show very uniform profiles, except very close to the walls. The free stream turbulence level was measured at 0.47 percent.

2-3 MODEL

Since the purpose of the investigation was to study thoroughly the effect of the finite end of the cylinder on the features of the flow, it was essential, due to the many related parameters of the problem (Section 1-4), to minimize the influence of some of those parameters, namely, the boundary layer, free-stream turbulence, and aspect ratio. In order to lessen the influence of the boundary layers the cylinder was extended inside the test section to a distance where the tip was situated at about the middle of it. Running the wind speed at about 22.8 m/sec, given the limitation of the speed range, helped serving at least three objectives. The first was to attain a low turbulence level in the test section since at higher speeds the turbulence level tends to increase (See Smith, (1978)). The second objective was to obtain a low subcritical Reynolds number (with the adequate choice of the cylinder's diameter) which was one of the motivations of this investigation. Third, it helped reduce the amount of vibration of the model. The choice of the diameter was to be determined on the basis of obtaining a high aspect ratio cylinder. So in choosing a small diameter cylinder the aim of having a high aspect ratio is made more attainable. In addition this helped in reducing the blockage in the test section. However, while considering a small diameter cylinder, or equivalently, a high aspect ratio cylinder a possible vibration in the model was a factor that had to be taken into account.

Considering all the above factors in choosing the model. a stain-

less steel rod of diameter 0.635 cm was chosen for the present study. With the tip of the cylinder at about the middle of the test section, the aspect ratio was set at $\ell/D = 37$.

To introduce the model into the test section a hole was drilled in one side-wall of the test section. For the sake of holding the cantilevered model rigidly to one wall, a cylindrical block, through which a hole of the same diameter was drilled, was tightened to the outer side of the wall and the two holes were aligned. By using a washer to minimize the leakage, the model in addition, was held more firmly. The length of the extended hole by which the model was passed through into the test section was 4.4cm. To further insure the rigidity of the attachment of the model to the wall a bolt was tightened against the model through the wall of the cylindrical block. As we shall see later, measurements with the model spanning the whole test section were needed. That required drilling another hole in the opposite side-wall of the test section.

The vibration of the cantilevered model was feared to be vigorous but with the tunnel running the model did not show any apparent vibration. The vibration of the model spanning the whole test section was expected to even be less vigorous. The figure below shows a sketch of the cantilevered model with the corresponding coordinate system used.

2-4 HOT WIRES

Two single hot-wire probes were used for this investigation, in order to measure the magnitude of the mean velocity and the root-mean-square values. The probe sensors (Disa P11) consist of 5 μm.-diameter platinum-plated tungsten wires of length 1.2mm. The constant temperature anemometers were of the type Disa 55 M10. The output signals from the

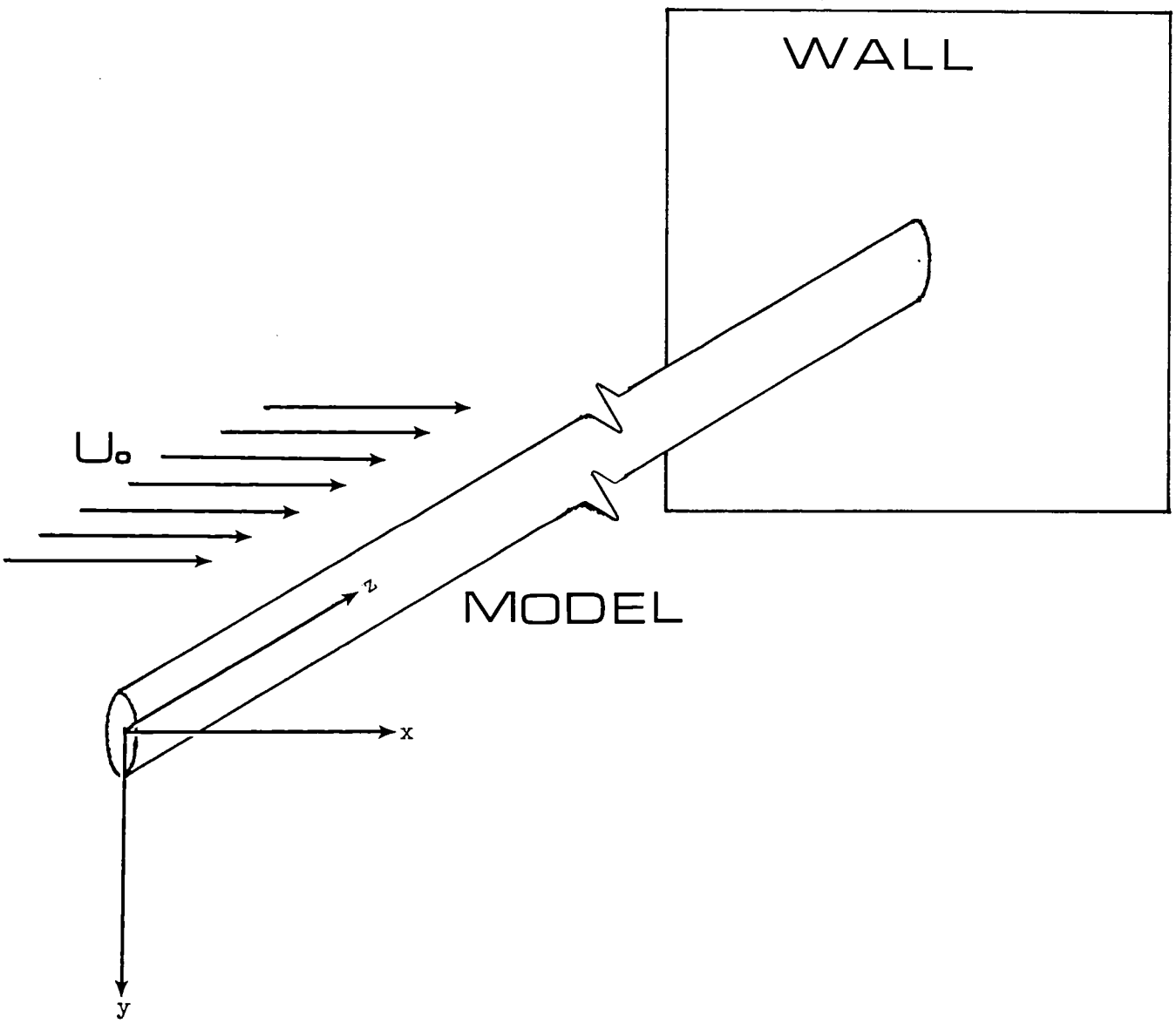
WALL
U_o
MODEL
z
x
y

anemometers were linearized by linearizers of the type 55 D10. The purpose of using two hot-wires was mainly to determine phase differences between the respective signals as will be explained later in the chapter (Section 2-6). Referring to the figure on the last page, the wire sensors were placed parallel to the z-axis, so that the values measured determine the magnitude of the velocity vectors in the x-y plane (see Figure 2-1). One of the hot wires, referred to as a reference probe, was movable in the y-z plane. It was supported by means of a probe support of diameter 0.95 cm which was attached to a traversing mechanism mounted outside the upper wall of the test section through a slot parallel to the z-axis. The center of the reference probe sensor could be placed to within 0.01 cm in both the y and z directions. The other hot-wire, referred to as a traversing probe, was movable in three dimensions. It was supported by a 0.635 cm-diameter brass cylinder which was attached to a traversing mechanism mounted on a frame built under the test section. depending on the nature of measurements (as will be explained later), the cylindrical probe support passed through a streamwise or spanwise-slotted plate. Figure 2-2 shows the model, the probes, and the traversing mechanisms with the spanwise-slotted plate arrangement. The center of the traversing probe sensor could be placed to within 0.01 cm in the three directions.

2-5 MEASUREMENT OF THE VORTEX SHEDDING FREQUENCY

There are various ways of determining the frequency of vortex shedding. Using a series of filters is a normal way of obtaining such frequency. The procedure of computing the frequency spectra involves processing the signal in different frequency intervals at different times. In addition, the fact that each filter has a finite band width

makes fine filtering not possible. This consequently creates a resolution problem especially when the nature of shedding involves a non-steady frequency. Another known procedure consists of constructing Lissajou figures. This is done by feeding a known signal with the signal in question on both axis of an oscilloscope and trying to obtain a steady figure (known as Lissajou figure). However, if the frequency of the vortex shedding is unsteady it becomes very difficult to establish a steady Lissajou figure. A fact that makes the determination of the frequency of vortex shedding rather difficult. What was done here for determining the frequency of vortex shedding, which is by far a more appropriate way, was generating autocorrelation functions and frequency spectra using a correlator of the type Honeywell Model SAI-43A in conjunction with a Fourier transform analyzer of the type Honeywell Model SAI-470. The frequency was thus determined by the power spectra generated by the analyzer. These spectra were displayed on an oscilloscope and recorded for later examination on an x-y recorder. From preliminary investigations it was found that the range of frequency components of interest did not exceed 700 Hz. That led to setting the range of frequency in the power spectra in this investigation at 0-1000 Hz with a resolution of 5 Hz. By displaying the frequency spectra on an oscilloscope a desired value of a frequency peak could then be determined precisely by an intensified light dot, scanning the screen of the oscilloscope, whose movement is monitored by the Fourier analyzer. To insure the existence of vortex shedding, a phase study is necessary by which a 180° phase shift between two signals from two hot-wires symmetrically-located with respect to the wake center-plane confirms the shedding phenomenon.

2-6 PHASE DETERMINATION

One of the procedures used in the present investigation was the determination of the phase shift between two periodic functions of the same frequency. Let us assume that a signal coming from one hot-wire contains a periodic component

$$F_p'(t)$$

If ω_o denotes the frequency of the periodic component, then the signal can be written as

$$F_p'(t) = \mathrm{Re}\left\{Ae^{i\omega_o t}\right\} \tag{2.1}$$

where A is the amplitude of the periodic function. Now let us assume that a second hot-wire signal contains a periodic function of the same frequency ω_o :

$$G_p'(t) = \mathrm{Re}\left\{Be^{i\omega_o t}\right\} \tag{2.2}$$

where B is the amplitude of the periodic function. If the signals of (2.1), and (2.2) are measured at different points in the flow then a phase shift may exist between them. Denoting such phase shift by ϕ, one may write (2.2), for instance, as

$$G_p'(t) = \mathrm{Re}\left\{Be^{i(\omega_o t + \phi)}\right\} \tag{2.3}$$

So given two signals as represented by (2.1), and (2.3) with an unknown phase shift ϕ , one would wish to calculate ϕ by utilizing the cross-correlation function between the given signals. In so doing the cross-correlation is given by (Bendat and Persol (1968))

$$R_{xy}(\tau) = \lim_{T \to \infty} \frac{1}{2T} \int_{-T}^{+T} F'_p(t)\, G'_p(t-\tau)\, dt \qquad (2.4)$$

which by proper substitution and integration can be shown to be

$$R_{xy}(\tau) = \mathrm{Re}\left\{ \frac{AB}{2}\, e^{i(\omega_o \tau - \phi)} \right\} \qquad (2.5)$$

The filtering of the signal about a desired frequency was necessary in order to avoid including more than one major frequency component in the correlation process, a situation that would complicate the effort of determining the phase shift since, as it will be apparant later, the signal of the hot-wire includes in some instances more than one periodic component. The result of Equation (2.5) will be utilized in confirming the vortex shedding nature of some components of interest and in determining the direction of propagation of those components (see Ayoub & Karamcheti).

2-7 TYPES OF MEASUREMENTS

The experiment included three phases. 1) Measuring the mean velocity and root-mean-square profiles at stations covering up to 12 diameters downstream of the cylinder's axis and up to 15 diameters in the spanwise direction away from the free end. The same type of measurements, restricted to the downstream direction, were made on the same model spanning the whole test section. 2) Constructing the frequency spectra of the fluctuating velocity, toward the outer boundary of the wake at stations covering up to 26 diameters away from the cylinder's free

end and up to 13 diameters downstream of the cylinder's axis. Similar spectra were also obtained for the two-dimensional model. 3) Cross-correlating the fluctuating signals of the two hot wires for phase information and other observations.

2-7.1 VELOCITY FIELD

The measurements of the velocity field took place on one side of the wake (along the positive y-direction, refer to the figure on Page 16). However, the symmetry in the velocity measurements was checked by comparing the values on both sides of the wake center-plane at $x/D = 3.0$, $z/D = 3.4$ and the variation in the mean speed values between the two sides was within about 5 percent. Even though such variation is still within the estimated experimental error of the experiment, it is beleived that the source of error is due to the unequal degree of interference of the guided tube of the hot-wire on both sides of the wake.

The mean velocity profiles were mainly used to determine the mean boundaries of the wake in the spanwise and streamwise directions. Due to geometric constraints the traversing probe, which was used to measure the mean velocity and the root-mean-square profiles, was introduced in the test section through a slotted plate whose slots were parallel to the streamwise direction. Such arrangement allowed a closer probing of the region immediately behind the cylinder and made the movement of the probe in the streamwise direction a continuous one so that the probe could be placed in any desired streamwise position. That of course put a limitation on the spanwise movement which could not be made as continuous, but it was judged at the time that it was a more convenient arrangement than the spanwise slotted plate (Figure 2.2).

The following table shows the streamwise and spanwise stations at which the mean velocity and root-mean-square profiles were measured. It is to be noted that for each spanwise station the measurements were made at all the indicated streamwise locations.

x/D	z/D
0.13	
0.38	1.45
0.65	
1.00	3.40
1.50	
2.00	7.50
2.50	
3.01	11.50
4.01	
6.01	15.50
9.01	
12.61	
(a) Streamwise Locations	(b) Spanwise Locations

In constructing the mean velocity profiles in the wake of the two-dimensional cylinder the traversing probe, due to geometric limitations, was placed at 0.45D off the center of the cylinder's span. The streamwise locations at which the profiles were measured were the same as those for the finite cylinder (see the Table above).

To determine the wake's boundaries let us introduce the "half-width" b of the wake which defines the vertical distance between the wake center-plane and the outer edge of the wake. In order to determine such length two definitions were adopted. The first defines the edge of the wake

as the point at which a maximum mean speed is obtained (Fage & Johansen 1927, 1928). The second defines the half-wake width as the one that corresponds to twice the distance that corresponds to the average mean of the minimum and the free stream speeds (Kovasznay 1949). In determining which definition is more convenient to use depends largely on two factors. First, on the degree of accuracy in determining the minimum speed at the wake-center plane. Second, on how exactly the maximum mean speed can be determined. As we shall see in the next chapter, considering the given factors, the first definition was used in the near-wake region while farther downstream the second definition was used.

2-7.2 FREQUENCY MEASUREMENTS

In calculating the frequency spectra the traversing hot-wire introduced in the test section through the slotted plate whose slots were parallel to the span of the cylinder (Figure 2-2). The chosen slotted plate, being different from the one used in the mean velocity measurements, allowed a continuous spanwise movement which made it possible to move the hot-wire in small steps. The steps at which the hot-wire was moved were finer toward the tip of the cylinder. Starting from the tip of the cylinder the hot-wire was moved in the spanwise direction in 0.25 diameter steps up to 4.50 diameters. From 4.50 diameters up to 13 diameters the hot-wire was moved in 0.50-diameter steps, and farther away from the tip the steps were not regular since the flow in that region exhibits two-dimensional character (judging from the spectra) and the steps varied from one downstream station to another with a maximum distance reached at 26 diameters. The off wake center position of the hot-wire varied from one downstream station to another but in

all cases it was located toward the edge of the wake in order to reduce including a lot of turbulence. The table below shows the downstream stations at which the frequency spectra of the velocity fluctuations were calculated.

x/D
0.10
0.97
3.44
6.03
8.53
11.09
13.46

2-7.3 CORRELATION MEASUREMENTS

As the power spectra were examined, a number of frequency components showed up consistently as the hot-wire was moved in the wake of the finite cylinder. To determine the nature of those frequency components a cross-correlation analysis was performed between the signals of the hot-wires symmetrically positioned with respect to the wake center-plane in order to determine the phase shift between the signals. Referring to the table of Section 2-7.2, the reference hot-wire was allowed to move spanwise at a single downstream station, at x/D = 0.10. The traversing probe, however, could be located at all the cited downstream stations. In performing the cross-correlation analysis on the frequency components at x/D = 0.10, both hot-wires were involved and the probes coulb be positioned symmetrically with respect to the wake center-plane. However, as the frequency components were examined at farther downstream stations the corss-correlation analysis was performed in the following manner.

For examining a certain frequency component the reference probe was fixed at a position where that particular frequency component was detected, then the traversing hot-wire would be placed at two mirror-image postions with respect to the wake center-plane and each time a cross-correlation function was computed between the approprietely filtered signals of both probes, and by displaying the correlation functions on the same graph the phase difference could thus be inferred.

2-8 CORRECTION TO MEASUREMENTS

When measurements are performed on a model placed in a test section of a wind tunnel, one of the desired objectives is that the characteristics of the flow measured are those that would exist if the model was placed in an open unbounded flow. The presence of walls constitutes the major reason behind what is called the interference effect on the characteristics of the flow being measured. The effect of such interference may be divided into two categories (Smith 1978): blockage effects and end effects. The concept of blockage refers to the fact that when a model is placed in the test section of a wind tunnel the free stream velocity would be affected in a proportionate manner to the reduction in the effective area of the cross-section normal to the flow direction. Besides the alteration in the value of the free stream velocity, the walls of the test section have the influence of constraining the wake of the model. End effects would be present in each case where the model is mounted inside the test section. One of such effects comes as a result of embedding one end or more in the wall boundary layer. This may alter the flow at spanwise positions away from the wall. This effect is dependent on the aspect ratio of the

model, and the particular geometry of its cross-section (Goldstein 1965).

The blockage effects are generally determined by the ratio of the body thickness to the width of the test section. If the model has a circular cross-section, as is the case in the present investigation, then the diameter replaces the thickness of the body and thus the ratio of the thickness of the model to that of the width of the test section is equal to 0.0139. The connection between the blockage and the change in free stream dynamic pressure was put in a mathematical relation by Maskell (1963). The corrected dynamic pressure is given by

$$\Delta q/q = \varepsilon C_D S/A_s \qquad (2.6)$$

where ε is a blockage factor determined by the magnitude of the base pressure, q is the dynamic pressure, C_D the drag coefficient, S the frontal area, and A_s the cross-sectional area of the test section. The assumptions underlying Maskell's formula imply that the form of the pressure distribution over the body and the origin of the wake (seperation point) are invariant under constraint. By considering the present investigation in which the model is a finite circular cylinder, the seperation point may vary under constraint. Furthermore, an experimental evidence by Ramamurthy and Lee (1973) indicates that the form of the pressure distribution around bluff bodies varies under constraint. This is in addition to the fact that the effective reduction in the area of the test section is not uniform in the spanwise direction. These facts preclude any consideration of such formula. The blockage effect, in sofar as the interpretation of the results of the present investigation is concerned, plays insignificant role. Besides, the blockage from

small-diameter models such as the one used in this investigation can be expected to be small and thus no correction for blockage effects was made.

The boundary layer on the wall of the test section may cause some effects along the span of the cylinder as pointed out earlier. These effects are expected to be of more significance with smaller aspect ratio cylinders. For two-dimensional models the experiments by Keefe (1961) showed that the Strouhal number for a cylinder did not vary for two different end conditions. A major part of the present investigation dealt with measuring the frequency of vortex shedding along the span of the cylinder. Also the geometric configuration of the model in the test section was in such a way that one end was embedded in the boundary layer while the other was in the free stream which was at 37 diameters away from the wall of the test section. With the consideration of those factors and the fact that the major objective of the present investigation was to determine the effect of the finite end, a correction for the effect of the boundary layer was not attempted.

Conducting the experiments in this investigation required running the wind tunnel (of closed-circuit tupe) over a lengthy period of time. This and the varying environmental conditions (pressure, temperature, etc.) are expected to influence the Reynolds number of the experiment. In order to account for the ever varying conditions in calculating the Reynolds number, the temperature in the test section as well as the barometric pressure were recorded each time a data point was taken. The following formula was used in calculating the actual Reynolds number:

$$Rex10^{-6} = \left[Rex10^{-6} \text{PER INCH CHORD AT } T_f = 60°F \text{ \& } P = 30.0 \text{ INCH Hg}\right] x \left[\text{CHORD IN INCH}\right] x \; K_B x K_T \qquad (2.7)$$

where K_B is the pressure correction factor, K_T is the temeprature correction factor. Therefore, based on the recorded conditions, the Reynolds number varied and the calculated values ranged between 9,713 and 10,198. The mean average of those values was taken as the nominal Reynolds number for the present study. This value was 9955.

The accuracy in the hot-wire measurements are affected by the variation in temperature. Since the anemometer signal was linearized, the temperature variation affects the linearized curve by shifting the curve in a linear manner (see Bradshaw 1971). Taking such temperature variation into account, the maximum error in measuring the mean speed was calculated at 6 percent.

CHAPTER 3

RESULTS AND DISCUSSIONS

3-1 INTRODUCTION

In this chapter, results of the outlined experimental steps in chapter 2 are discussed, starting by examining the velocity profiles which are used to determine the wake width whose variation in the downstream and spanwise directions is examined. The discussion is continued by examining the spanwise variation of the root-mean-square values of the velocity fluctuations at different transverse levels. Those observations are incorporated in the earlier results of the wake width study as well as in the results of the frequency and correlation analysis which constitute the latter part of this chapter.

3-2 VELOCITY FIELD

As was mentioned previously in chapter 2, the hot-wire probe was placed parallel to the span of the cylinder. Consequently, the magnitude of the mean velocity values measured by the hot-wire indicates that of the velocity vector in the plane normal to the span of the cylinder (x-y plane)*. Figure 3-1 shows the mean speed profiles across the wake of the finite cylinder at a spanwise location (z/D) of 1.45 diameters and for the downstream positions that extend from a value of x/D = 0.13 up to a value of x/D = 12.61. The horizontal axis corresponds to the local mean speed normalized with respect to that of the free stream. The value of the normalizing free stream speed was

---

* The reference for the coordinate system should be made to the figure shown on page 16 (Section 2-3).

measured at each station independently (every time a single profile was measured) at a distance of about 9 diameters off the wake center-plane ($y/D \simeq 9$). The vertical axis shows the distance (in diameters) off the wake center-plane. The profiles at $x/D = 0.13$ and 0.38 do not show data points at the wake center since they were taken at the shoulder of the cylinder and so the hot-wire was obstructed by the surface of the cylinder. Referring to the speed profile at $x/D = 0.13$, the closest data point to the wake center is at $y/D = 0.496$ and the magnitude of the normalized speed at this location is greater than the other values of the same profile. This value was taken as the maximum speed in this profile, since at this location the hot-wire probe was at about 0.082mm from the surface of the cylinder and any attempt of positioning the probe closer to the cylinder's surface was feared might damage the probe. The reliability of the hot-wire reading at any position was determined by measuring the ratio of the root-mean-square value of the velocity fluctuations (rms) to the local mean speed ($u'_{rms}/\overline{U}$) which at this closest position to the cylinder's surface was 11 percent. As for the other data points of the same profile, the hot-wire signal was quite reliable since the value of $u'_{rms}/\overline{U}$ did not exceed 4 percent.

The velocity profile at $x/D = 0.38$ starts with the closest data point to the cylinder's surface at $y/D = 0.420$ at which the normalized speed is 0.315. At this location the reliability of the hot-wire signal is very poor since a value of $u'_{rms}/\overline{U}$ was about 81 percent. The maximum mean speed was measured at $y/D = 0.575$ at which the $u'_{rms}/\overline{U}$ was about 3 percent.

Further downstream at $x/D = 0.65$, the mean speed values around

the wake center show high $u'_{rms}/\overline{U}$ values, specifically at y/D = 0.160, 0.339, and 0.417 which range between 57 percent at y/D = 0.16 and 72 percent at y/D = 0.417. The maximum mean speed occurs at y/D = 0.575 at which the ratio $u'_{rms}/\overline{U}$ is about 6 percent.

At x/D = 1.0, the hot-wire signal about the wake center shows more reliable measurements than those observed at the previous stations, however, the ratio $u'_{rms}/\overline{U}$ still shows fairly high values ranging between 45 percent at y/D = 0.0 and 50 percent at y/D = 0.472. The maximum mean speed was determined precisely by moving the hot-wire probe in a continuous manner until a maximum mean speed was obtained.

Similarly, at x/D = 1.50, the maximum mean speed was sharply defined while the ratio $u'_{rms}/\overline{U}$ was evaluated at the wake center and at y/D = 0.472 and had values of 38 and 47 percent respectively.

At x/D = 2.00, the maximum mean speed could still be sharply located by moving the hot-wire probe continuously and recording the mean speed values while the values of the ratio $u'_{rms}/\overline{U}$ at the wake center were still high.

At further downstream locations, two facts are observed; first, the signal of the hot-wire becomes more reliable toward the wake center as evidenced by evaluating the ratio $u'_{rms}/\overline{U}$ which shows significant reduction from the values observed in the earlier profiles, and second, the maximum mean speed is no longer as sharply defined.

By examining the mean speed profiles at x/D = 6.00, 9.00, 12.61, it is evident that the speed profiles show very little variation between the values at the wake center and the speed of the free stream. For the profiles at x/D = 6.00, 9.00, 12.61, the difference is 2.6,

1.0, and 0.2 percent, respectively. This seems to be a clear indication that at this spanwise location (z/D = 1.45), the hot-wire probe was getting out of the wake as the downstream distance was increased.

By looking at the profiles at x/D = 0.65, 1.0, one notices a dip in the mean speed values in the vicinity of the wake center. As pointed out earlier, the hot-wire signal in this region is not reliable. Furthermore, in such region, there may be a reverse flow in which case the hot-wire would not distinguish the direction of the flow and thus negative speeds (taking the sign of the downstream direction as positive) might well have been recorded.

Figure 3-2 shows the mean speed profiles across the wake of the finite cylinder at a spanwise location of 3.4 diameters away from the tip. Consider the speed profile at x/D = 0.13, the closest transverse position to the cylinder at which the mean speed was measured is at y/D = 0.496. At the next position away from the cylinder (y/D = 0.575), the speed is at its maximum.

At x/D = 0.38, the speed profile shows a well defined maximum speed measured at y/D = 0.653. Furthermore, the maximum speed of the profile at x/D = 0.65 occurs at y/D = 0.732. The profiles at x/D = 0.13 and 0.38 do not extend to the wake center, due to the presence of the cylinder's body; however, the profile at x/D = 0.65 extends to the wake center with unreliable measured value of the speed at this location as indicated by the measured value of the ratio $u'_{rms}/\bar{U}$ of 47 percent.

Now let us compare the first three profiles of Figure 3-2, namely the ones at x/D = 0.13, 0.38, 0.65, with the respective ones of Figure 3-1. At x/D = 0.13, the maximum speed of Figure 3-2 occured

at y/D = 0.575 while the maximum speed of Figure 3-1 occurred at y/D = 0.496. Similarly, at x/D = 0.38 and 0.65, the respective maximum speeds of the profiles of Figure 3-2 occurred at y/D = 0.653 and 0.732 while the respective maximum speeds of the profiles of Figure 3-1 occurred at y/D = 0.575 and 0.575. The trend displayed here by the three profiles indicates clearly that a slight widening in the wake width is experienced as one moves from the spanwise location (z/D) of 1.45 to that of z/D = 3.40.

Continuing to examine the profiles of Figures 3-2, 3-3, 3-4, 3-5, and 3-6 while keeping in mind the two questions: 1) how well can the maximum speed in each profile be defined, and 2) how reliable are the measured values of the speed at the wake center, results in the following. In the first six downstream locations of each figure, a well defined maximum speed could be determined for each profile. On the other hand, the speed at the wake center for those locations was not defined with high certainty.

Beyond that, namely at x/D > 2.0, locating a maximum speed for a profile becomes difficult as the downstream distance is increased. However, the reliability of the hot-wire at the wake center, improves.

It is to be stressed at this stage that a clear cut degree of certainty in the determination of the mean speed at the wake center on one hand and in determining a well defined maximum speed on the other, is not always clear. For instance, for z/D = 1.45, the ratio $u'_{rms}/\overline{U}$ at x/D = 2.0 and at the wake center is 41 percent while at x/D = 2.50, the ratio is 27 percent, unlike the case for z/D = 5.4 where the ratio $u'_{rms}/\overline{U}$ at x/D = 2.0 is 42 percent and at x/D = 2.50, it is 42 percent. This raises the question that the evaluation of

the wake width be done on a case by case basis. However, examining the spanwise variation of the wake width (as seen in Figure 3-8) requires a consistent criterion at each value of x/D.

It is observed that as the spanwise distance is increased (away from the tip) the speed profiles start to appear like those for the two-dimensional case (Figure 3-7). Also, the profiles at the last three or four downstream stations of Figure 3-7 seem to look similar in appearance to those measured by Smith (1978) at Re = 8730 and 21030 as well as to those measured by Bloor and Gerrard (1966) at Re = 16,000.

3-3 WAKE WIDTH

Figure 3-8 shows the spanwise variation of the half-wake width at various downstream stations. As was pointed out in the preceding section, the wake experiences a slight widening at x/D = 0.13, 0.38, 0.65, as one moves from the spanwise position of z/D = 1.45 to that at z/D = 3.40. However, speaking about the spanwise behavior of the wake width is more appropriately done if the wake width at any spanwise location is considered with respect to the wake width at a far distance from the tip, where it would tend to be uniform in the so-called two-dimensional region. The uniformity of the wake width in our case is manifested, at least, in the last two spanwise locations, namely at z/D = 11.50 and 15.50, as can be seen in Figure 3-8. So in basing the wake width behavior on that at z/D = 15.50, it is observed that the statement made earlier regarding the spanwise widening of the wake width at x/D = 0.13, 0.38 and 0.65 still holds and the difference between the wake width at the spanwise locations at z/D = 1.45 and 15.50 for the cited downstream positions are 13.7, 11.9, and 11.9

percent, respectively.

Beyond x/D = 0.65, the trend in the spanwise behavior of the wake width seems to reverse itself; closer to the tip the wake width starts to show larger values than those at z/D = 15.50, a behavior which continues to prevail at all the downstream stations (Figure 3-8). It also can be observed that the difference between the near-tip wake width and that at far positions from the tip increases with increasing downstream distance.

The downstream development of the wake width at different spanwise stations is shown in Figure 3-9 which clearly shows that at far downstream distances, the wake width towards the tip of the cylinder is wider than at positions away from it. Also, one observes that as z/D is increased, the curves begin to have a similar appearance to one another. Furthermore, comparing these curves with that in the two-dimensional case (Figure 3-10), it becomes apparent that at downstream locations beyond 3-4 diameters, the curves are quite similar. The dotted lines in Figures 3-9 and 3-10 separate two regions labelled Region I and Region II. The wake width determined in Region I was based on locating the position (y/D) of the maximum speed, where as the wake width in Region II was based on the method outlined by Kovasznay (1949). One can see that in Region I of Figure 3-10, two unconnected data points at x/D = 1.50 and 2.00 are shown. Those points correspond to the wake width whose determination is based on the criterion used in Region II. The discrepancy between the wake width (evaluated according to the two criteria used in both regions) at x/D = 1.50 and 2.00 is quite noticable. This becomes more understandable by examining

the raw data at x/D = 1.50 and 2.00 in which one finds that at x/D = 1.50, a well defined maximum speed could be determined and the ratio $u'_{rms}/\overline{U}$ at the wake center is about 38 percent; where as at x/D = 2.00, a well defined maximum speed is not so well determined and the raw data show that the maximum speed occurs at two (y/D) positions, a fact that makes evaluating the wake width, based on locating the maximum speed, highly uncertain. On the other hand, the ratio $u'_{rms}/\overline{U}$ at the wake center is about 30 percent, a value which is far less than the respective ones for the finite cylinder case (Figure 3-9). It is to be noted that unlike the two-dimensional cylinder case, for the finite cylinder's case, a maximum speed was always well defined at x/D = 2.00 for all the investigated spanwise positions.

3-4 ROOT-MEAN-SQUARE PROFILES

In this section, we try to investigate the variation of the root-mean-square values (rms) of the velocity fluctuations in three directions (x,y,z) by plotting the spanwise variation of these values at appropriately selected transverse positions (y/D) for each of the downstream stations investigated.

As was observed earlier, when discussing the speed profiles (Section 3-2) and the wake width (Section 3-3), the signal of the hot-wire in the vicinity of the wake center had various degrees of uncertainty in view of the ratio $u'_{rms}/\overline{U}$. This was taken into consideration when the rms profiles were plotted.

Starting with the downstream station at x/D = 0.13, Figure 3-11 shows a group of curves that show the spanwise variation of the rms values at different transverse positions (y/D) beginning at y/D = 0.57.

The vertical coordinate in the figure indicates the percentage of the local rms values normalized with respect to the free-stream speed. It can be observed that a slight increase in the rms level (turbulence level) is experienced towards the tip of the cylinder with a leveling off in the curves over the span as y/D is increased.

Further downstream at x/D = 0.38 (Figure 3-12), the curve that corresponds to y/D = 0.57 shows an interesting increase in the turbulence level at z/D = 3.4, while at the closer position to the tip (z/D = 1.45) the turbulence level remains rather low. A similar increase is also observed at higher y/D but to a lesser degree.

At x/D = 0.65 (Figure 3-13), the region of higher turbulence level seems to widen (as observed from the curve that corresponds to y/D = 0.57) while the turbulence level at the spanwise position closest to the tip (z/D = 1.45) maintains a relatively lower level. At y/D = 0.65, the curve looks very similar in appearance to that observed at x/D = 0.38, y/D = 0.57.

At x/D = 1.0 (Figure 3-14), the turbulence level towards the tip (at z/D = 1.45) shows the highest turbulence value with a decreasing trend as the spanwise distance is increased. This attitude is clearly observed for the curves at y/D = 0.79 and 0.94 which also can be observed in Figure 3-15 for y/D = 0.79 and 0.94.

The behavior observed in Figures 3-14 and 3-15 for the curves that correspond to the first couple of y/D positions, starts to change at x/D = 2.00 (Figure 3-16) where the turbulence level at the closest position to the tip (z/D = 1.45) starts to experience a decrease in its value relative to other spanwise locations for the same y/D, as can be seen from the curve that corresponds to y/D = 0.79, and to a lesser

degree to y/D = 0.94.

The turbulence level at z/D = 1.45 keeps on decreasing in value relative to other spanwise locations for the same y/D, as the downstream distance is increased, a behavior which is illustrated clearly at x/D = 2.50 (Figure 3-17) for the curves that correspond to y/D = 0.63 and 0.79. At this downstream station, a new trend starts to develop in the curves that correspond to the tip region and that is, while the turbulence level at z/D = 1.45 is becoming smaller with respect to the rest of the spanwise locations (for the same y/D), the curves show a bump between z/D = 2.00 and 7.00 as the transverse distance (y/D) approaches the outer edge of the wake. This is exemplified in the curve that corresponds to y/D = 0.79 which lies inside the wake boundary, in contrast to the curve that corresponds to y/D = 2.34 which lies outside the wake.

So far, the fact that the turbulence level at z/D = 1.45 is continuing to get smaller with respect to the values at far spanwise positions from the tip, with increasing x/D, has been visually clear from Figures 3-16 and 3-17. However, at the remaining downstream stations a quantitative support is necessary. To do so, we chose three curves in each figure that correspond to different y/D levels and computed the percentage difference between the turbulence level at z/D = 1.45 and z/D = 15.5 for each curve. Then we examined how such difference varies with downstream distance for the same y/D. The transverse levels were chosen at y/D = 0.63, 0.79, and 1.35. These levels lie within the wake boundary. The curves that lie outside the wake show very little, if any, spanwise variation and are not interesting for the present discussion.

Considering Figures 3-18 and 3-19, which correspond to the respective downstream stations x/D = 3.0 and 4.0, one finds, by examining the data, that the difference between the turbulence level at z/D = 1.45 and z/D = 15.5, for the cited y/D levels, are 20, 17, and 14 percent in Figure 3-18, while the respective differences in Figure 3-19 are 33, 24, and 39 percent, a clear evidence that a relative drop in the turbulence level at z/D = 1.45 is increasing with distance.

Continuing the same procedure with Figure 3-20, corresponding to the downstream station x/D = 6.0, one finds that the differences between the turbulence level at z/D = 1.45 and that at z/D = 15.5, for the cited y/D levels, are 61, 54, and 30 percent which further shows an increasing trend in the relative drop in the turbulence level at z/D = 1.45, except at y/D = 1.35. This trend is also true in Figures 3-21 and 3-22. At x/D = 9.00 (Figure 3-21), the difference in turbulence level between z/D = 1.45 and z/D = 15.5, for the same y/D are 75, 72, and 52 percent and those differences rise even higher as the downstream distance is increased; for at x/D = 12.61 (Figure 3-22), the values are 82, 81, and 70 percent. The reason for the behavior at y/D = 1.35 in Figure 3-20 is not precisely known.

As can be seen in Figures 3-20, 3-21, and 3-22, the transverse range is extended to the wake center so several new curves are plotted. The curves in those figures show a drop in turbulence level towards the tip of the cylinder (at z/D = 1.45). Choosing the curves of y/D = 0.0, 0.16, and 0.47, we compared the turbulence level at z/D = 1.45 with that at z/D = 15.5 for Figures 3-20, 3-21, and 3-22. The results show that in Figure 3-20, the differences between the turbulence level at

z/D = 1.45 and that at z/D = 15.5, for the cited y/D positions, are 70, 69, and 66, respectively, as opposed to the corresponding differences in Figure 3-21 which are 80, 80, and 78 percent. The same trend is even emphasized further in the curves of Figure 3-22, where the respective differences are 86, 85, and 84 percent.

We have thus far observed how the turbulence level in the tip region, specifically at z/D = 1.45, has been dropping increasingly below that at 15.5 diameters from the tip at all the transverse positions, as the downstream distance is increased. As the reader may remember, this trend starts at a downstream station of about 2.50 diameters from the cylinder. The observation made here is that as the downstream distance is increased, the outer boundary of the wake (i.e. the wake boundary along the direction of the span) is being pushed toward the wall supporting the root of the cylinder. The observation was based by following the relative drop in turbulence level between two points along the span at the same transverse level with downstream distance. It is also of interest to note that the level of turbulence at z/D = 1.45 approaches that in the free stream with increasing downstream distance. This observation about the behavior of the wake boundary in the spanwise direction is in conformity with the earlier observation made when discussing the velocity profiles (Section 3-2) In addition to that, a flow visualization made by Okamoto and Yagita (1973) provides a further evidence to the same effect.

The behavior of the rms curves at x/D = 0.38 and 0.65 show, as observed earlier, bumps (Figure 3-12, and 3-13). These bumps may be associated with a fluid mechanical phenomenon that is responsible for the turbulence generation. What makes this behavior different

from that observed at x/D = 2.5 and further on downstream, is that the curves show quite a dramatic high level of turbulence despite the small respective spanwise variation in the wake width.

The fact that the rms curves that correspond to x/D = 2.50 and further on downstream show bumpy shapes in the tip region may be explained by the fact that at those downstream stations the spanwise variation in the wake width is greater toward the tip than away from it, which leads us to consider the following cases: first, when the hot-wire probe is outside the wake boundary in the transversal direction of all spanwise positions, it is more subject to the influence of the wake in the tip region than at positions away from it. Second, the probe is immersed in the wake in the tip region but outside the wake at positions away from the tip. The third case is when the probe is within the wake boundary at all spanwise locations. This case is obviously the same referred to in the preceding paragraph where the turbulence activity in the tip region casues the observed behavior in the rms curves. This idea (high turbulence activity) seems to incorporate well in the discussion of the frequency analysis, which is the topic of the next section.

3-5 FREQUENCY ANALYSIS

The frequency components in the near-wake were studied by constructing the power spectra of the hot-wire signals at different spanwise and streamwise positions, as has been discussed earlier in Section 2-7. The clarity of the discussion of the frequency analysis will be well served by surveying the spanwise positions for each individual downstream station. The analysis at each position includes the features of the frequency components appearing in each spectrum and the relation of

these components to the vortex-shedding phenomenon.

The closest downstream station to the cylinder was at x/D = 0.10. Starting at the tip of the cylinder (z/D = 0), the hot-wire was placed at the transverse position (y/D) of 0.7 diameter off the wake center. The power spectrum shows a single frequency component of 240 Hz; the spectrum at z/D = 0.25 and 0.50 show that the same component persists as illustrated in Figure 3-23. Each power spectrum in Figure 3-23 is part of a wider frequency range spectrum for which the range is between 0 and 1000 Hz. An explanation for why such range was considered is included in Chapter 2. The spectrum at z/D = 0.75 starts to show a transitional behavior which is characterized by a wider frequency band extending from less than 150 Hz up to about 240 Hz (Figure 3-23.d), with a prominent peak at about 230 Hz. The transitional character seems to disappear in the next one diameter without any apparent change in the structure of the power spectrum. The multi-peaked spectrum around 240 Hz, observed when the transition first started, at z/D = 0.75, seems to be retained, however, as the spectrum at z/D = 1.75 shows (Figure 3-23.e). The appearance of the frequency component at 240 Hz in the tip region, as opposed to the shedding frequency component appearing in the so-called two-dimensional region, far from the tip invites the question with regard to its relation to the shedding phenomenon. In answer to such question, the two hot-wire probes (traversing and reference probes) were placed at mirror-image positions with respect to the wake center-plane and a phase study, by constructing the cross-correlation function, was performed. The hot-wire probes were thus located at each spanwise location at which the frequency 240 Hz was observed, and the correlation functions show that

(after filtering the two signals between 200 and 300 Hz) the signals are about 180 degrees out of phase as Figure 3-24 shows, indicating that such frequency component is a shedding one. As with regard to the peak at 230 Hz that has been observed in the spectrum of Figure 3-23.d, it seems that it does not represent a simultaneous shedding phenomenon for if it did, it would imply the existence of two cells (Ayoub & Karamcheti) which would mean that the component at 230 Hz that appears at z/D = 0.75 (Figure 3-23.d), should get more prominent as the distance is increased away from the tip. This does not happen to be the case as is revealed by the spectra at z/D = 1.0, 1.25, and 1.50 (not shown). This argument seems to be supported, even further, when considering the fact that each spectrum is the result of 32000 averages. Therefore, the multi-peaked spectra seem to indicate a slight oscillation in the shedding frequency with time.

As the spanwise distance is increased by increments of a quarter of a diameter, beyond z/D = 1.75, the spectra at z/D = 2.0 and 2.25 start to show an emergence of a lower frequency component alongside the first one already observed. Such component is characterized by a wide frequency band that extends from about 150 to 180 Hz, as shown by the spectrum at z/D = 2.25 (Figure 3-25). The cross-correlation functions of the two hot-wire signals placed at y/D = $\pm$0.7, at z/D = 2.25, and filtered successively between 200 and 300 Hz and 110 and 200 Hz are shown in the same figure (Figure 3-25) indicated by (a) and (b), respectively. The cross-correlation (b) clearly characterizes the lower component (between 150 - 180 Hz) as a non-shedding one. This component dominates the spectrum in the next half diameter, where the spectra were constructed at z/D = 2.5, 2.75 and 3.0. The results

at z/D = 2.75 and 3.0 are shown in Figure 3-26 where (a) represents the power spectrum at z/D = 2.75 and (b) represents the spectrum at z/D = 3.0. The cross-correlation analysis at those locations, where the hot-wire signals were filtered between 110 and 200 Hz, are shown in Figure 3-27, indicated by (a) at z/D = 2.75 and (b) at z/D = 3.0. The cross-correlation functions illustrate the non-shedding nature of this frequency component (150-180 Hz), as indicated by the zero phase shift between the filtered hot-wire signals. This frequency component continued to exist in the next diameter, namely at z/D = 3.25, 3.50, 3.75, and 4.0. Furthermore, starting at z/D = 3.25 a higher frequency component starts to emerge alongside this component manifesting itself by a cluster of peaks around 600 Hz.

This new component becomes the dominant one at and beyond z/D = 4.25, with an increasing trend toward higher ranges of frequency with increasing distance from the tip. The word "component" being used to refer to a cluster of frequency peaks is an intended expression to imply that those peaks represent one single component with an oscillatory behavior with time. The increasing trend in the frequency of this component with increasing distance is apparent as the spectra at different spanwise positions show. Figure 3-28 shows the spectra at z/D = 4.25, 6.5, 8.5, and 10.0, and, as one can see, the cluster of prominent peaks tends to have lesser number of peaks with increasing distance. The nature of this component, which started to appear in the spectra at 3.25 diameters from the tip, proved to be a shedding component. The corss-correlation test, as shown in Figure 3-29, indicates that the component shown in Figure 3-28 is a shedding one. The hot-wire probes used for the cross-correlation test were placed at mirror-image positions with respect to

the wake center-plane and filtered as follows: at z/D = 4.25, the hot-wire signals were filtered between 520 and 650 Hz; at z/D = 6.5 the signals were filtered between 520 and 700 Hz; at z/D = 8.5 the signals were filtered between 540 and 700 Hz; at z/D = 10, the signals were filtered between 600 and 700 Hz. As the spanwise distance is increased, the spectra become single-peaked as shown at z/D = 13, and 18 (Figure 3-30). The cross-correlation test in Figure 3-31, where the hot-wire signals were filtered between 600 and 750 Hz, indicates that the component at z/D = 18 (see Figure 3-30) is shedding as well.

Several points are to be noted here. First, the statement regarding the trend in the frequency increase of the component with increasing distance from the tip can be visually verified by looking at the power spectrum of Figure 3-28. However, it is not directly established as to how much the central frequency is equal to in each spectrum. That was answered by constructing the auto-correlation function of each signal from which the central frequency was determined by measuring the time of the first half period of the function. Based on such procedure, the estimated central frequency in Figure 3-28.a is 609 Hz and in Figure 3.28.b it is 675 Hz. The frequency of the single-peaked spectra was however determined precisely by the spectrum analyzer as outlined in Chapter 2 and, therefore, the prominent peak in Figure 3-28.d corresponds, for instance, to a frequency of 690 Hz and those of Figure 3-30 to a frequency of 700 Hz each.

The second point is that the spectra presented in this text are only a sample of many spectra systematically computed over the surveyed span according to the plan outlined in Chapter 2. The conclusions drawn from those presented are in complete conformity with the observa-

tions that would have been made had all the measured spectra been included in the presentation.

The third point is that the multi-peaked spectra reduce their number of peaks with increasing distance from the tip. The spectra at z/D = 13 and 18 (Figure 3-30) represent a range in which the spectra are characterized by a single prominent peak with a constant frequency with the spanwise distance. The spectra that correspond to spanwise distances of less than 13 diameters showed lesser values in peak frequency.

Very similar measurements to the above were performed at the next downstream station, namely, at x/D = 0.97. The reference hot-wire probe was restricted to the downstream position at x/D = 0.1 and its signal, in conjunction with that of the traversing probe, were used for the cross-correlation study. The technique of testing the shedding phenomenon at this station (x/D = 0.97) and further on downstream has been discussed previously in Chapter 2.

Starting at the tip of the cylinder (z/D = 0), the traversing hot-wire probe was placed at y/D = 0.7 and the power spectrum showed a single prominent peak at a value of 240 Hz (Figure 3-32a) with the same component appearing at z/D = 0.50 (Figure 3-32b). At z/D = 1.0 (Figure 3-32c), the component was best evident by placing the probe at y/D = 2.3. However, at z/D = 1.50, y/D = 2.3 (Figure 3-32d), the spectrum showed fairly weak peaks of about 240 and 150 Hz. The peak (240 Hz) seems to be enhanced by decreasing y/D, as evident from Figure 3-32.e, at y/D = 0.88. The fact that the peak corresponding to the smaller frequency did not do so, shows, if nothing else, the extend of the flow complexity at the tip region. The frequency component (240 Hz) just observed is evidently the same

component observed at the earlier downstream station (x/D = 0.10), which then was proved to be a shedding component. To insure its shedding nature at the present downstream station (x/D = 0.97), the reference probe was placed at x/D = 0.1, y/D = -0.79, z/D = 0.0 and the traversing probe was placed at mirror-image positions with respect to the wake center-plane, namely at x/D = 0.97, y/D = $\pm$ 0.79, z/D = 2.0. Then, on each side of the wake, the cross-correlation function was computed between the filtered signals (between 200 and 300 Hz) of the reference probe and that of the traversing probe, with the latter's signal delayed. The two cross-correlation functions were then displayed as shown in Figure 3-33. It can be inferred from this figure that the frequency component in question is a shedding one. This component could still be observed further at z/D = 2.25 and 2.50, however, it becomes weaker farther along the span.

The component between 150 and 180 Hz starts to show its presence solely at z/D = 2.75 with lesser clarity than it was observed at the earlier downstream station (x/D = 0.10) due, perhaps, to increasing background turbulence with increasing downstream distance. Figure 3-34 shows the spectra at z/D = 3.0 and 3.75 where such component could be detected. To show that this component is similar in nature to that observed at x/D = 0.10, the technique employed in testing the nature of the component observed at closer spanwise position to the tip (240 Hz) was implemented with the reference probe placed at x/D = 0.1, y/D =-0.7, z/D = 2.75 and the traversing probe placed at x/D = 0.97, y/D = $\pm$0.7, z/D = 3.75 The signals of both probes were filtered between 100 and 200 Hz and the signal of the traversing one delayed. That yielded the correlation

functions shown in Figure 3-35 which evidently prove that the phenomenon associated with this frequency component is the same as that observed at x/D = 0.10.

The higher frequency component starts to appear in the spectra at about z/D = 4.5, where the spectra are characterized by many peaks as illustrated at z/D = 5.5 (Figure 3-36a). The group of peaks starts to shift to higher frequencies while the number of prominent peaks diminishes until one single prominent peak is left as the spectra in Figure 3-36b,c illustrate. The spanwise range between about z/D = 4.5 and 14 is the range within which such gradual frequency shift takes place. The nature of this component in this range was tested by the correlation analysis used so far. The correlation functions shown in Figure 3-37 corresponds to the spanwise positions z/D = 5.5 and 12. The reference probe, in testing the component of Figure 3-36.a, was placed at x/D = 0.10, y/D = -1.0, z/D = 4.0 and the traversing probe was placed at x/D = 0.97, y/D = $\pm$ 1.0, z/D = 5.5. The signals were then filtered between 550 and 700 Hz with the signal of the traversing probe delayed. Similarly, in testing the nature of the component of Figure 3-36.c, the reference probe was placed at x/D = 0.10, y/D = -1.0, z/D = 10.0 and the traversing probe was placed at x/D = 0.97, y/D = $\pm$ 1.0, z/D = 12. The signals were filtered between 600 and 750 Hz with the signal of the traversing probe delayed. It is evident that the correlation functions of Figure 3-37 illustrate the shedding nature of this component.

The range in which the spectra become single-peaked with constant frequency starts at z/D = 14, and since the extent of the measurements was up to 26 diameters from the tip, several spectra within this range

were constructed in order to insure the constancy in the frequency. The spanwise locations at which the spectra were constructed were at z/D = 14, 16, 18, 20, 23, 25, and 26 and in all the spectra, the frequency kept a constant value. Figure 3-38 shows the spectra at z/D = 14 and 26 in which the frequency of the single-peaked spectra was equal to 700 Hz. The shedding test was preformed,in this range, at three spanwise locations, namely, at z/D = 14, 20, and 26. The correlation functions shown in Figure 3-39, which correspond to z/D = 26, sum up the findings of the tests done at the other two spanwise locations. In Figure 3-39, the reference probe was placed at x/D = 0.10, y/D = -1.0, z/D = 24 and the traversing probe at x/D = 0.97, y/D = $\pm$ 1.0, z/D = 26. The signals were then filtered between 600 and 750 Hz with the signal of the traversing probe delayed. It is evident that the frequency component (700 Hz) is a shedding one.

As the spanwise survey of the second downstream station comes to an end, few points are observed. The distribution of the different frequency components is still generally similar to that observed in the first downstream station (x/D = 0.10). That is, there are four spanwise ranges that start from the tip with a range over which the component of about 240 Hz prevails, followed by a range in which the component 150-180 Hz exists. The third range starts with a higher frequency component which is gradually shifting to higher values until the fourth range is attained in which the gradually increasing peak frequency attains a constant value of 700 Hz. Unlike in the first downstream station, the frequency component between 150 and 180 Hz appears at a closer position to the tip. It is clear that such

component is propagating in the downstream direction. However in order to substantiate its spanwise spread, as the observation above might suggest, it is required that a spanwise phase study be made. This, in addition, would help acquire more insight into the characteristics of this component. Such study will be presented in the following section.

It is also observed that at x/D = 0.97 the constant frequency (700 Hz) starts to prevail at a spanwise distance, z/D = 14, while at x/D = 0.10 such frequency starts at z/D = 13.

The next downstream station was located at x/D = 3.44. The power spectra were computed at very similar spanwise locations to those of the previous downstream stations, x/D = 0.10 and 0.97. Starting from the tip of the cylinder it is observed from the spectra that the low shedding component (240 Hz) is discernable in the first 2.5 diameters. The peaks are not as clear as those appearing in the respective positions at x/D = 0.10, for instance. It is noticed that the component (between 150 and 180 Hz) shows up at a very close position to the tip of the cylinder alongside the low shedding component. Figure 3-40 shows the spectrum at z/D = 0.25 in which both components are discernable. It is also observed that the low shedding component is not single-peaked. The non-shedding component is of the same order of magnitude as that of the low shedding one.

In order to provide a characterization check on the nature of the non-shedding component the correlation functions between the filtered signals of the reference and traversing probes were computed. The

reference hot-wire was placed at x/D = 0.10, y/D = -0.70, z/D = 2.25 and the traversing probe was placed at two mirror-image positions with respect to the wake center-plane, at x/D = 3.44, y/D = $\pm$ 2.0, z/D = 0.25. The two signals were filtered between 100 and 200 Hz with the traversing probe's signal delayed. The computed correlation functions are shown in Figure 3-41. The Figure shows that the phase difference between the signals from the two mirror-image positions is zero. Similarly the test was conducted on the nature of the same component at the spanwise locations z/D = 0.0, 0.5, 0.75, 1.0, 1.25, 3.25, 3.75, 4.25, and 5.5 and the zero-phase shift between the filtered signals (between 100 and 200 Hz) from both sides of the wake was proven in each case.

It is expected that at the present downstream station and farther downstream both components (the low shedding component and the non-shedding one) become less visible with downstream distance in view of the increase in the background turbulence and three-dimensionality of the flow. Therefore, the cross-correlation analysis, besides providing a characterization check on the nature of these components, plays an additional role in confirming their existence. Examining the spanwise positions in the tip region reveals that in some cases the spectra show clearly one or two of these components as in shown for instance, in Figure 3-42. The shedding nature of the low frequency component was confirmed at the spanwise locations z/D = 2.0, and 3.5, and as a matter of illustration, Figure 3-43 shows the correlation functions between the filtered signal of the reference probe and that of the traversing one, where the reference probe was placed at x/D = 0.10,

y/D =-1.0, z/D = 0.0 and the traversing probe placed at x/D = 3.44, y/D = $\pm$ 2.0, z/D = 2.0. The signals were filtered between 200 and 300 Hz with the traversing probe's signal delayed.

The high frequency component for this downstream station shows up in the spectrum at z/D = 2.0 with multiple peaks centered at about 600 Hz. In following the spectra computed along the span it is observed that the peak frequency is constant beginning with the spanwise station z/D = 13 and continuing up to z/D = 25. The shedding character of this component was confirmed by computing the correlation functions between the properly filtered signal of the traversing hot-wire probe and that of the reference probe. Three spanwise positions were used for this test, at z/D = 3.5, 9.0, and 16.

In the following downstream stations the existence of the low frequency components in the tip region was proved mainly through the cross-correlation analysis. Each of these components retained its character throughout the remaining downstream stations. The correlation functions in Figure 3-44 are shown in order to illustrate the existence as well as the character of the low frequency component (between 150 and 180 Hz) at x/D = 8.53, z/D = 1.25. Similarly, Figure 3-45 illustrates the case for the component at 240 Hz, at x/D = 8.53, z/D = 4.0. It is to be mentioned that similar figures were constructed at the downstream stations x/D = 6.03, 8.53, 11.09, and 13.46.

At x/D = 6.03 the constant value of the high frequency component (700 Hz) starts to appear in the spectrum at the spanwise distance z/D = 16; at x/D = 8.53 this component starts at z/D = 16; at x/D = 11.09 it starts to appear at z/D = 15; and finally at x/D = 13.46 it starts

at z/D = 16. This shows that the outer spanwise boundary toward the tip of the region in which the uniform shedding component exist gets closer to the wall.

The frequency of vortex shedding for the model spanning the whole test section was measured at the middle of the span at the respective downstream stations at which the frequency spectra were constructed for the finite cylinder case. The frequency thus measured was consistently less than the uniform value of the frequency measured for the finite cylinder. The difference in frequency was less than 2 percent and no explanation is offered as to why this decrease in frequency was experienced.

3-5.1 FEATURES OF THE NON-SHEDDING FREQUENCY COMPONENT

As we have learned so far from the last section, the non-shedding frequency component showed up for the first time at some distance from the tip of the cylinder when the spanwise positions for the downstream station x/D = 0.10 were surveyed. However, at x/D = 0.97 traces of this component showed up at closer locations to the tip. In all those measurements the hot-wire probe was located at some distance off the wake center-plane. When the probe was placed on the center-plane and moved toward the tip of the cylinder at different stations, a more interesting behavior of this component was revealed. The first attempt was tried at the downstream station x/D = 0.97. The traversing hot-wire probe (which was used for the investigation) was first placed at z/D = 0.0 and the power spectrum was computed. The spectrum showed

a strong frequency component similar in range to that of the non-shedding component discussed in the previous section. The strong appearance of this component was not accompanied by any other frequency component. When the hot-wire probe was moved 0.25 diameter away from the tip and the spectrum was computed, the same frequency component showed up. The spectra at z/D = 0.0, and 0.25 are shown in Figure 3-46a, b. At the next spanwise location, z/D = 0.50, the power spectrum (Figure 3-46c) shows two frequency components. The low frequency component is apparently the same one observed previously at z/D = 0.0, and 0.25. On the other hand the higher frequency component is the low frequency shedding component at 240 Hz which seems to subside from the spectrum at the next spanwise position, z/D = 0.75 (Figure 3-46d). The fact that the low frequency shedding component (at 240 Hz) shows up in the wake center as Figure 3-46c depicts is somehow unexpected. This however, will be explained by the fact, often observed in the wakes of bluff bodies, that the wake physical center-plane fluctuates with time and so the hot-wire probe in such case would be exposed to the effect of the shedding frequency at some times and to the double shedding frequency at others. As a matter of fact, when the original spectrum from which Figure 3-46c was taken was examined, a frequency component corresponding to double the vortex shedding frequency could be observed. The fluctuation in the wake center-plane seems to offer the most reasonable explanation for the appearance of the low shedding frequency component apart from the possibility of misplacing the hot-wire probe on the exact wake center. As it is observed from Figure 3-46d, there are two dominating frequency components, the lower component that is similar to the one already observed in Figure 3-46a and b, and the

higher one that corresponds to a value which is equal to about double the value of the low shedding component (480 Hz). The appearance of the frequency component at 480 Hz is a reassurance that the component at 240 Hz is a shedding one. Figure 3-46 in general demonstrates clearly that the non-shedding frequency component makes its presence more strongly felt at the wake center. Such strong showing makes the study of its propagative behavior more accessible especially when considering the fact that this component was observed at some distance away from the tip, as was already noted in the pervious section. To perform such study the two hot-wire probes (traversing and reference) were used for the cross-correlation analysis as follows: The reference hot-wire probe was placed at x/D = 0.10, y/D = -1.0, z/D = 3.0 and the traversing probe was placed, for a selected downstream station, in a succession of spanwise positions along the wake center and in each position the cross-correlation function between the filtered signals of both probes was computed with the signal of the traversing probe delayed. The first phase study was done, for the downstream station x/D = 0.97, at the spanwise positions z/D = 0.0, 0.50, and 0.75. Figure 3-47 shows the cross-correlation functions between the filtered signals (between 100 and 200 Hz) of the traversing and reference hot-wire probes. In Figure 3-47a the phase shift deduced from the time to the maximum correlation from the origin is -8.1 degrees. At z/D = 0.50 (Figure 3-47b) the phase shift is 52.76 degrees, and finally the phase shift at z/D = 0.75 (Figure 3-47c) is 50.10 degrees. With reference to section 2-6 we could represent the filtered signal of the reference probe by $\mathrm{Re}\left\{ Ae^{i(\omega t)} \right\}$ and the traversing hot-wire's signal by $\mathrm{Re}\left\{ Be^{i(\omega t + \phi)} \right\}$. Hence by delaying the traversing probe's signal and performing the cross-

correlation $\mathrm{Re}\left\{\frac{AB}{2}\ e^{i\ (\omega\tau\ -\ \phi)}\right\}$ results. So given a phase shift ϕ of -8.1 degrees one could see that the event corresponding to the frequency ω , received by the reference hot-wire probe, happened before it was received by the traversing probe by a time proportional to 8.1. Similarly from Figure 3-47b, where ϕ is 52.76 degrees, we find that the event received by the traversing hot-wire probe took place before it did at the reference probe by a time proportional to 52.76. Since the reference probe was kept fixed at the same location in both cases it can be deduced that the event which corresponds to the non-shedding frequency component took place at the spanwise position, z/D = 0.50 before it did at z/D = 0.0. This means a propagation of that component in the spanwise direction from the position z/D = 0.50 to that at z/D = 0.0. On the other hand the very slight shift deduced from figures 3-47c and 3-47d leaves the question of propogation between z/D = 0.50 and z/D = 0.75 uncertain. However, the best that can be said at this point is that the component seems to be confused in choosing its direction of propogation between these two positions.

At the downstream station, x/D = 3.44 the power spectra were computed at several spanwise locations. With the hot-wire probe placed at the wake center the spectra were computed at z/D = 0.0, and 1.0, and 2.0 as Figure 3-48 shows. It is readily seen that the non-shedding component is not as easily recognizable as it was at the downstream station x/D = 0.97 (See Figure 3-46). It is interesting to note, though, that as the hot-wire probe is moved away from the tip the non-shedding component becomes more recognizable. The relative strong showing of the non-shedding component at z/D = 2.0 is also reflected by the strong cross-correlation between the signal of the traversing

probe at that location and that of the reference probe as Figure 3-49c so illustrates. This seems to suggest that the non-shedding component tends to show its strength toward the outer spanwise of the wake (see Figure 3-18). The same concept will be returned to as the downstream stations x/D = 6.03, and 8.53 are discussed below.

Figure 3-49 shows the cross-correlation functions between the signal of the reference hot-wire probe, placed at x/D = 0.10, y/D =-1.0, z/D = 3.0, and that of the traversing probe, placed at x/D = 3.44, y/D = 0.0 at the spanwise positions z/D = 0.0, and 2.0. The maximum correlation at z/D = 0.0 (Figure 3-49a) occurs at a phase shift of -40.34 degrees. At z/D = 1.0 (Figure 3-49b) the maximum correlation occurs at -94.9 degrees. By utilizing the results of section 2-6, the non-shedding component seems to propagate from the spanwise position z/D = 0.0 to that at z/D = 1.0. However, the propagation between the spanwise positions z/D = 1.0, and 2.0 seems to be favored in the reversed direction since a maximum, at the spanwise position z/D = 2.o (Figure 3-49c), occurs at a phase shift of 151 degrees from the origin.

The next wake center surveyed was at the downstream station x/D = 6.03. The power spectra were computed at the spanwise positions z/D = 0.0, 1.0, and 3.0 as seen in Figure 3-50. The spectra show how the non-shedding component becomes more discernable as the spanwise position is moved inward away from the tip. It is interesting to notice that such component seems to show more clearly in the spectra toward the outer spanwise edge of the wake. That seems to be confirmed by a reference to Figure 3-20 which describes the spanwise distribution of the root-mean-square values of the velocity fluctuations at the downstream station x/D = 6.0 and further shows that at y/D = 0.0 the

spanwise position of z/D = 3.0 is likely to be closer to the edge of the wake than the position z/D = 1.0.

Figure 3-51 tries to describe a propagative behavior, if any of the non-shedding component at x/D = 6.03 by constructing cross-correlation functions between the filtered signal (between 100 and 200 Hz) of the reference hot-wire probe and that of the traversing hot-wire probe (filtered in the same manner). The reference probe was situated at x/D = 0.10, y/D = -1.0, z/D = 3.0 and the traversing probe at the spanwise positions z/D = 0.0, 1.0, and 3.0. The correlation functions indicated by a, b, and c, correspond to the respective spanwise positions. In Figure 3-51a the maximum correlation occurs at a phase shift of -122.03 degrees while the maximum correlation of the figure that corresponds to the spanwise location z/D = 1.0 occurs at -152.54 a fact that reflects an inward propagation between the two spanwise positions. At z/D = 3.0 the maximum correlation occurs at 93.6 degrees (Figure 3-51c) which may suggest that a reversal in the direction of propagation has occured, namely an outward spanwise propagation between z/D = 3.0, and 1.0. However, by examining the cross-correlation function at a spanwise position of z/D = 2.0 (not shown) it seems unclear as to which direction the propagation is favored in the spanwise ranges between z/D = 2.0 and 3.0, and between 1.0 and 2.0. This comes as a result of an existence of two maximum correlations at z/D = 2.0, occuring at phase shifts of 120, and -240 degrees from the origin. This leads to the suggestion that a propagation in the non-shedding component seems likely to occur in either direction between z/D = 1.0, and 2.0. likewise, the propagation between z/D = 2.0, and 3.0 is likely in either

direction.

Now let us consider the downstream station x/D = 8.53 and look first at the power spectra computed at the wake center for different spanwise positions starting from the tip of the cylinder. Figure 3-52 shows those spectra computed at the spanwise positions z/D = 0.0, 1.0, 3.0, and 3.5. As it is seen from the spectra at 0.0, and 1.0 no trace of the non-shedding component is observable. However, at z/D = 3.0, and 3.5, the component becomes increasingly discernable. This behavior seems to be in conformity with what has been observed that the non-shedding component becomes more discernable as the outer edge of the boundary is approached. This is also reflected in the cross-correlation functions at the respective spanwise positions. Therefore, if we look at the cross-correlation functions in Figure 3-53 it becomes readily acceptable that in a certain spanwise region the non-shedding component seems to show most strongly and that this region is around the outer spanwise boundary of the wake.

The functions shown in Figure 3-53 correspond to the cross-correlation functions between the signal of the reference hot-wire probe, at x/D = 0.10, y/D = -1.0, z/D = 3.0 and that of the traversing probe, at x/D = 8.53, y/D = 0.0, at the spanwise positions z/D = 0.0, 1.0, 3.5, and 4.5 with the two signals filtered between 100 and 200 Hz and the signal of the traversing probe delayed. At z/D = 0.0 (Figure 3-53a) the maximum correlation is shifted from the origin by an angle of -175.42 degrees, and at z/D = 1.0 (Figure 3-53b) the maximum correlation

is shifted by an angle of -195.25 degrees. In utilizing the results of section 2-6 it is concluded that an inward propagation in the non-shedding component takes place from the spanwise position z/D = 0.0 to that at z/D = 1.0. However, when the correlation function at z/D = 3.0 (Figure 3-53c) is examined, it is found that the maximum correlation takes place at a shifted angle of 47.2 degrees. This may suggest that a reversal in the direction of propagation occurs, i.e. a propagation in the non-shedding component takes place from the spanwise location z/D = 3.0 to that at z/D = 1.0. On the other hand, by examining the correlation curve at z/D = 4.5 (Figure 3-53d) in which a maximum correlation occurs at a phase shift of -187.2 degrees from the origin, a conclusion may be drawn that suggests that an inward spanwise propagation between z/D = 3.0, and 4.5 exists.

CHAPTER 4

CONCLUSIONS

In this chapter a summary of the findings of the present investigation along with suggestions for future work are presented.

1. Due to the finite configuration of the model studied, in order to describe the boundary of the wake one has to keep in mind that the wake is bounded in the cross-wise as well as in the spanwise directions. The present investigation reveals that the distance between the cross-wise boundaries of the wake, known as the wake width, can be described in the following manner. In the vicinity of the cylinder, the spanwise variation of the wake width shows that the wake is narrower in the tip region than it is away from it. However, at further downstream distances, the spanwise variation in the wake width shows that the wake becomes wider toward the tip. This spanwise behavior of the wake width in the immediate vicinity to the cylinder is supported by the experimental study conducted by Okamoto & Yagita (1973) in which it was reported that the flow near the tip seperates at closer positions to the back of the cylinder than at spanwise positions away from the tip.

The outer spanwise boundary of the wake, on the other hand, seems to get closer to the root of the cylinder with increasing downstream distance. This observation, which is qualitative in nature, is based on analyzing the mean speed profiles (sec. 3-2) and the root-mean-square profiles of the velocity fluctuations (sec. 3-4). These constitute independent pieces of evidence in support of this behavior.

which is further supported by the flow visualization presented by Okamoto & Yagita (1973).

The spanwise measurements of the turbulence level as represented by the root-mean-square values, at different transverse levels y/D seem to offer a good tool for a qualitative description of the behavior of the outer spanwise boundary of the wake. It is expected, however, that by measuring the turbulence quantities in three directions a quantitative description of the outer spanwise wake boundary would be better obtained.

2. Based on the spectral study it was found that the flow over the finite cylinder in the immediate vicinity of the cylinder can be characterized by four regions:

a. A tip region where the vortex shedding occurs at a lower frequency (240 Hz) than the frequency experienced in the so-called "two-dimensional" region where the value of the frequency of the vortex shedding is about three times as large. The tip region extends from the exact tip location to about two diameters away from it. Within this region the vortex shedding is more regular, in the sense that the frequency changes less with time at positions farther along the span.

b. An intermediate region adjacent to the first one where a frequency component (between 150 and 180 Hz) of a non-shedding character is present. The spanwise range over which this frequency component is detected is about two diameters. The power spectra show that this component is wide-band, and hence less regular.

c. A third region characterized by a non-regular vortex shedding where the spectra are multi-peaked, with a central frequency of about 600 Hz at the beginning, and as the distance is increased away from the tip the central frequency increases gradually and the spectra become narrow-band. This process continues till a single peaked-spectrum with a constant frequency is reached. The span-wise range for this region extends from a distance of about 3 diameters from the tip to about 13 diameters away from it. This spanwise behavior in the frequency of shedding conforms with the observation made by Okamoto & Yagita (1973).

d. A so-called "two-dimensional" region which covers the rest of the span with the exception of the root region where the boundary layer is most effective. The frequency in this region is due to vortex shedding and its value remains constant throughout. The value of the frequency in this region is comparable with the value measured in the wake of the two-dimensional model (i.e. when the cylinder spans the whole test section) with a difference of less than 2.0 percent.

3. Far downstream from the cylinder the low shedding component at 240 Hz and the non-shedding component could be detected in the tip region through either the cross-correlation functions, or to a lesser degree, the power spectra. There is, in addition, evidence that the non-shedding component spreads in both spanwise directions.

The start of the "two-dimensional" region seems to get closer to the root of the cylinder with increasing downstream distance.

4. There is evidence that the non-shedding component, at frequencies between 150 and 180 Hz, is due to a flapping motion of the outer spanwise edge of the wake. This motion seems, also, to induce some form of propagation, at the same frequency, in the velocity fluctuations. The origin of this component and its relationship to the shedding regimes present remain a topic for further investigation.

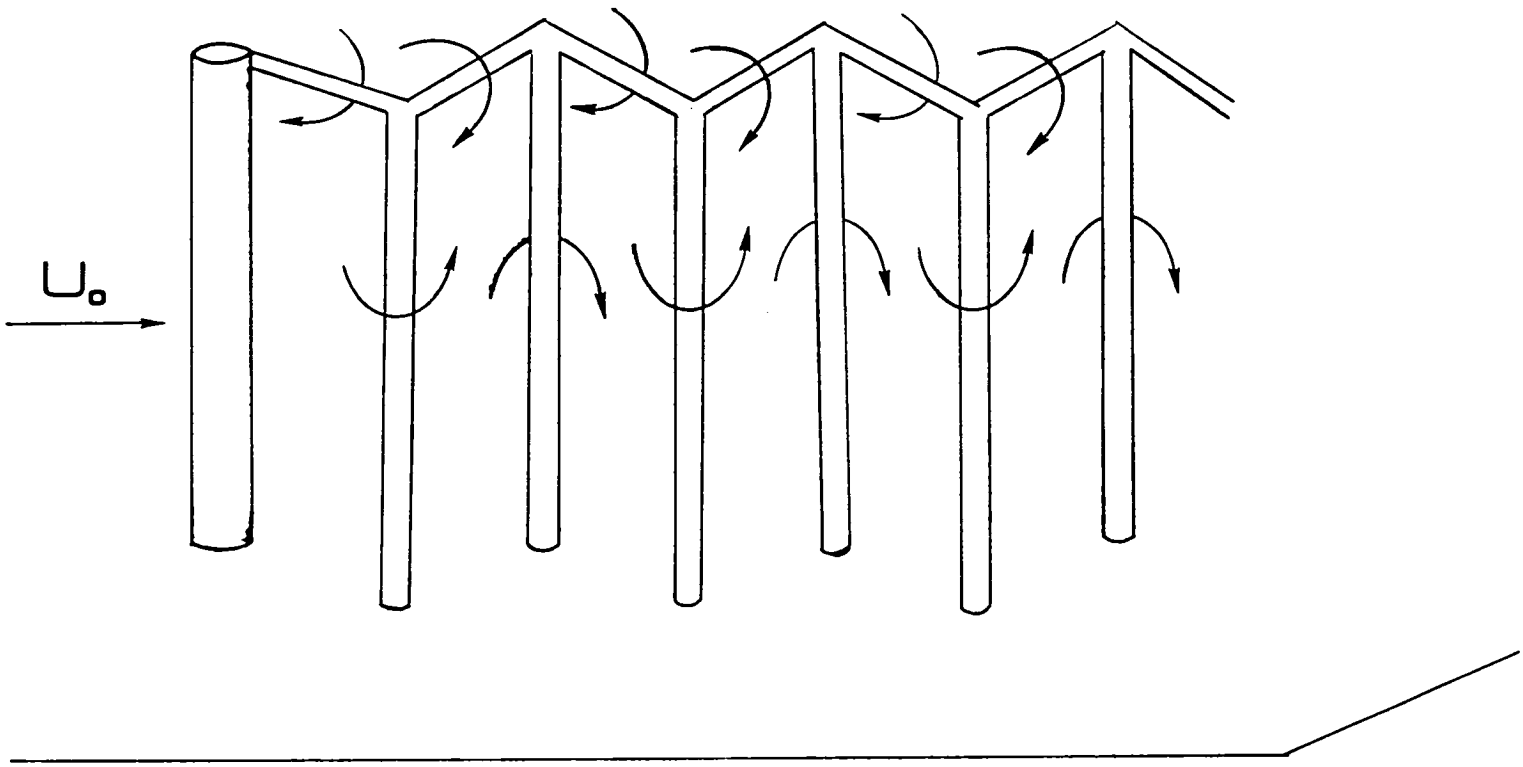

Figure (1-1) Taneda's vortex model of the flow past a finite cylinder (Re less than 100) .

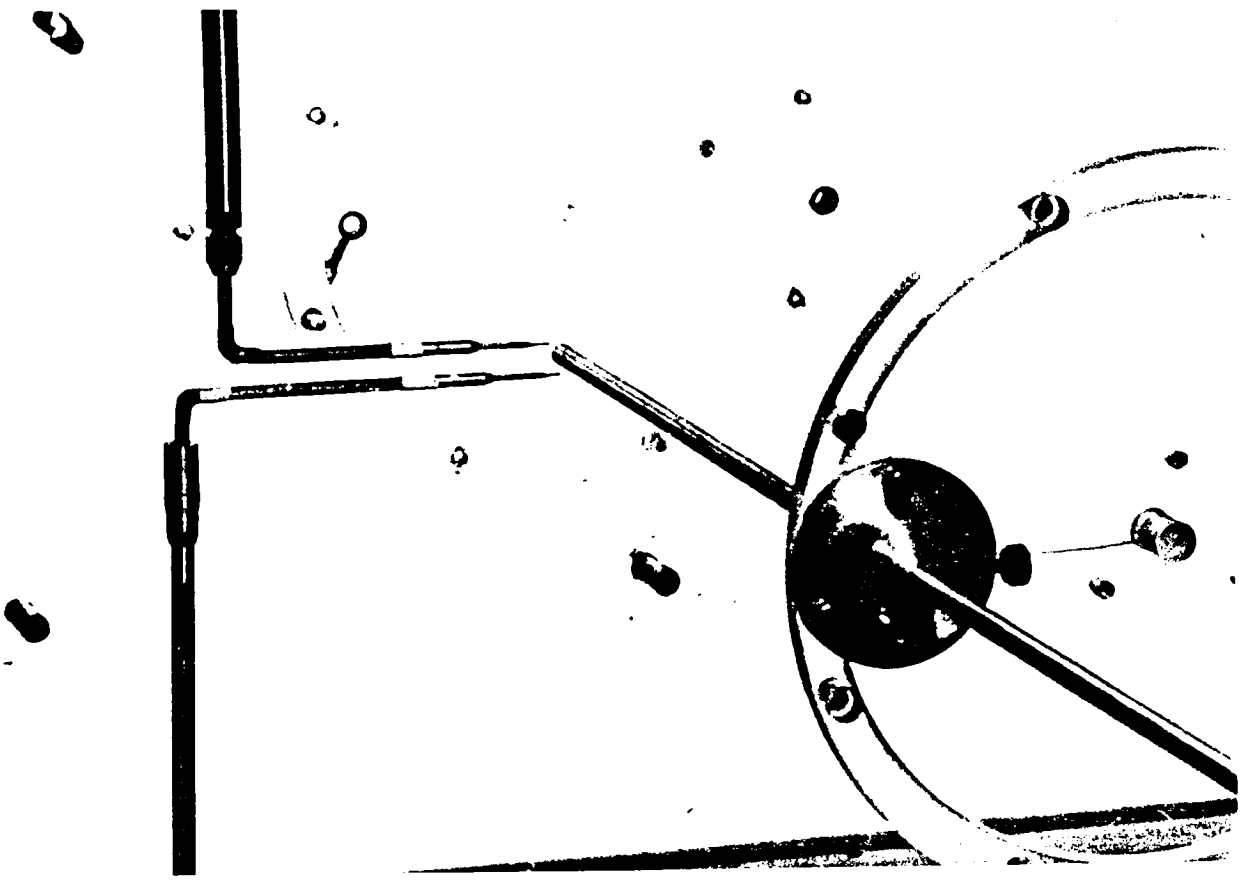

Figure(2-1) Side view of the test section with model and hot-wire probes.

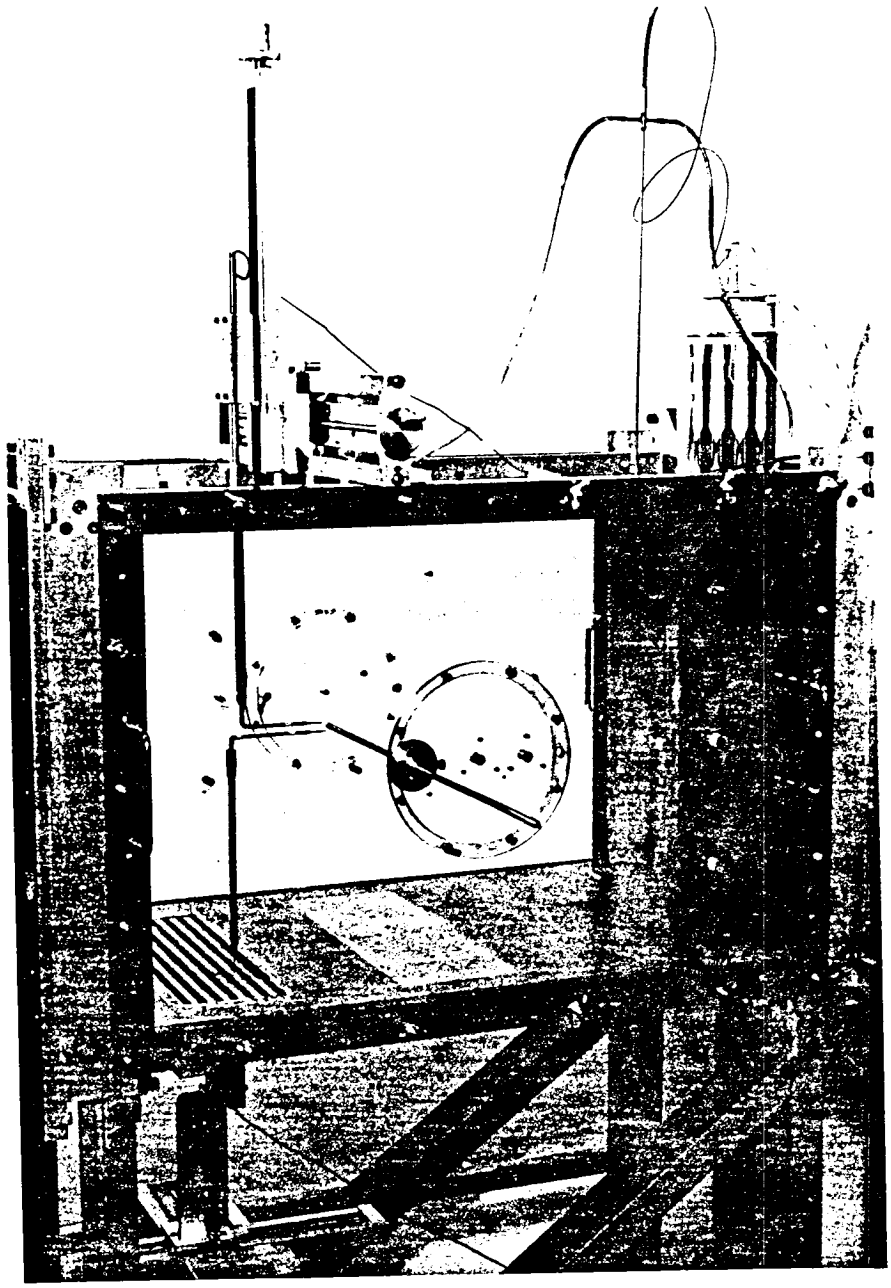

Figure(2-2) General view of the test section with model , hot-wire probes,and traversing mechanisms.

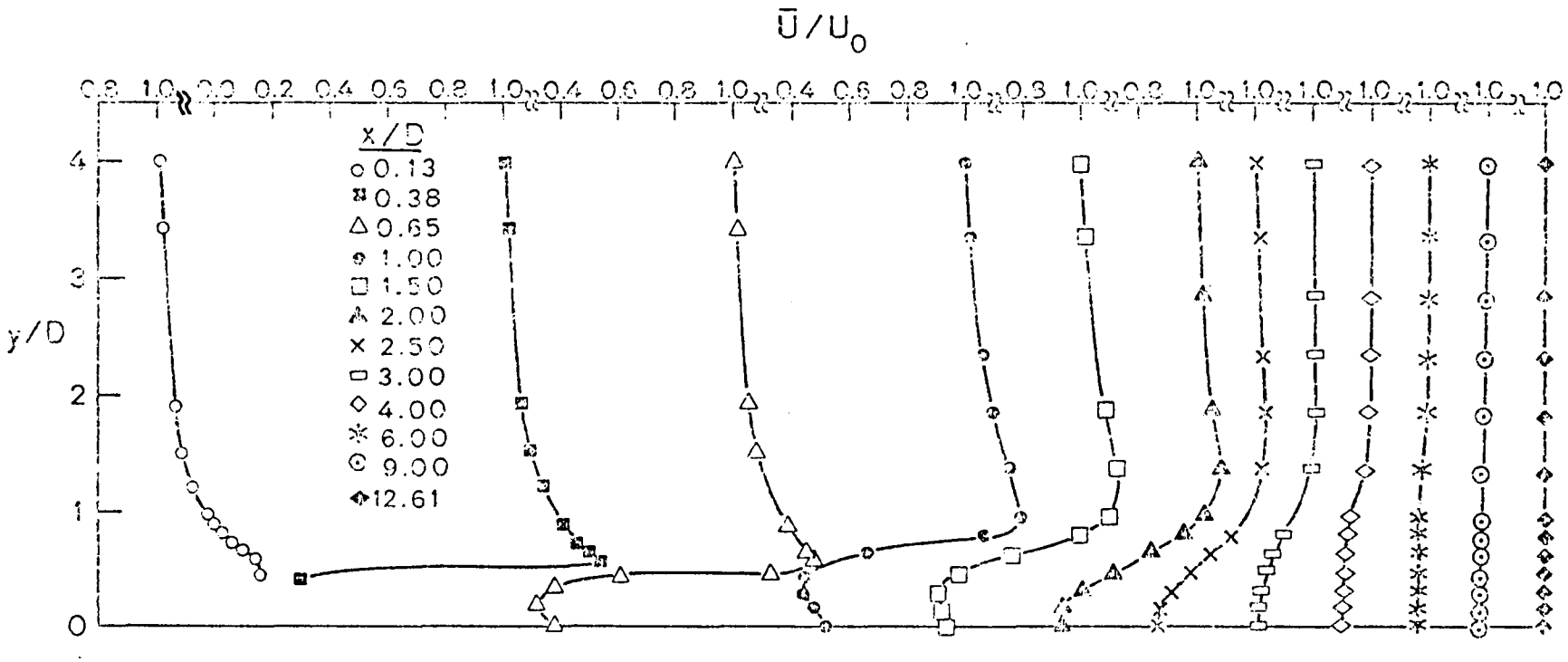

Figure(3-1) Mean speed profiles across the wake of a finite circular cylinder at Re = 9955, z/D = 1.45 .

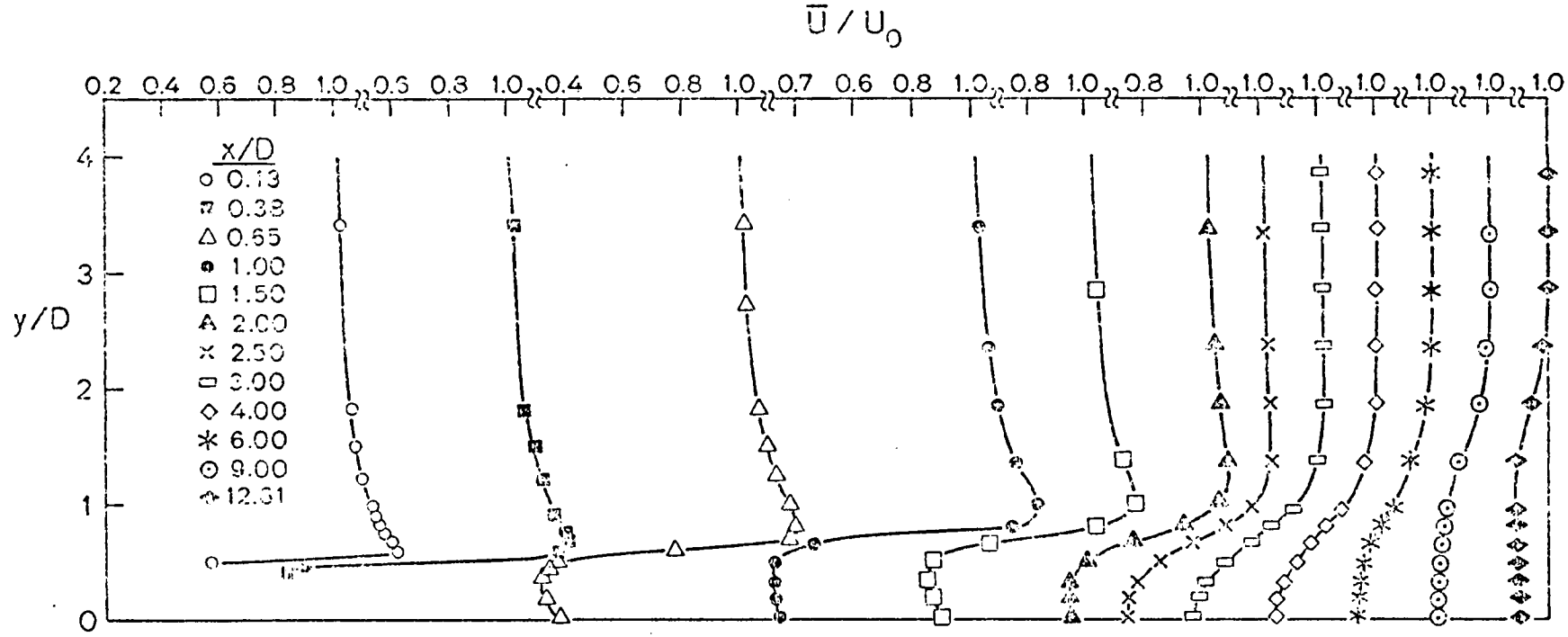

Figure(3-2) Mean speed profiles across the wake of a finite circular cylinder at Re = 9955, z/D = 3.4 .

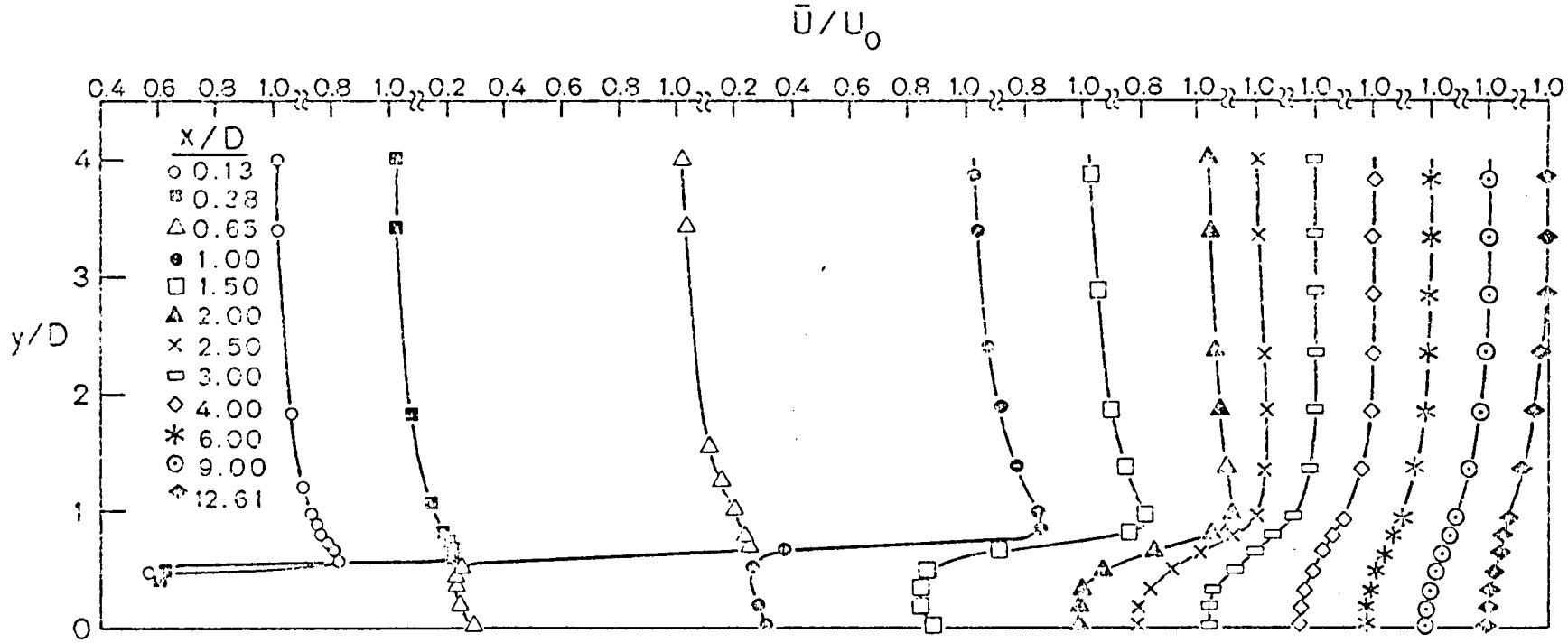

Figure(3-3) Mean speed profiles across the wake of a finite circular cylinder at Re = 9955,z/D = 5.4.

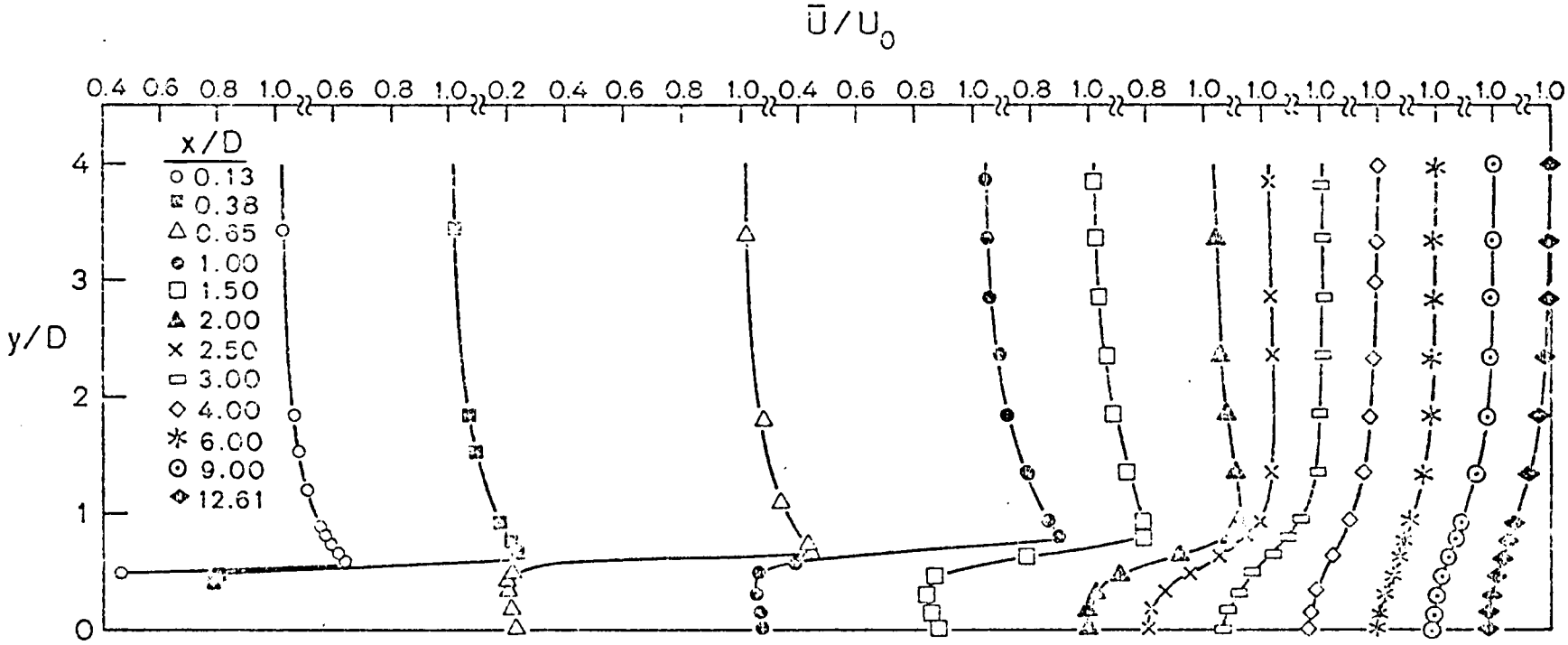

Figure(3-4) Mean speed profiles across the wake of a finite circular cylinder at Re = 9955, z/D = 7.5.

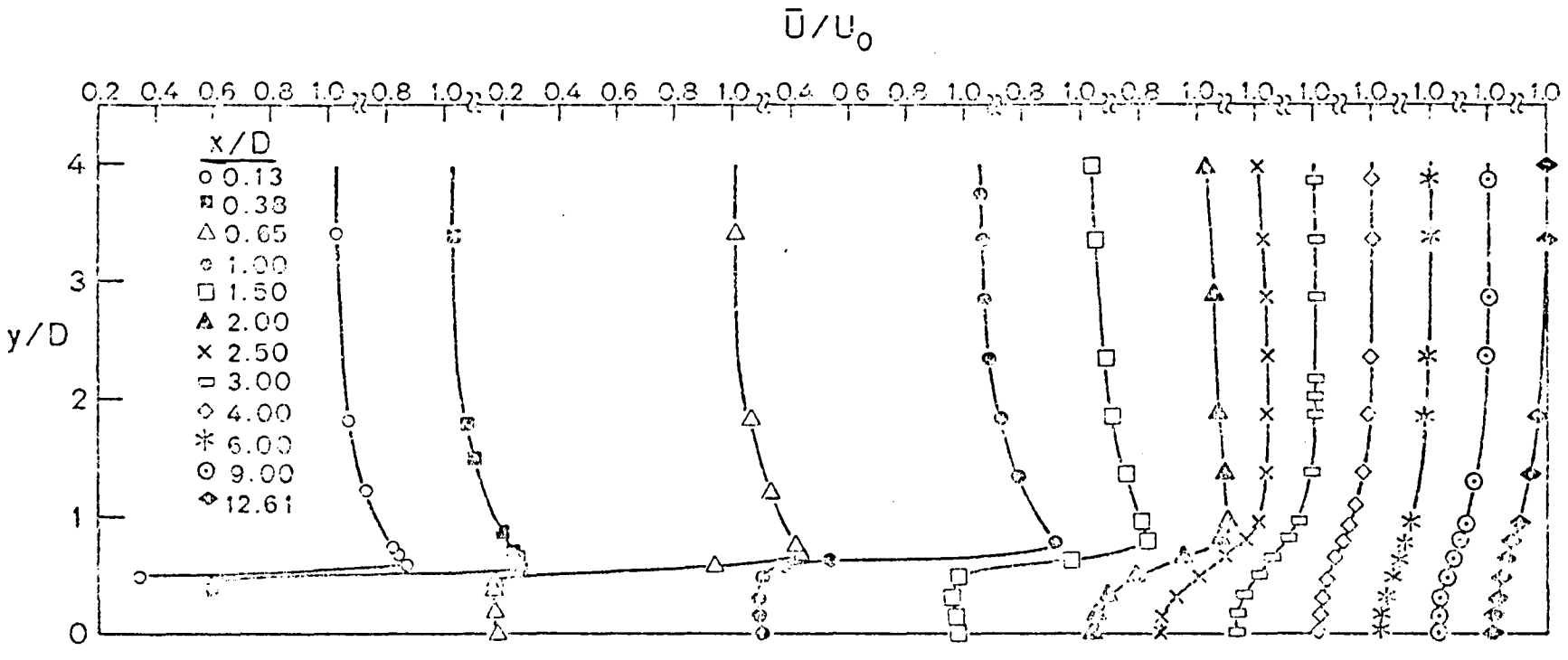

Figure(3-5) Mean speed profiles across the wake of a finite circular cylinder at Re = 9955, z/D = 11.5.

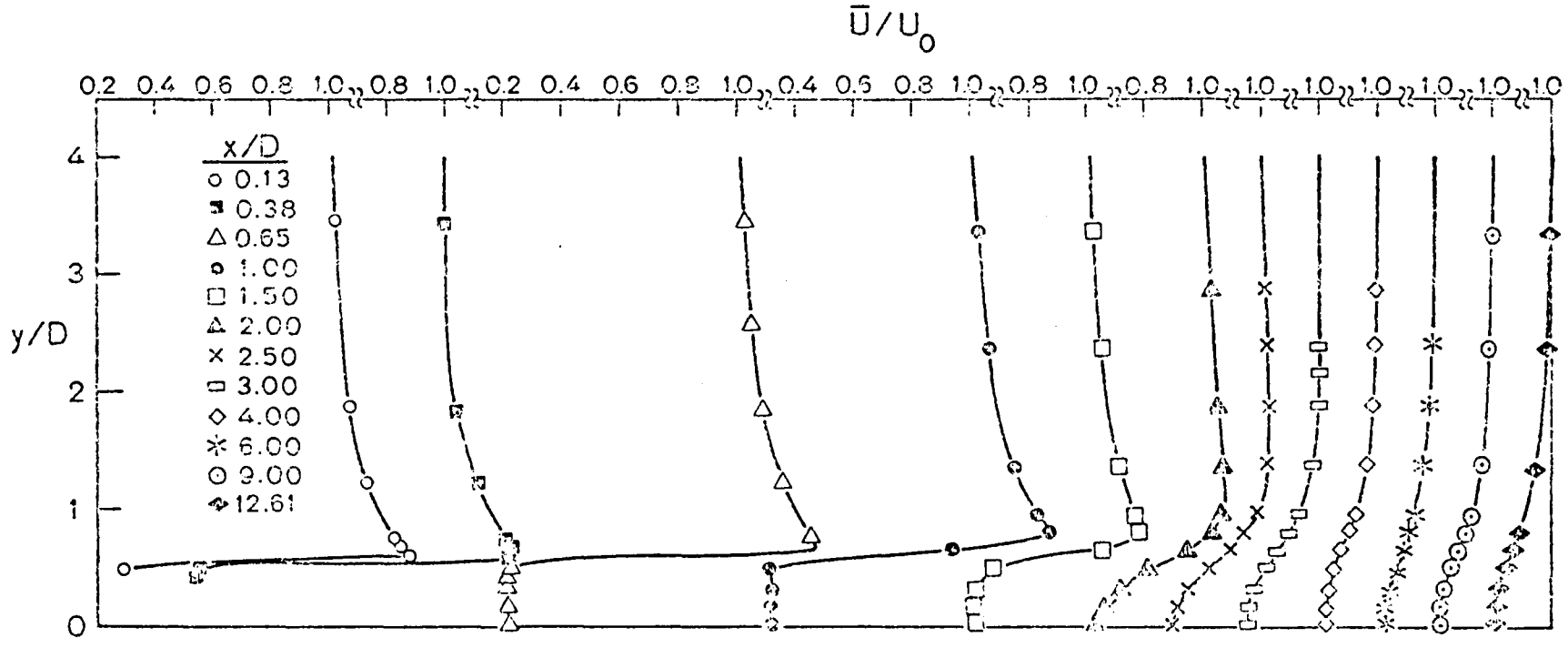

Figure(3-6) Mean speed profiles across the wake of a finite circular cylinder at Re = 9955, z/D = 15.5.

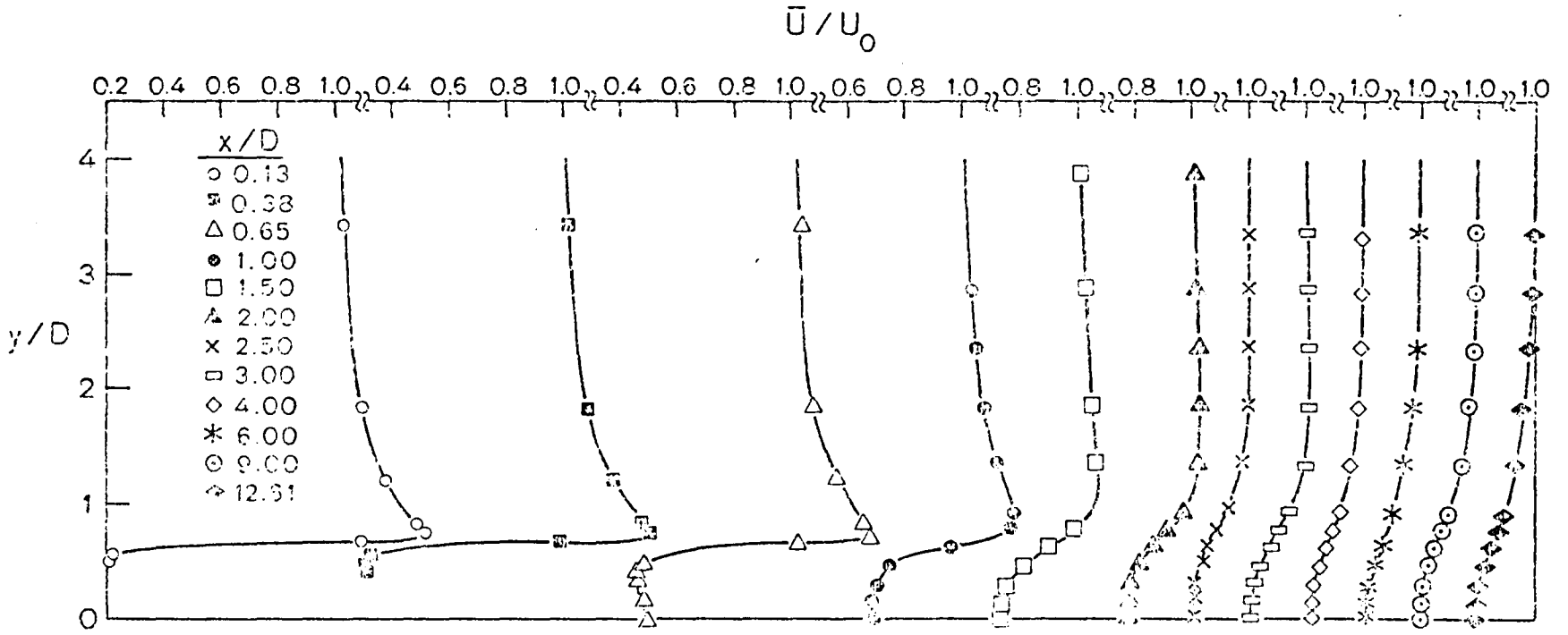

Figure(3-7) Mean speed profiles across the wake of a two-dimensional cylinder, Re = 9955.

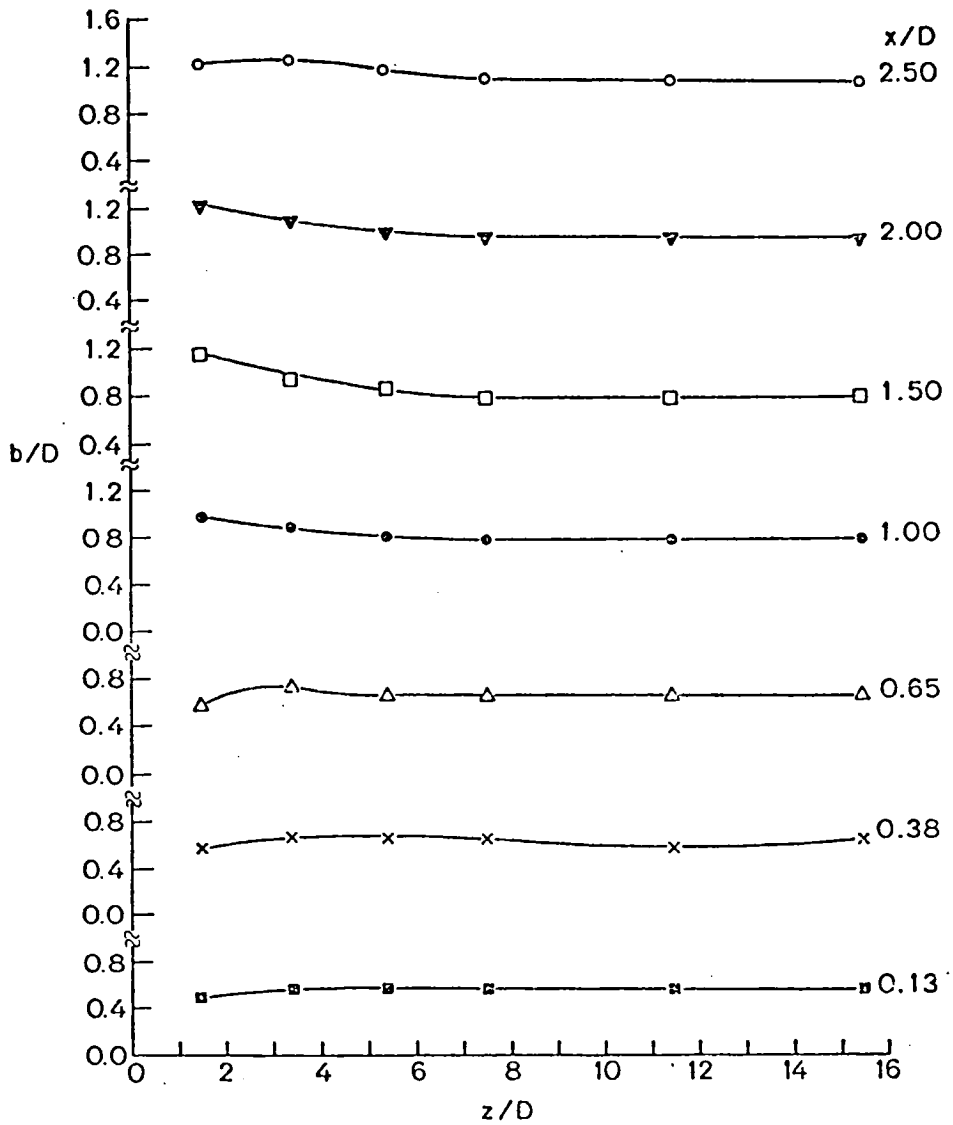

Figure(3-8a) Spanwise variation of wake width, Re = 9955.

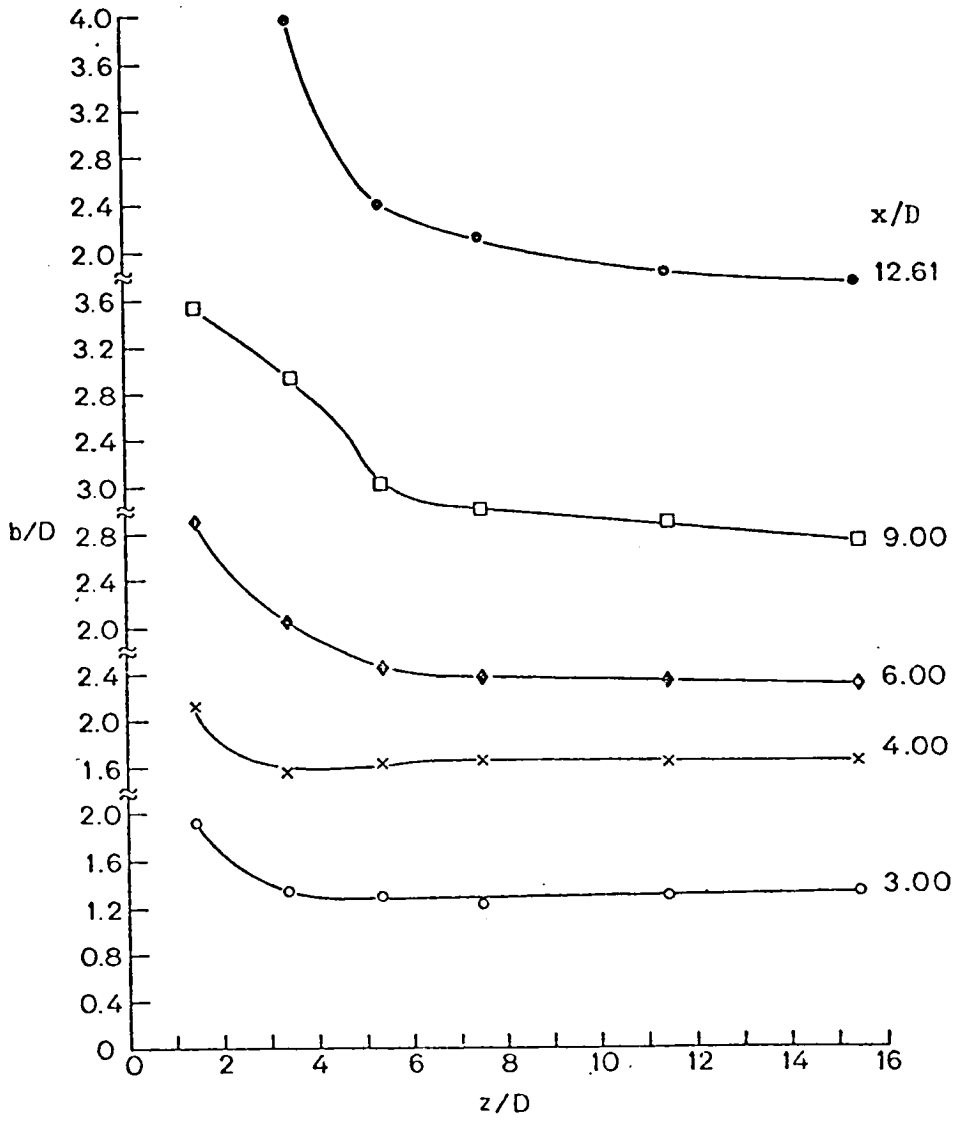

Figure(3-8b) Spanwise variation of wake width, Re = 9955.

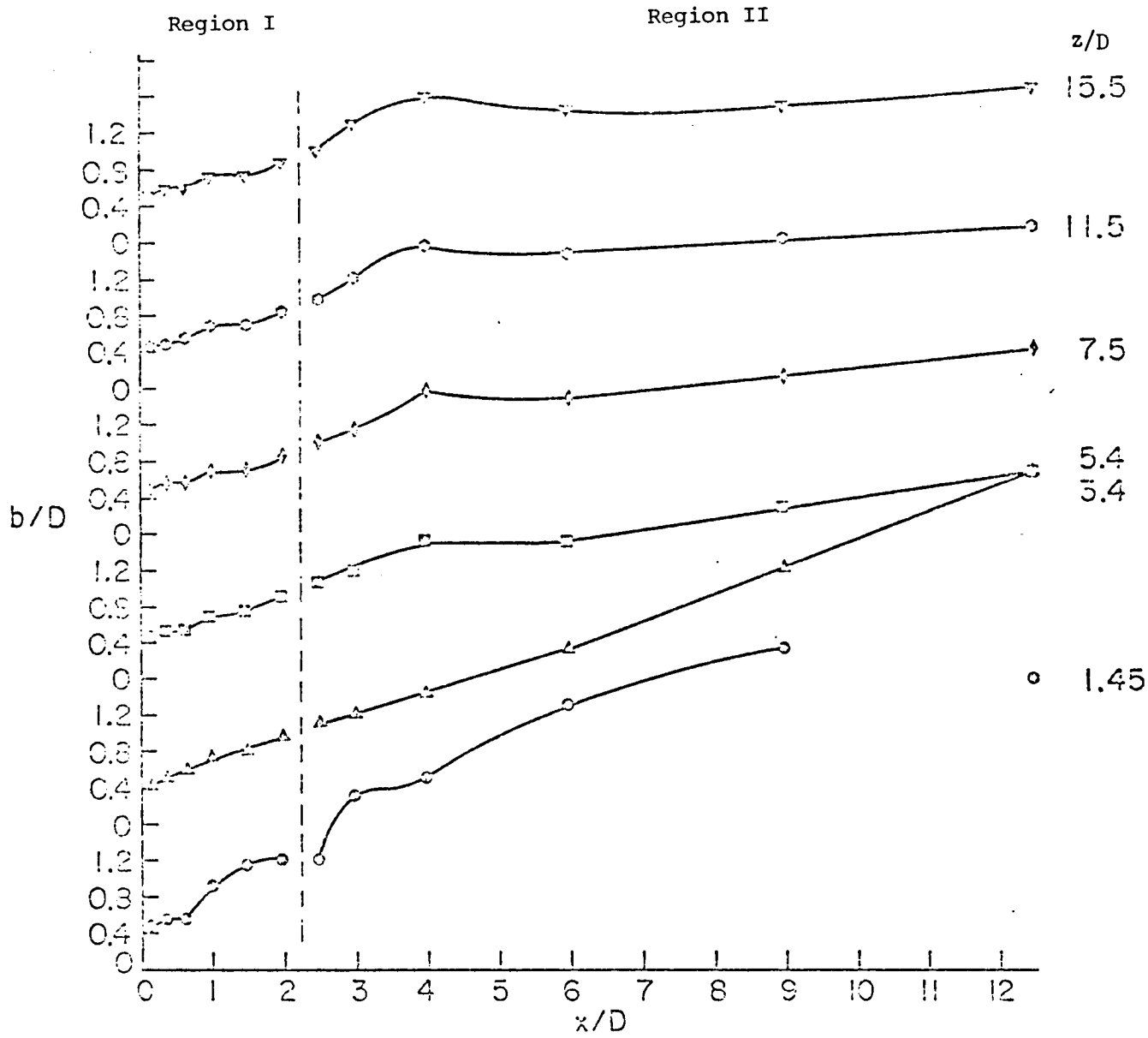

Figure(3-9) Streamwise variation of wake width , Re = 9955.

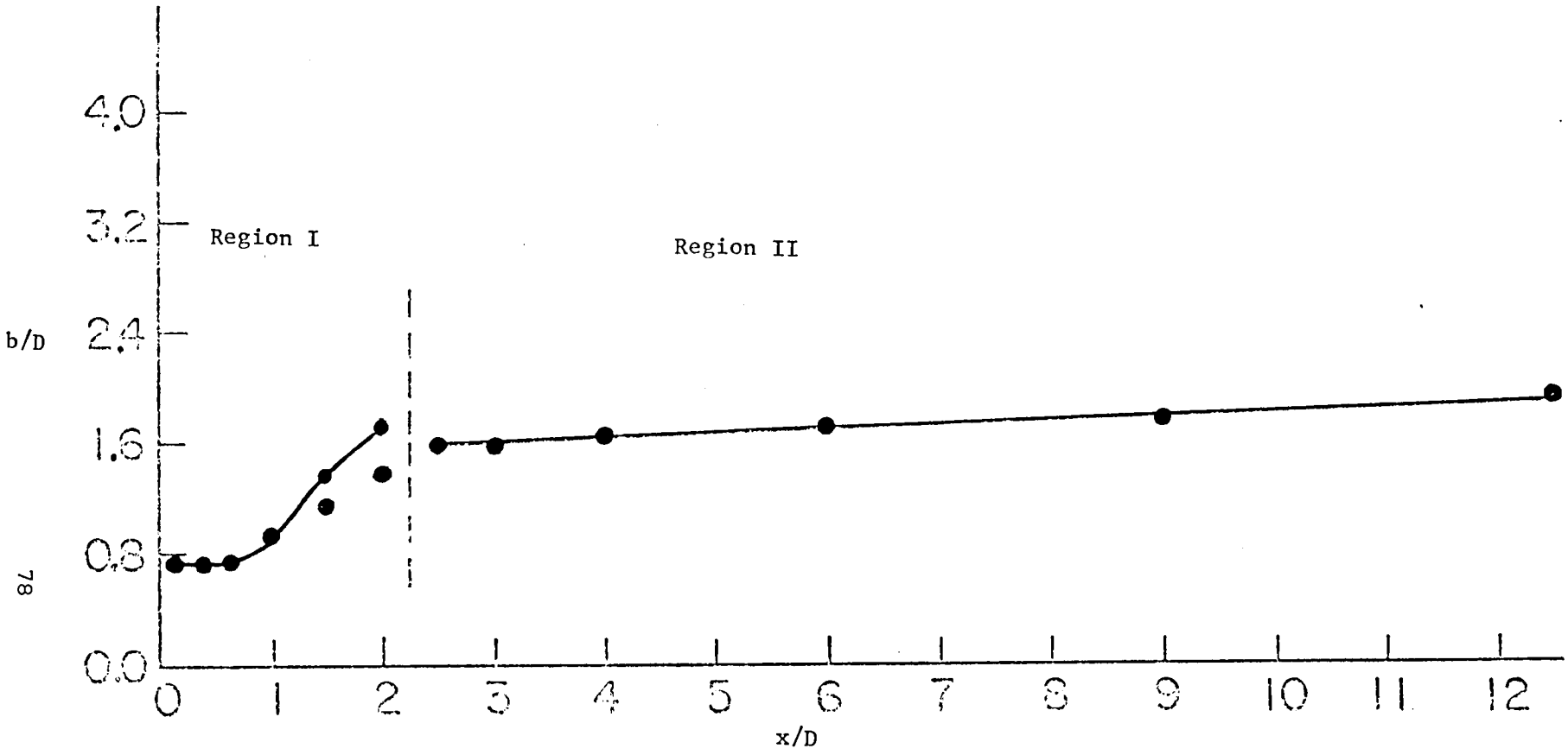

Figure(3-10) Streamwise variation of wake width for the case of a two-dimensional cylinder , Re = 9955.

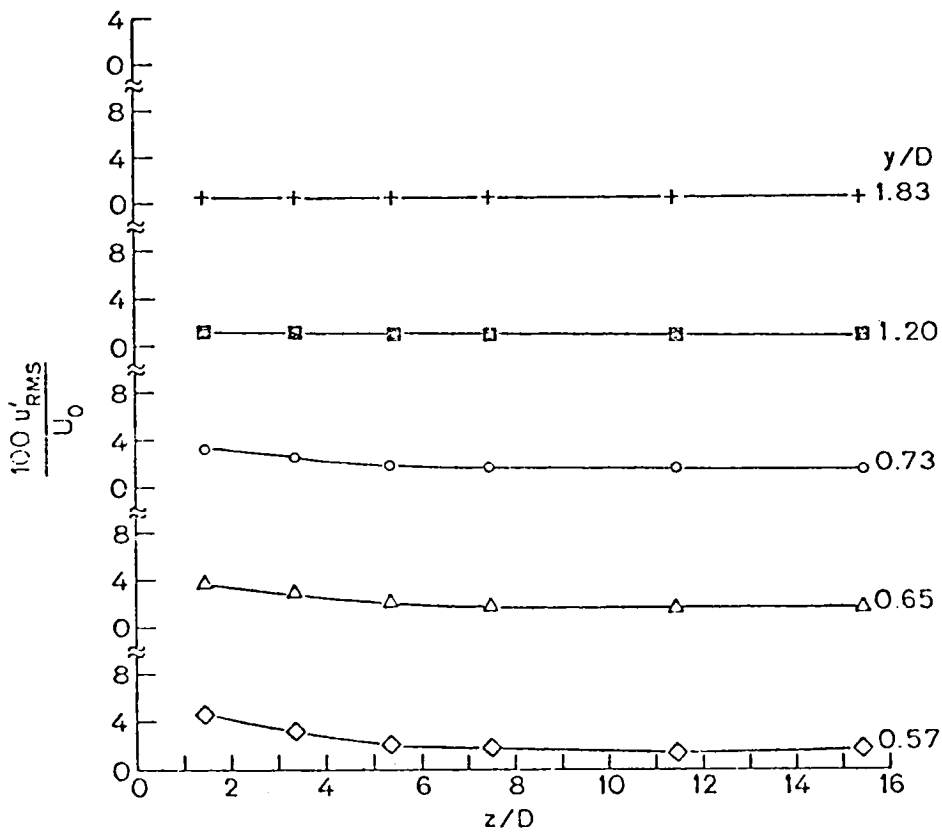

Figure(3-11) Spanwise variation of root-mean-square values of velocity fluctuations, x/D = 0.13.

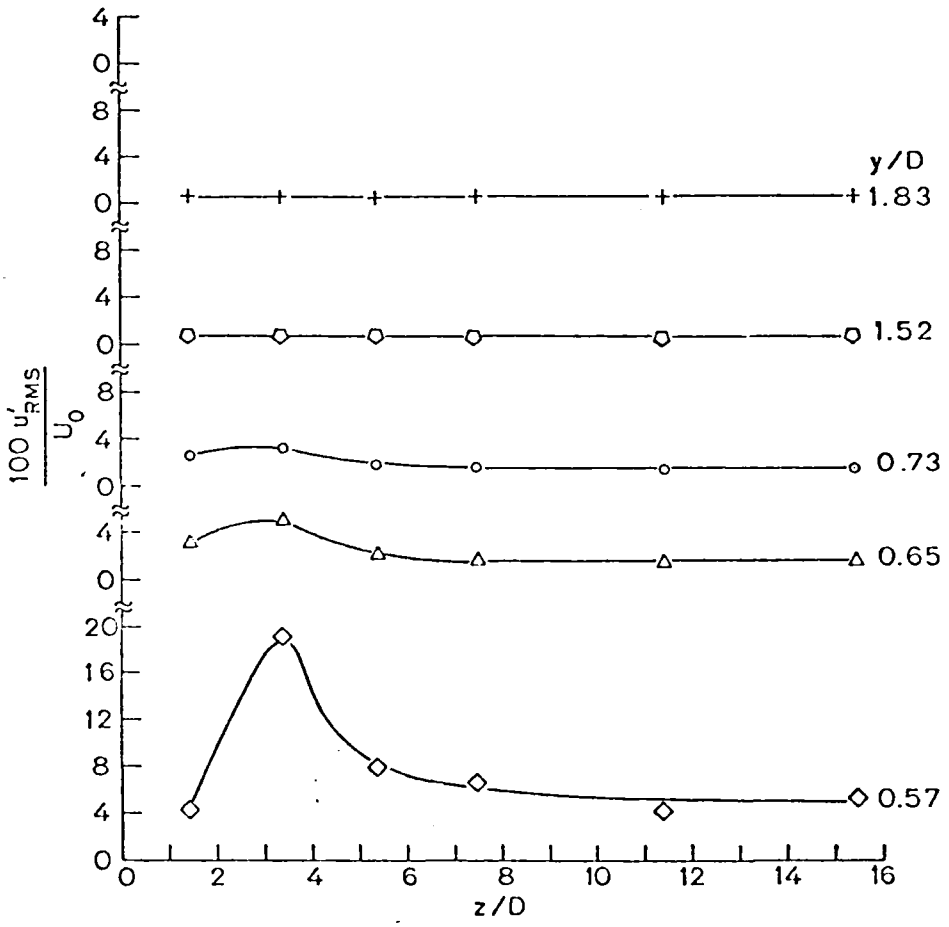

Figure(3-12) Spanwise variation of root-mean-square values of vlocity fluctuations, x/D = 0.38.

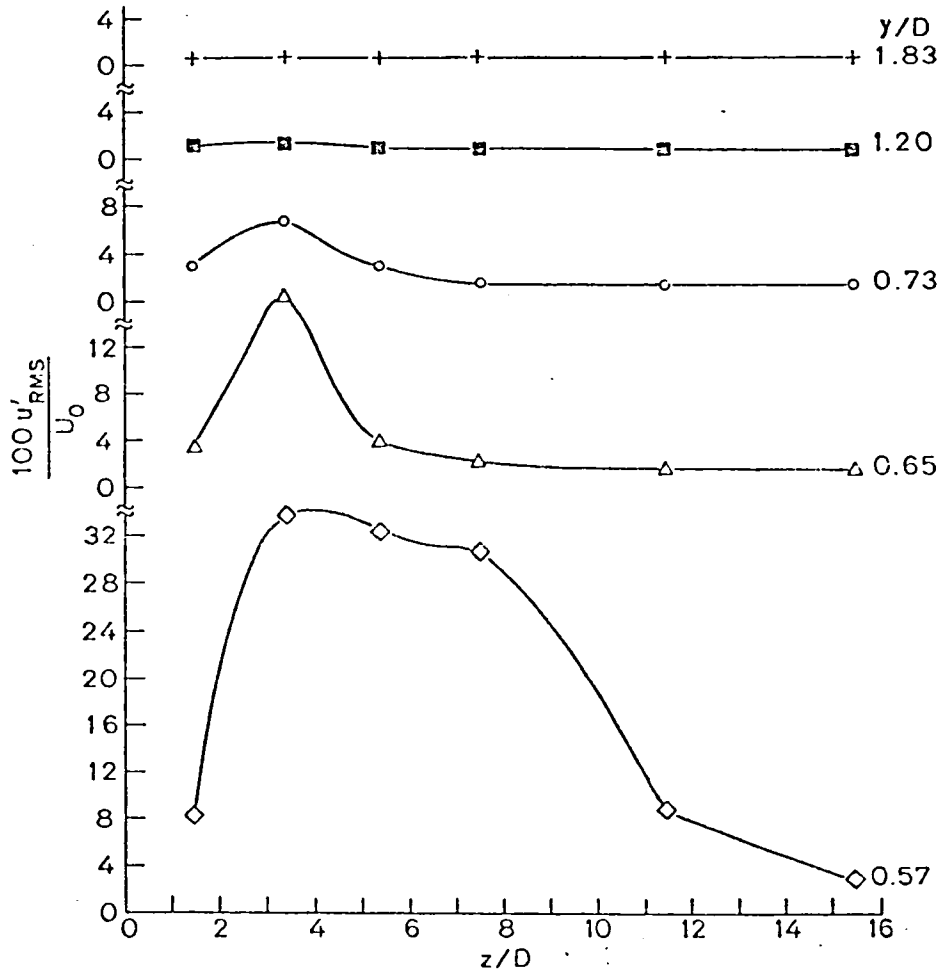

Figure(3-13) Spanwise variation of root-mean-square values of velocity fluctuations, x/D = 0.65.

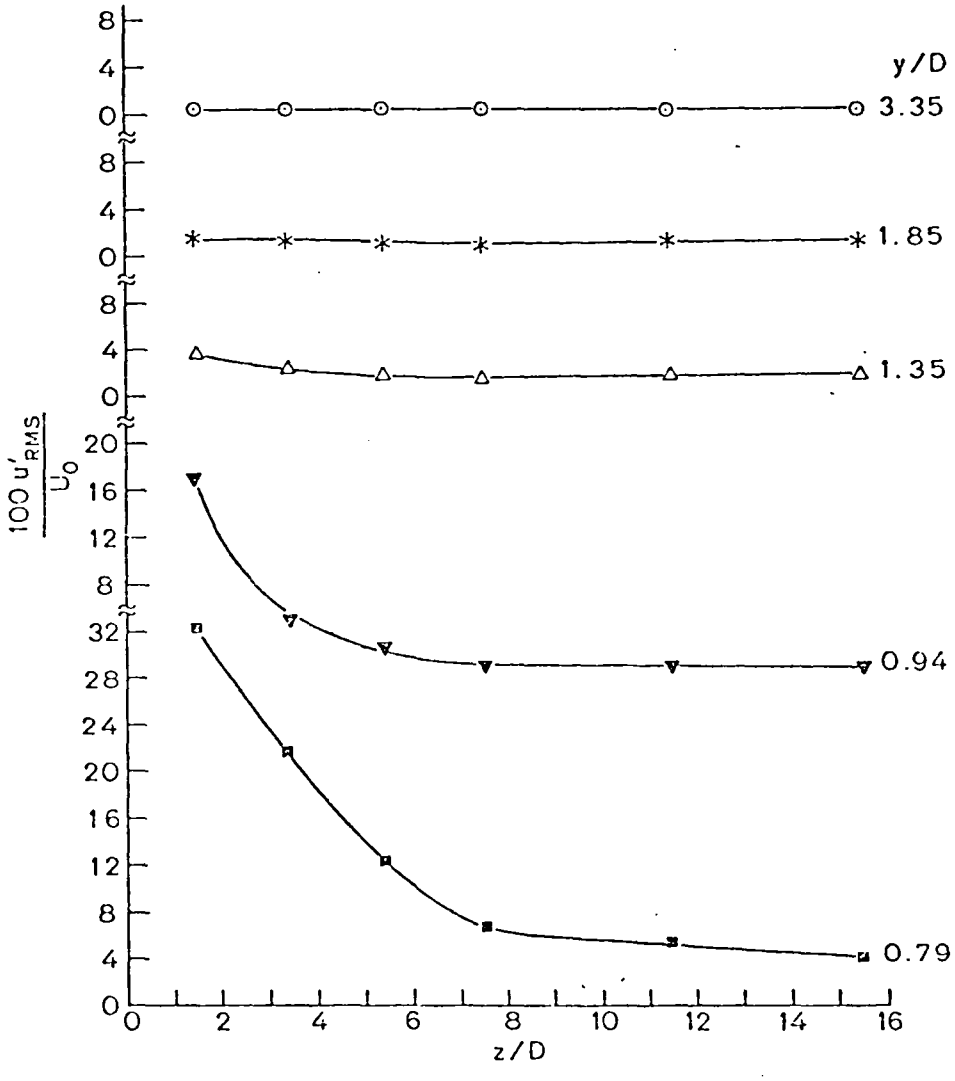

Figure(3-14) Spanwise variation of root-mean-square values of velocity fluctuations, x/D 1.0.

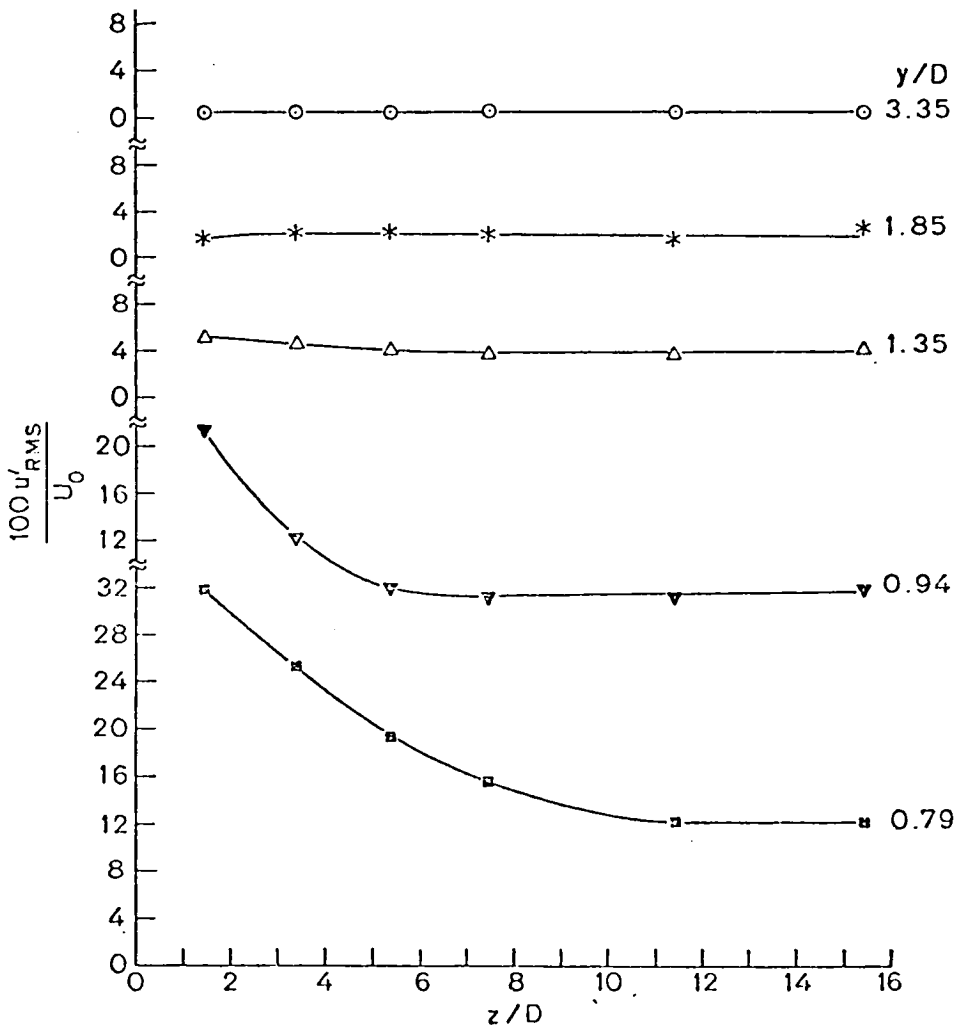

Figure(3-15) Spanwise variation of root-mean-square values of velocity fluctuations, x/D = 1.5.

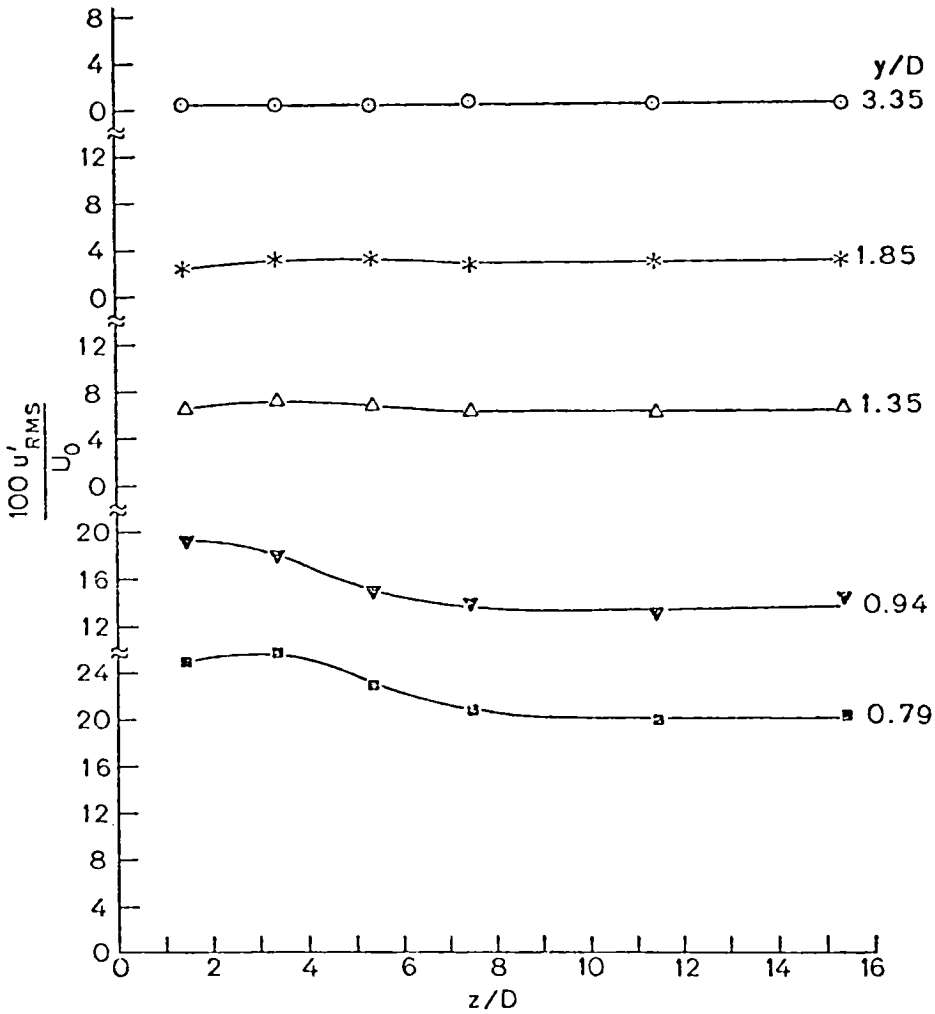

Figure(3-16) Spanwise variation of root-mean-square values of velocity fluctuations ,x/D = 2.0.

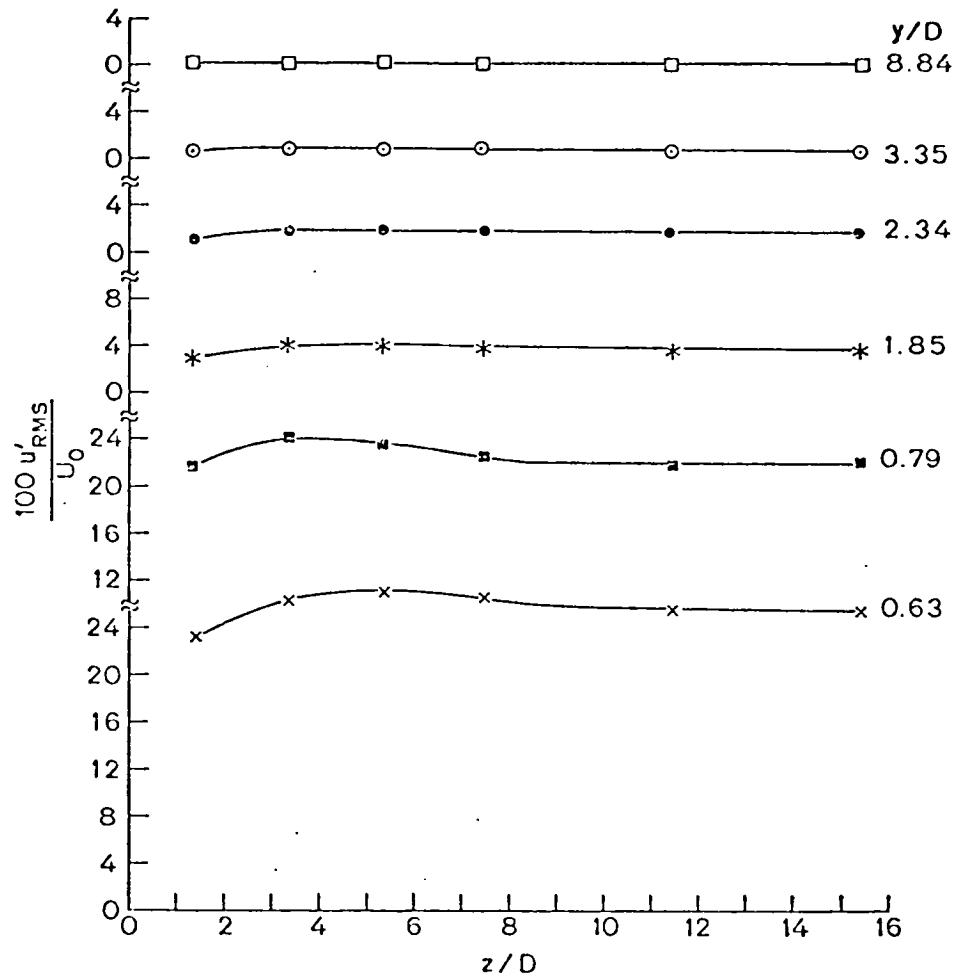

Figure(3-17) Spanwise variation of root-mean-square values of velocity fluctuations, x/D = 2.5.

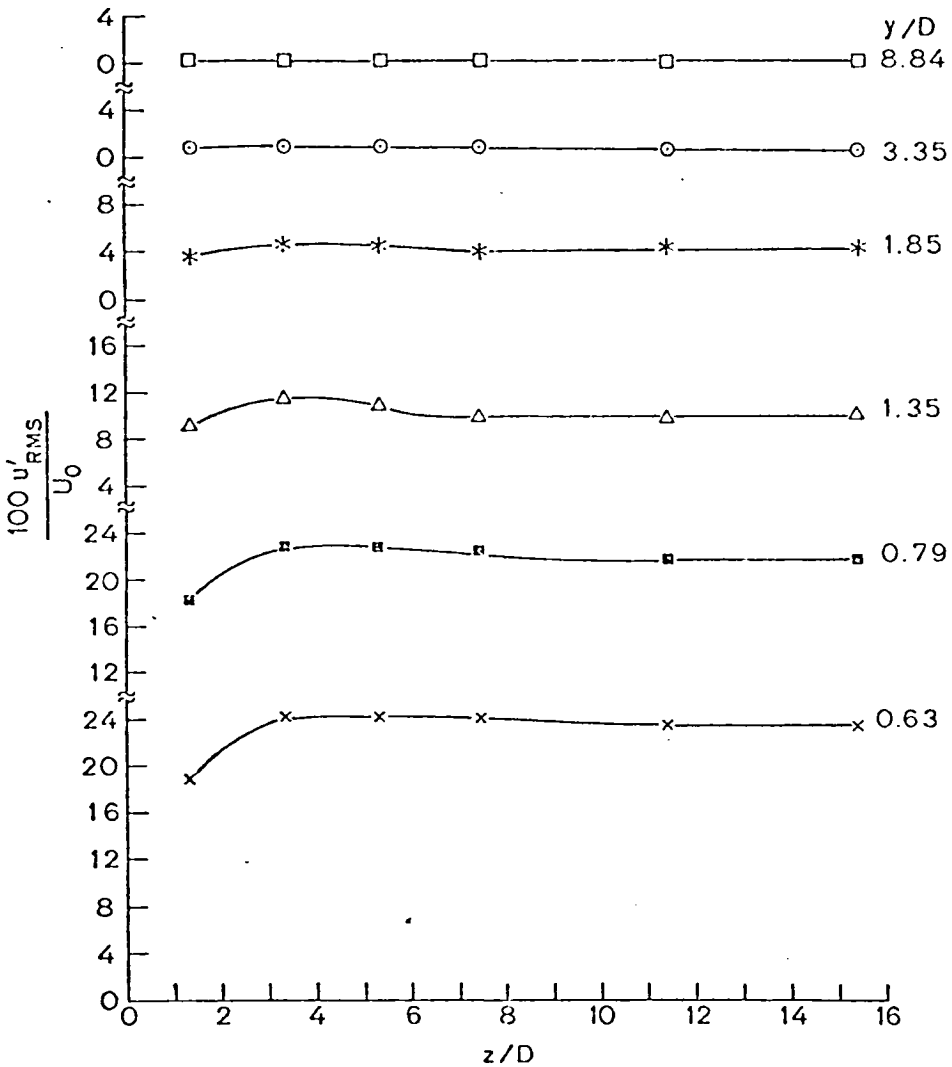

Figure(3-18) Spanwise variation of root-mean-square values of velocity fluctuations, x/D = 3.0.

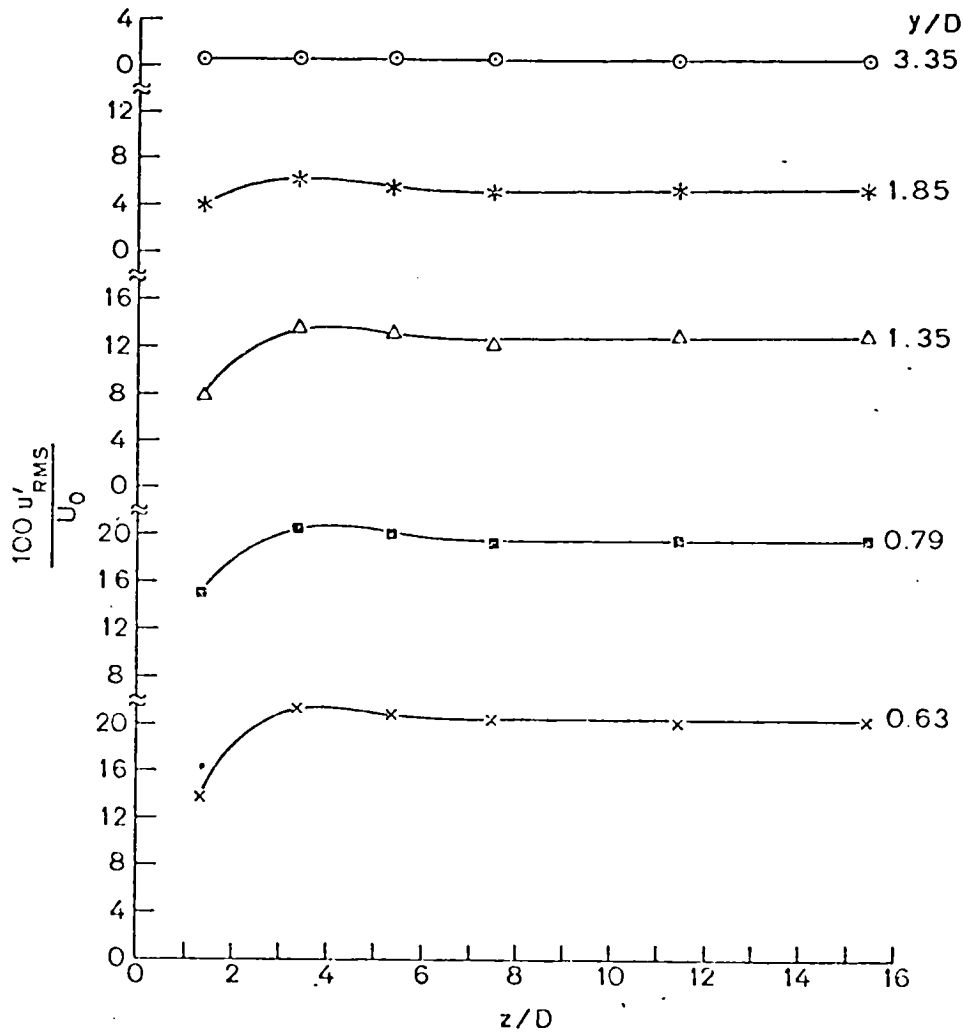

Figure(3-19) Spanwise variation of root-mean-square values of velocity fluctuations, x/D = 4.0.

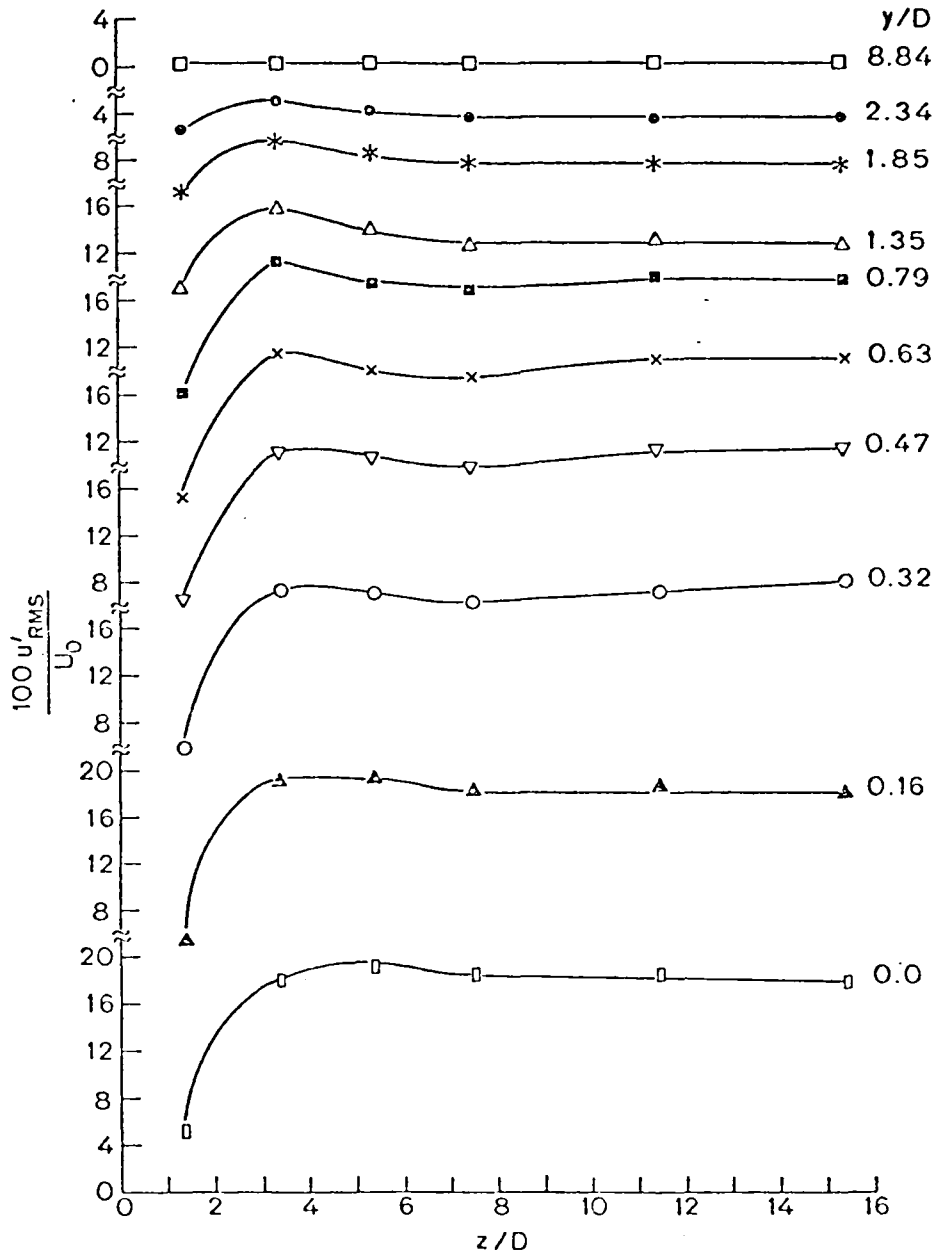

Figure(3-20) Spanwise variation of root-mean-square values of velocity fluctuations, x/D = 6.0.

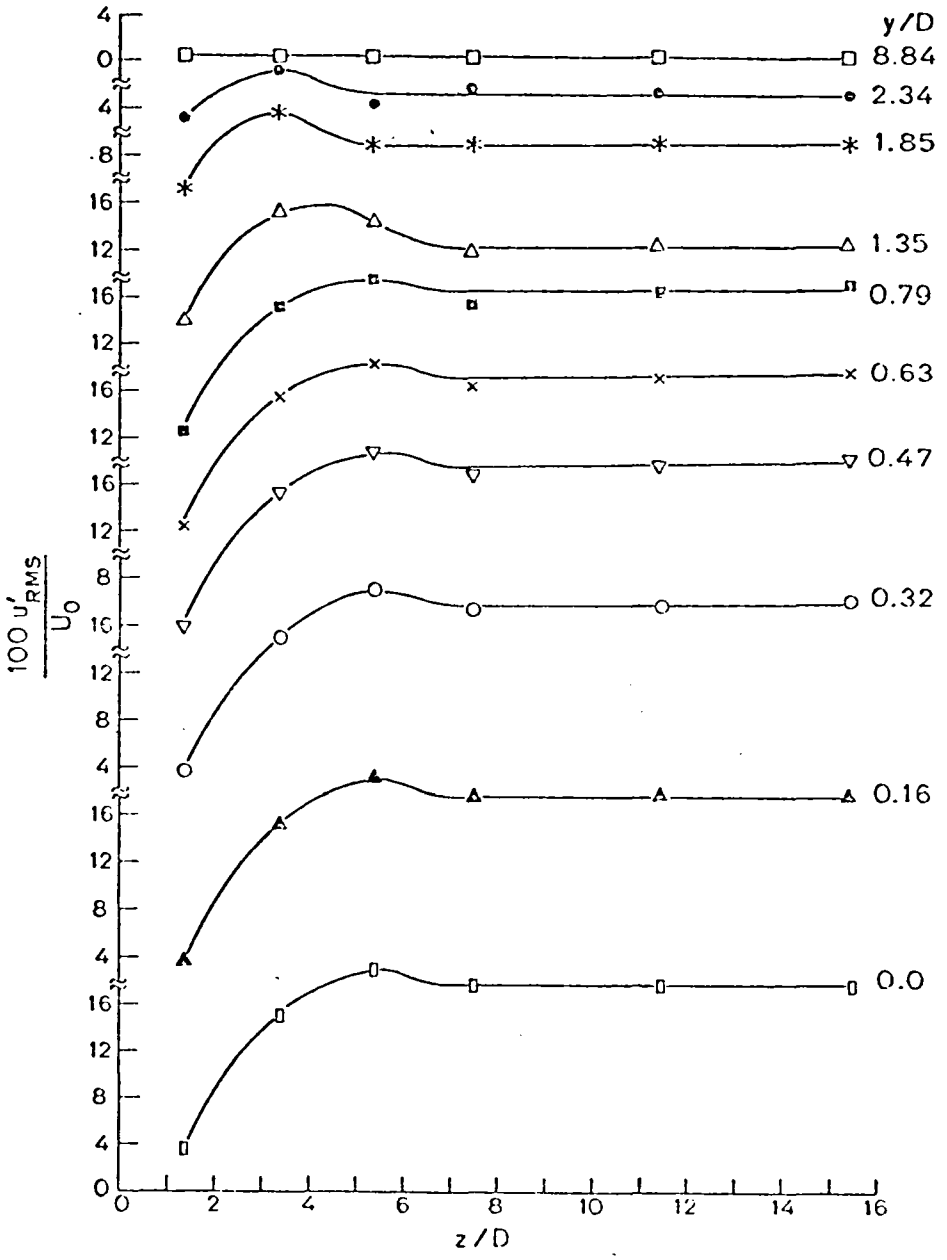

Figure(3-21) Spanwise variation of root-mean-square values of velocity fluctuations, x/D =9.0.

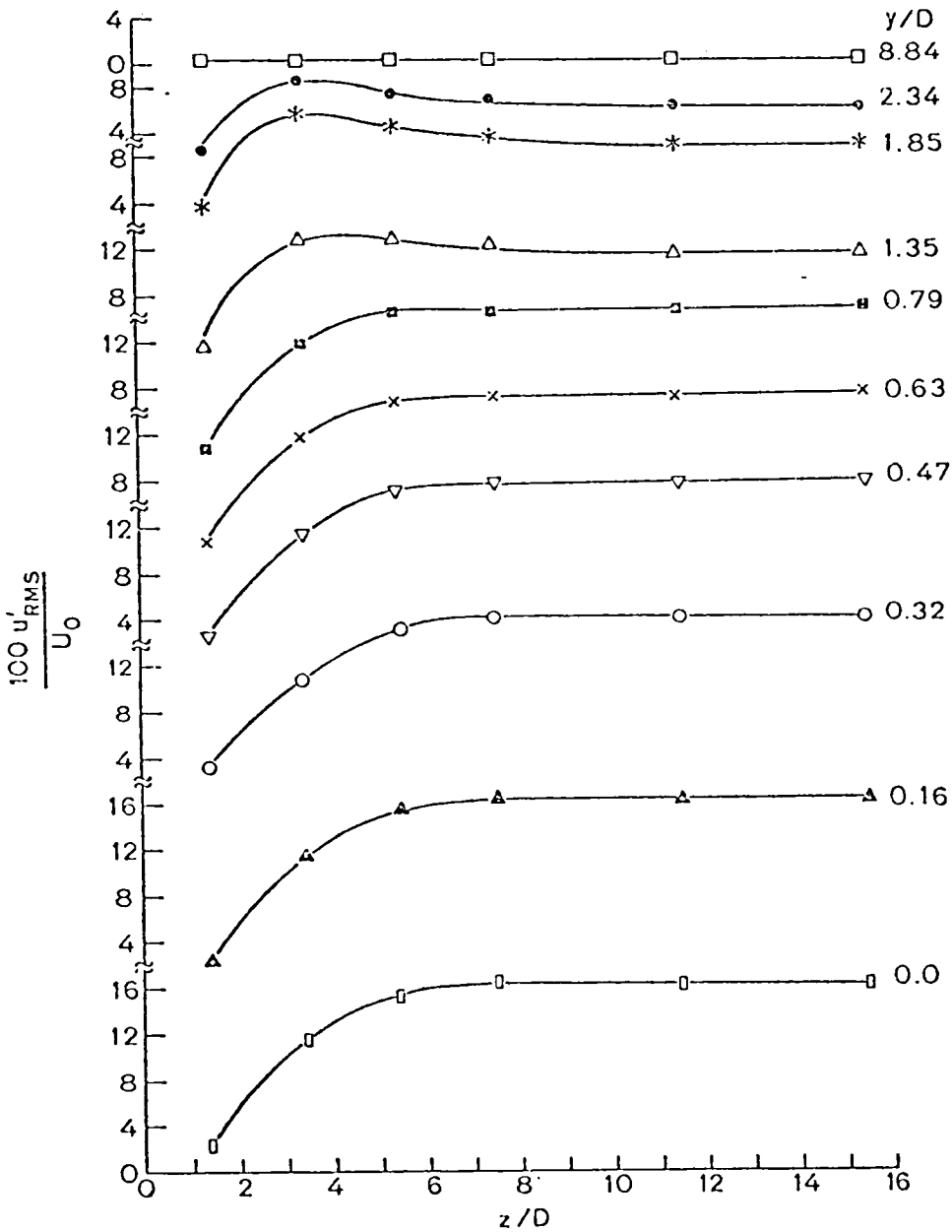

Figure(3-22) Spanwise variation of root-mean-square valuea of velocity fluctuation, x/D = 12.6.

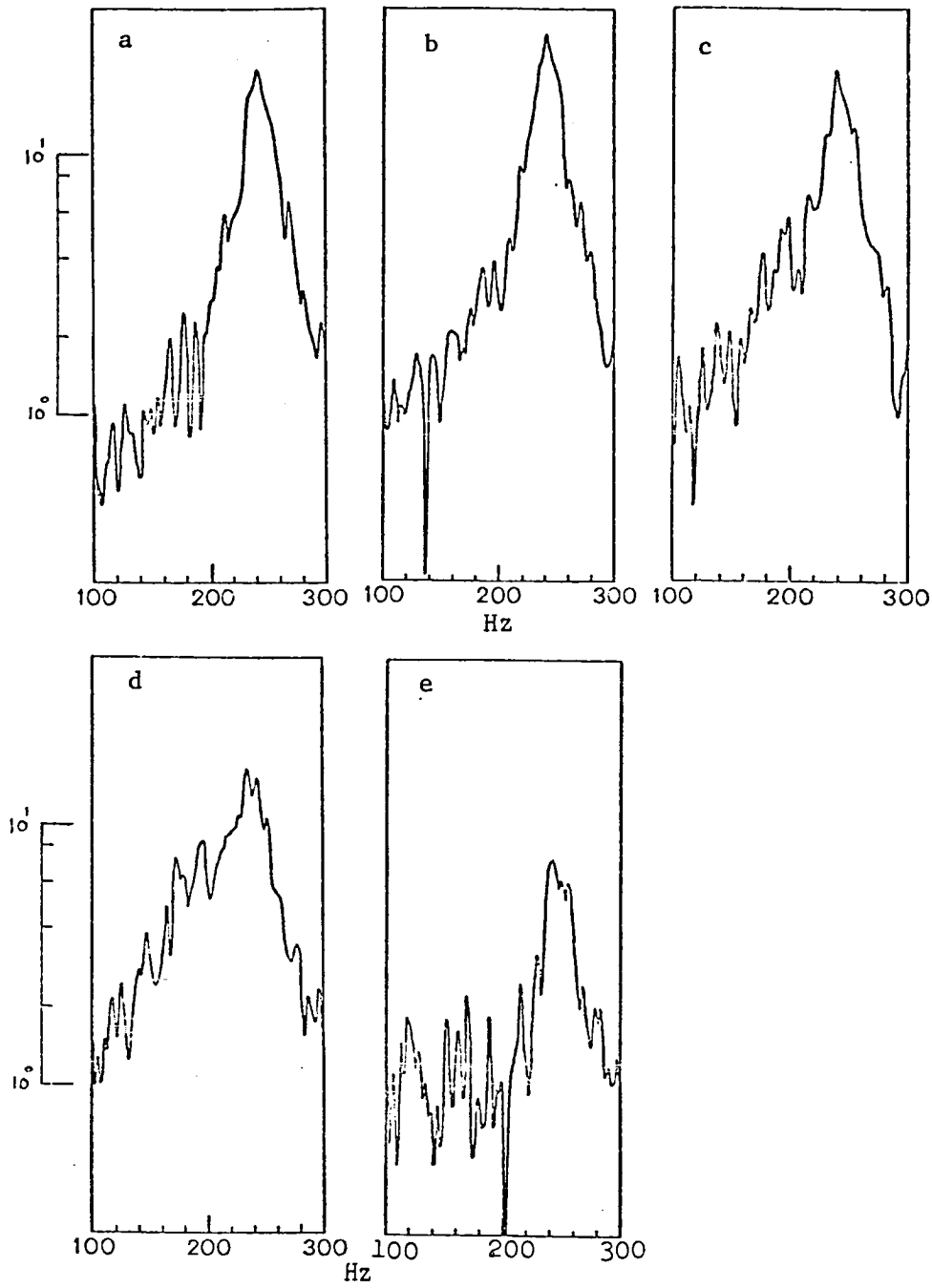

Figure (3-23) Frequency spectra of hot-wire signals at x/D = 0.10, y/D = 0.70 and spanwise positions (a) z/D = 0.0, (b) z/D = 0.25, (c) z/D = 0.50, (d) z/D = 0.75, (e) z/D = 1.75 Re = 9955.

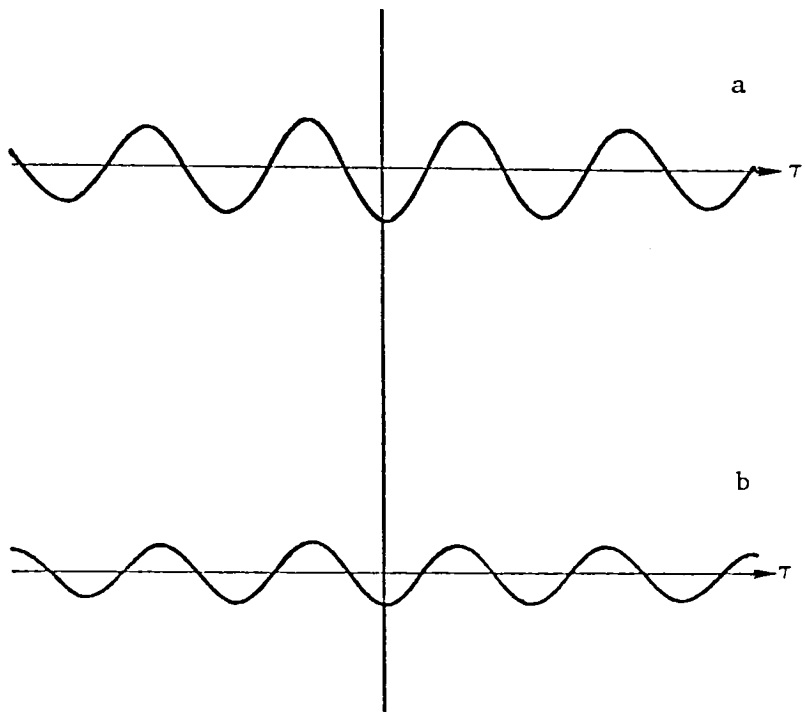

Figure (3-24) Cross-correlations between two hot-wire signals (filtered between 200 and 300 Hz) with both reference and traversing probes placed at mirror-image positions of 0.70D with respect to wake center, x/D = 0.10 and spanwise positions (a) z/D = 0.0, (b) z/D = 1.75. Re = 9955.

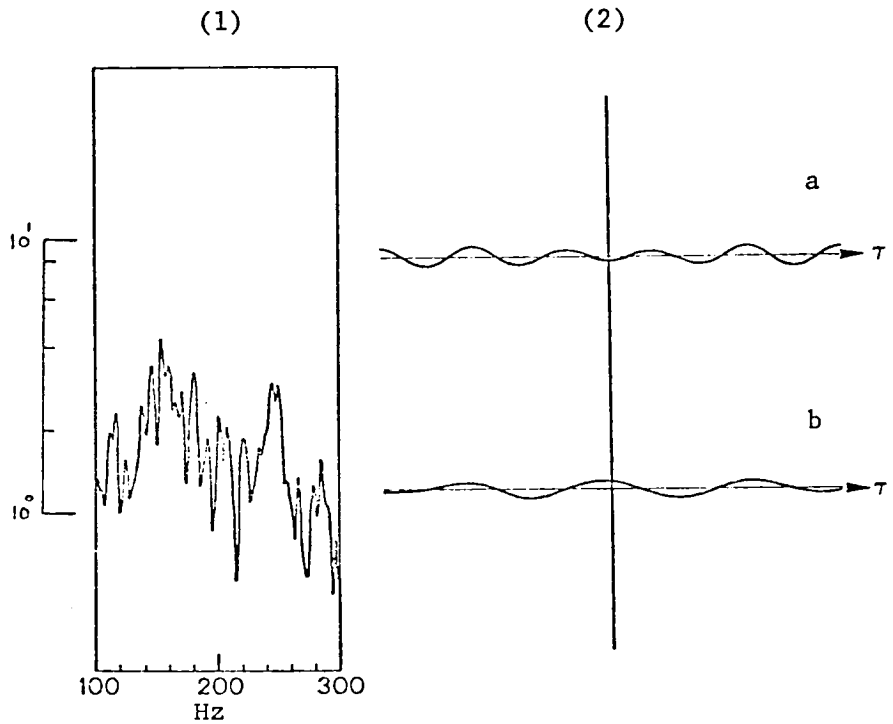

Figure (3-25) (1) Frequency spectrum of hot-wire signal at x/D = 0.10, y/D = 0.70, z/D = 2.25. (2) Cross-correlations between two hot-wire signals with both reference and traversing probes placed at mirror-image positions at y/D = 0.70 with respect to the wake center and x/D = 0.10, z/D = 2.25. Bandpass filters at (a) between 200 and 300 Hz, (b) between 110 and 200 Hz. Re = 9955.

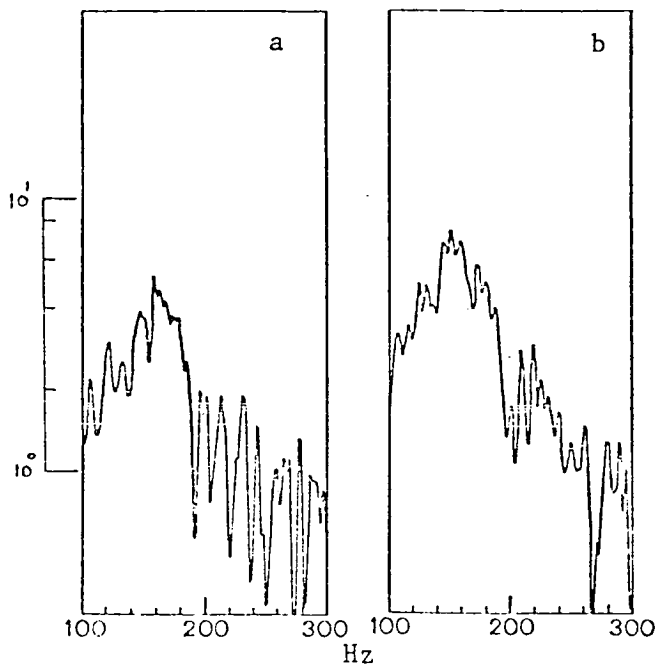

Figure (3-26) Frequency spectra of hot-wire signals at x/D = 0.10, y/D = 0.70, and spanwise position (a) z/D = 2.75, (b) z/D = 3.0. Re = 9955.

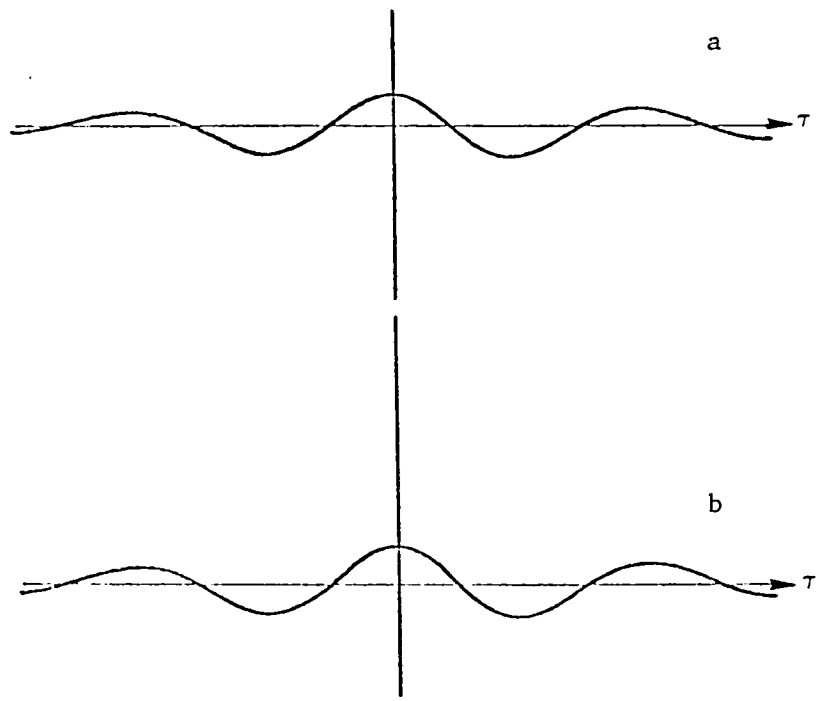

Figure (3-27) Cross-correlations between two hot-wire signals (filtered between 110 and 200 Hz) with both reference and traversing probes placed at mirror-image positions at y/D = 0.70 with respect to wake center, x/D = 0.10 and spanwise positions (a) z/D = 2.75, (b) z/D = 3.0. Re = 9955.

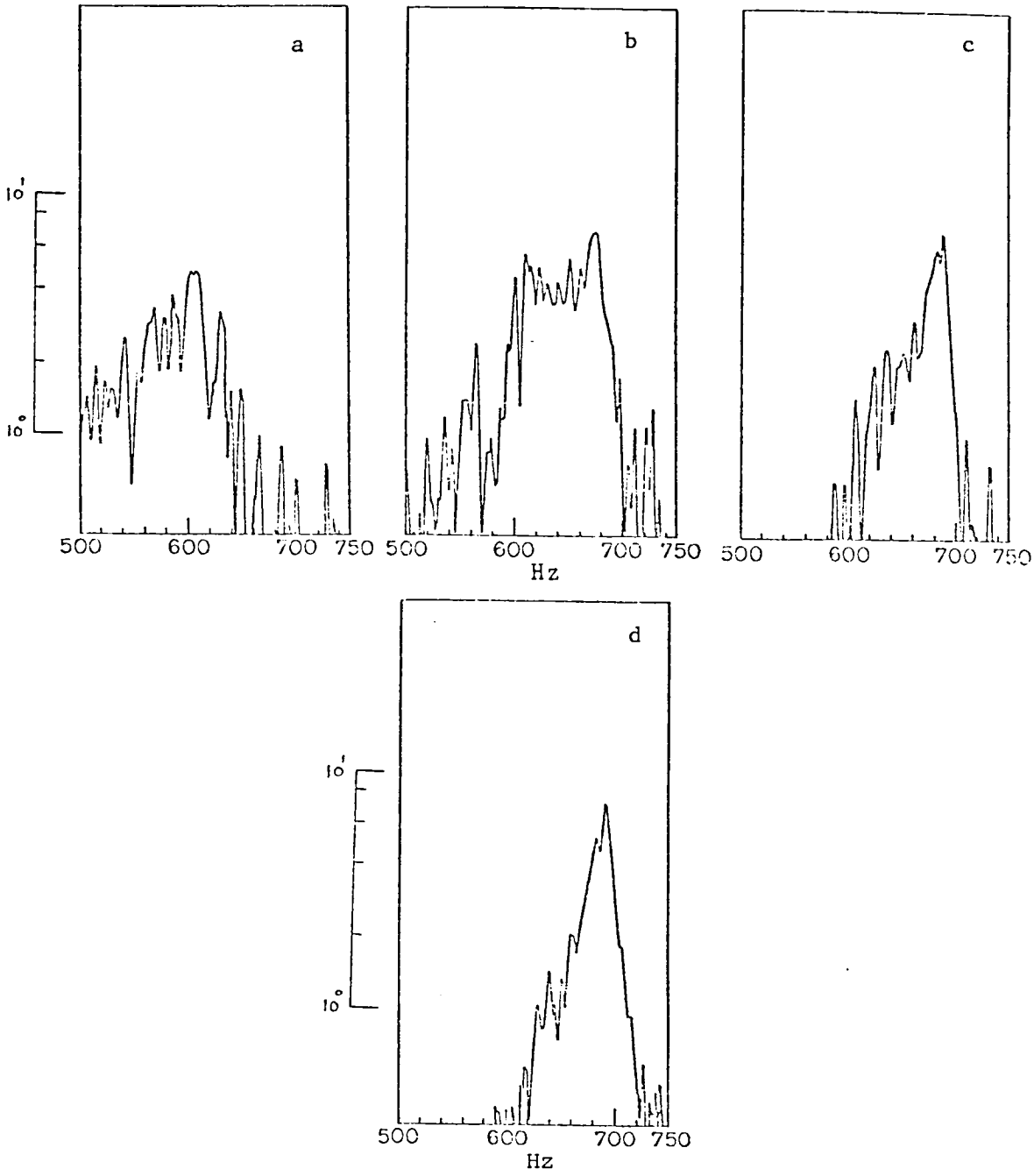

Figure (3-28) Frequency spectra of hot-wire signals at x/D = 0.10 and (a) y/D = 0.70, z/D = 4.25, (b) y/D = 1.0, z/D = 6.5, (c) y/D = 1.0, z/D = 8.5, (d) y/D = 1.0, z/D = 10.0. Re = 9955.

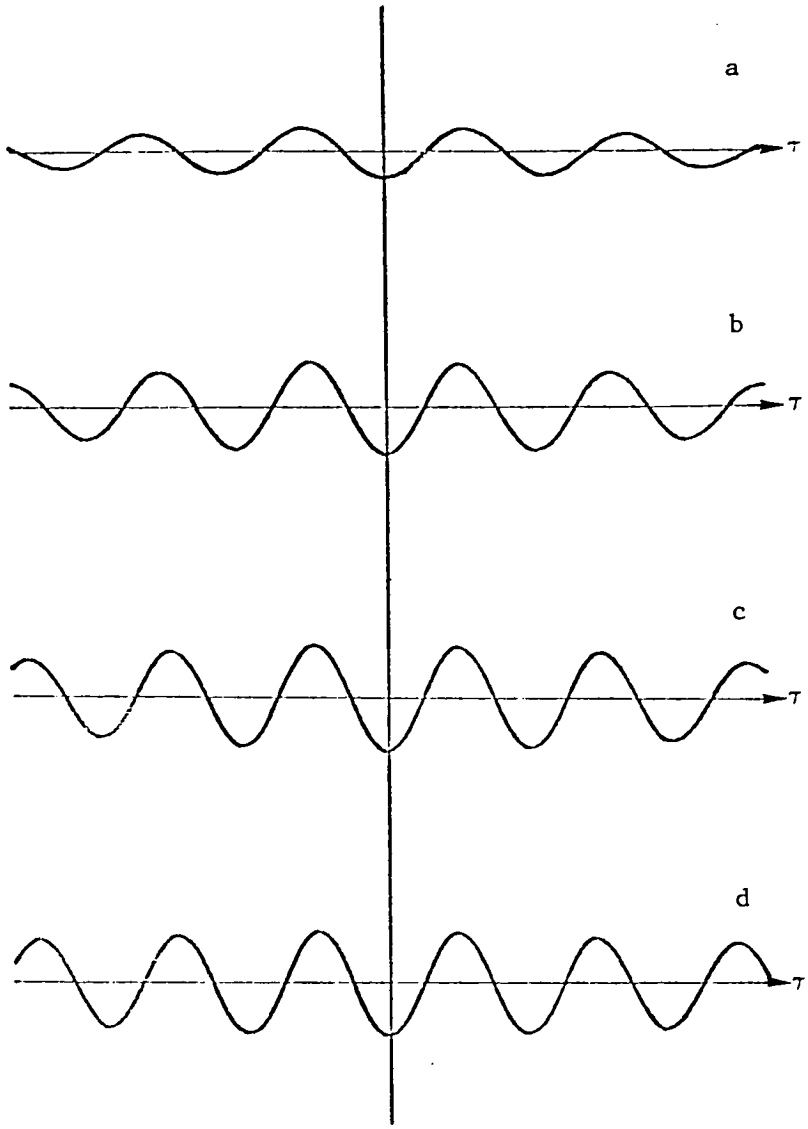

Figure (3-29) Cross-correlations between two hot-wire signals with both reference and traversing probes placed at x/D = 0.10 and (a) y/D = ± 0.70, z/D = 4.25 (with signals filtered between 520 and 650 Hz), (b) y/D = ± 1.0, z/D = 6.5 (with signals filtered between 520 and 700 Hz), (c) y/D = ± 1.0, z/D = 8.5 (with signals filtered between 540 and 700 Hz), (d) y/D = ± 1.0 ,z/D=10.0(with signals filtered between 600 and 700 Hz). Re= 9955.

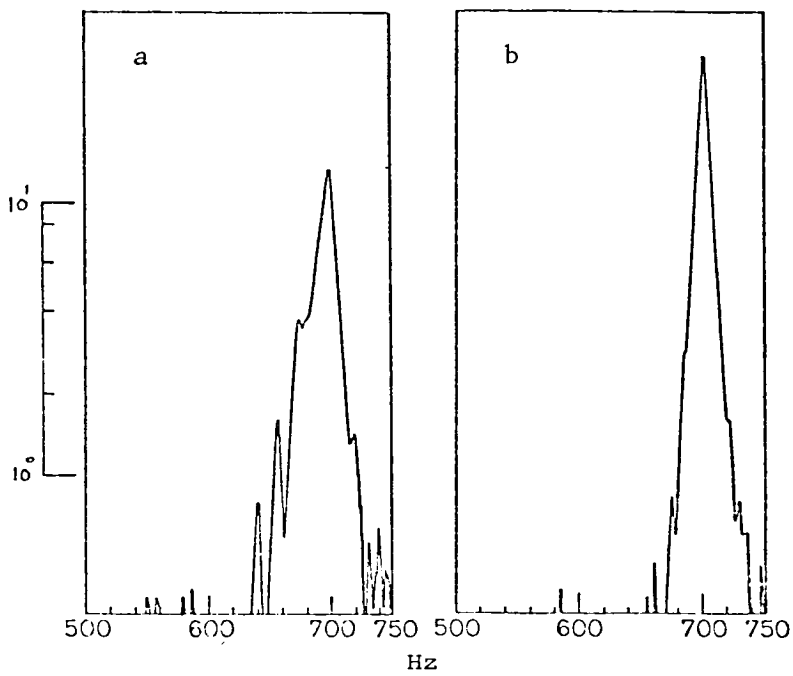

Figure (3-30) Frequency spectra of hot-wire signals at x/D = 0.10, y/D = 1.0, and (a) z/D = 13, (b) z/D = 18. Re = 9955.

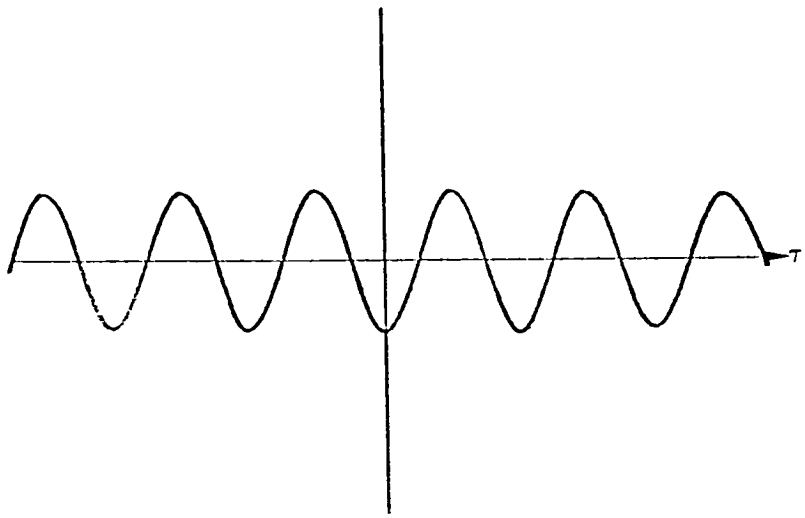

Figure (3-31) Cross-correlation between two hot-wire signals (filtered between 600 and 750 Hz) with both reference and traversing probes placed at x/D = 0.10, y/D = $\pm$ 1.0, z/D = 18. Re = 9955.

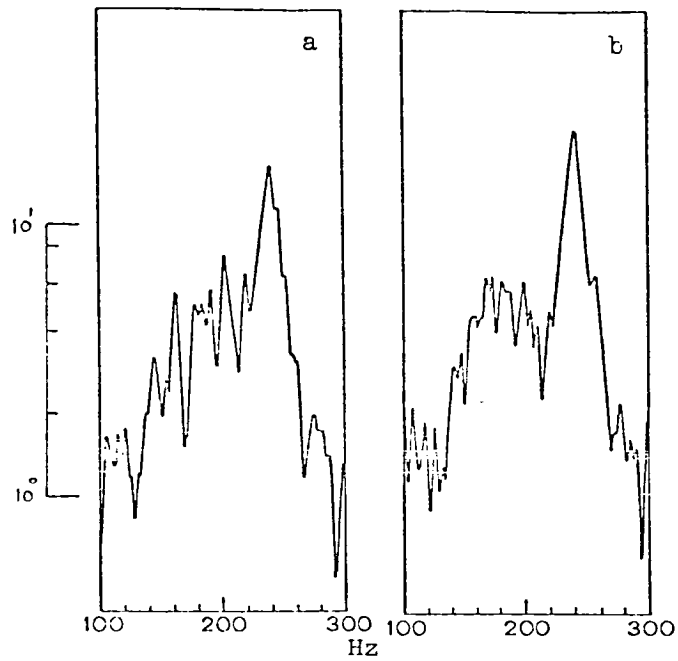

Figure(3-32),(a), and(b) . For legend see next page.

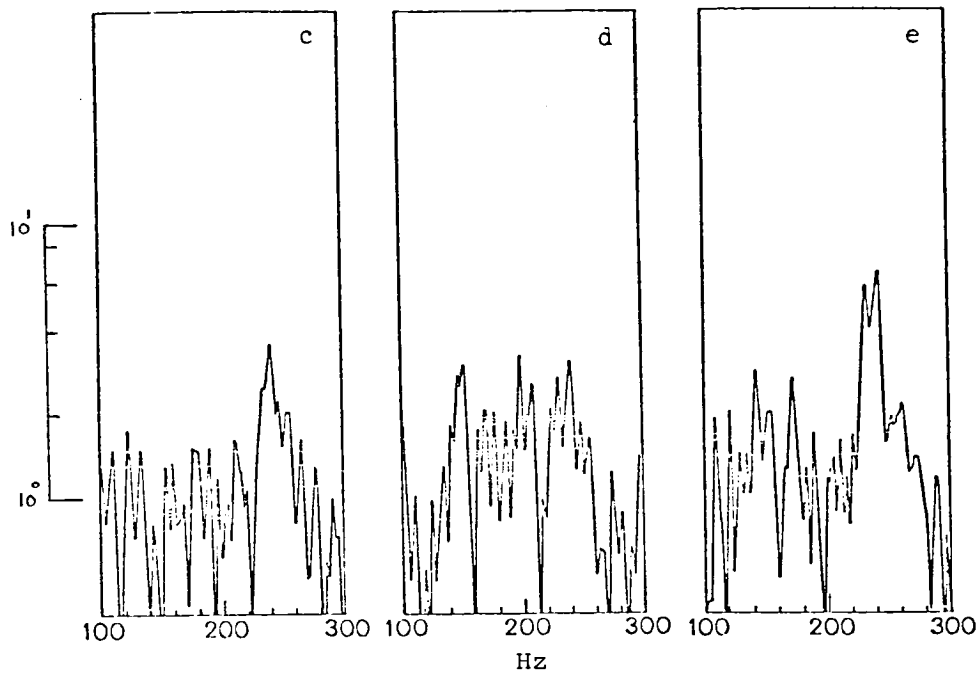

Figure (3-32) Frequency spectra of hot-wire signals at x/D = 0.97, and (a) y/D = 0.70, z/D = 0.0, (b) y/D = 0.70, z/D = 0.50, (c) y/D = 2.3, z/D = 1.0, (d) y/D = 2.3, z/D = 1.5, (e) y/D = 0.88, z/D = 2.0. Re = 9955.

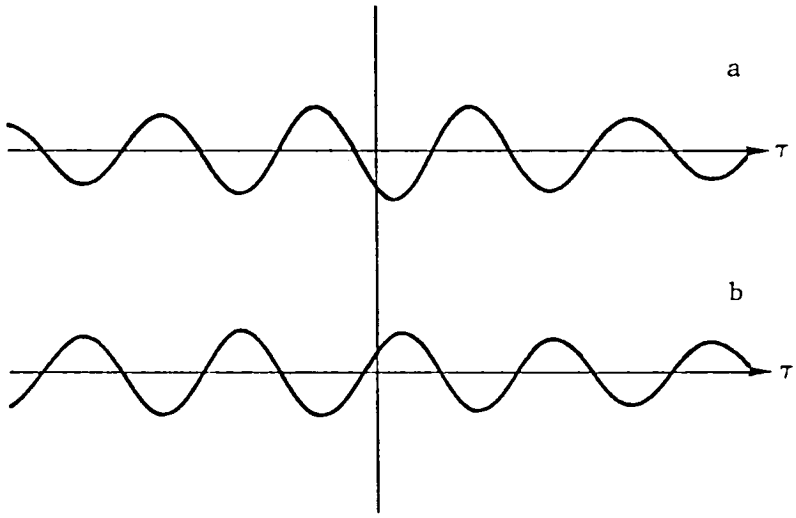

Figure (3-33) Cross-correlations between two hot-wire signals (filtered between 200 and 300 Hz) with reference probe placed at x/D = 0.10, y/D = -0.79, z/D = 0.0, and traversing probe at (a) x/D = 0.97, y/D = -0.79, z/D = 2.0, (b) x/D = 0.97 y/D = 0.79, z/D = 2.0. Re = 9955.

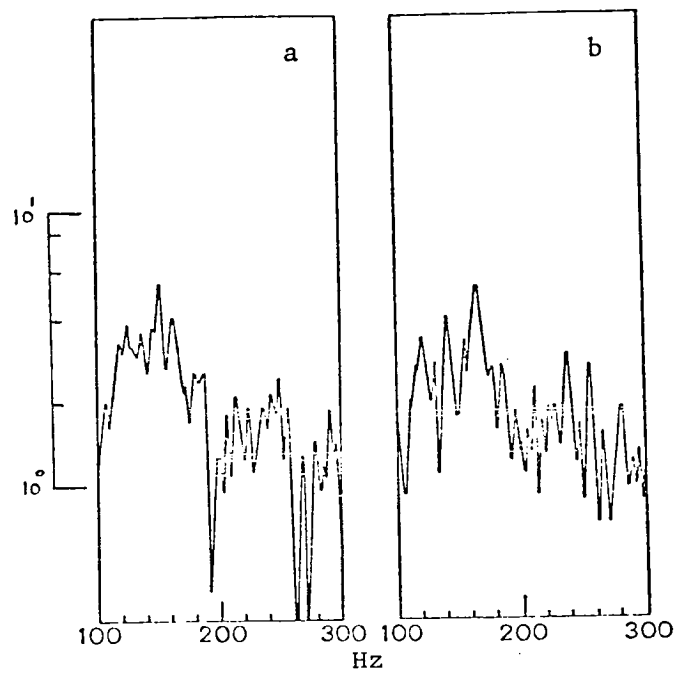

Figure (3-34) Frequency spectra of hot-wire signals at x/D = 0.97, and (a) y/D = 0.79, z/D = 3.0, (b) y/D = 0.76, z/D = 3.75. Re = 9955.

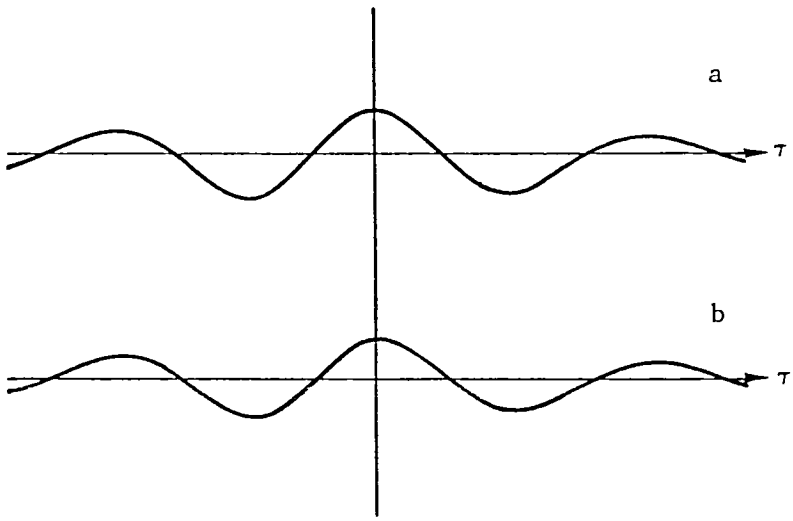

Figure (3-35) Cross-correlations between two hot-wire signals (filtered between 100 and 200 Hz) with reference probe placed at x/D = 0.10, y/D = -0.70, z/D = 2.75, and traversing probe at x/D = 0.97, z/D = 3.75, and (a) y/D = -0.70, (b) y/D = 0.70 Re = 9955.

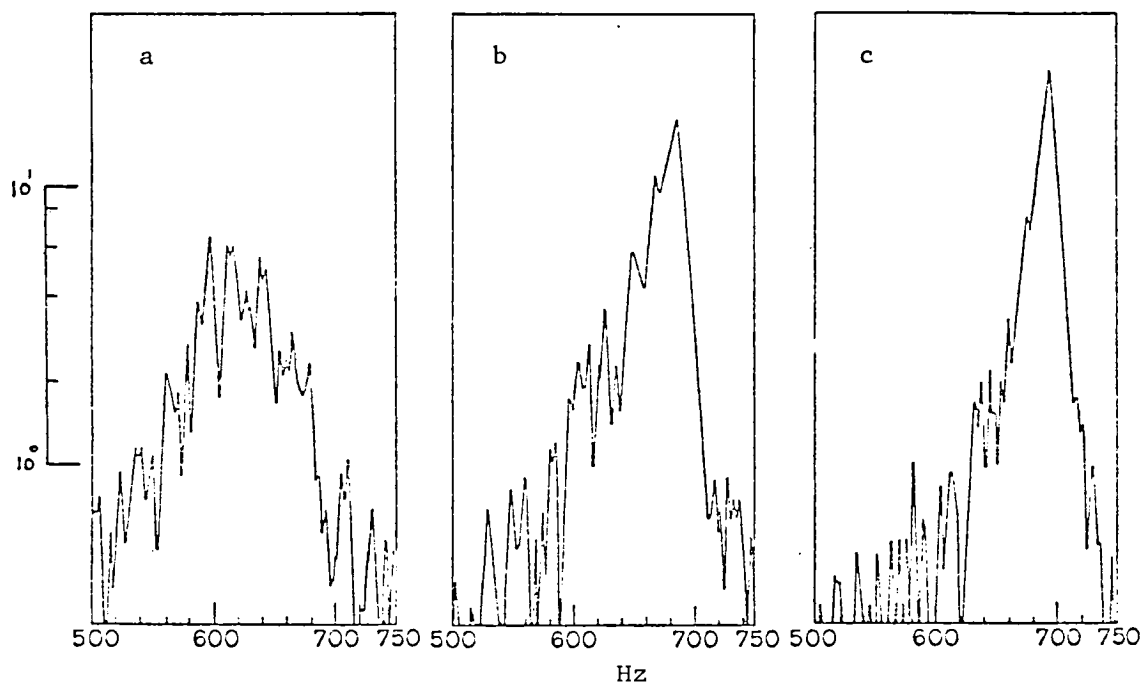

Figure (3-36) Frequency spectra of hot-wire signals at x/D = 0.97, y/D = 1.0, and (a) z/D = 5.5, (b) z/D = 9.0, (c) z/D = 12.0. Re = 9955

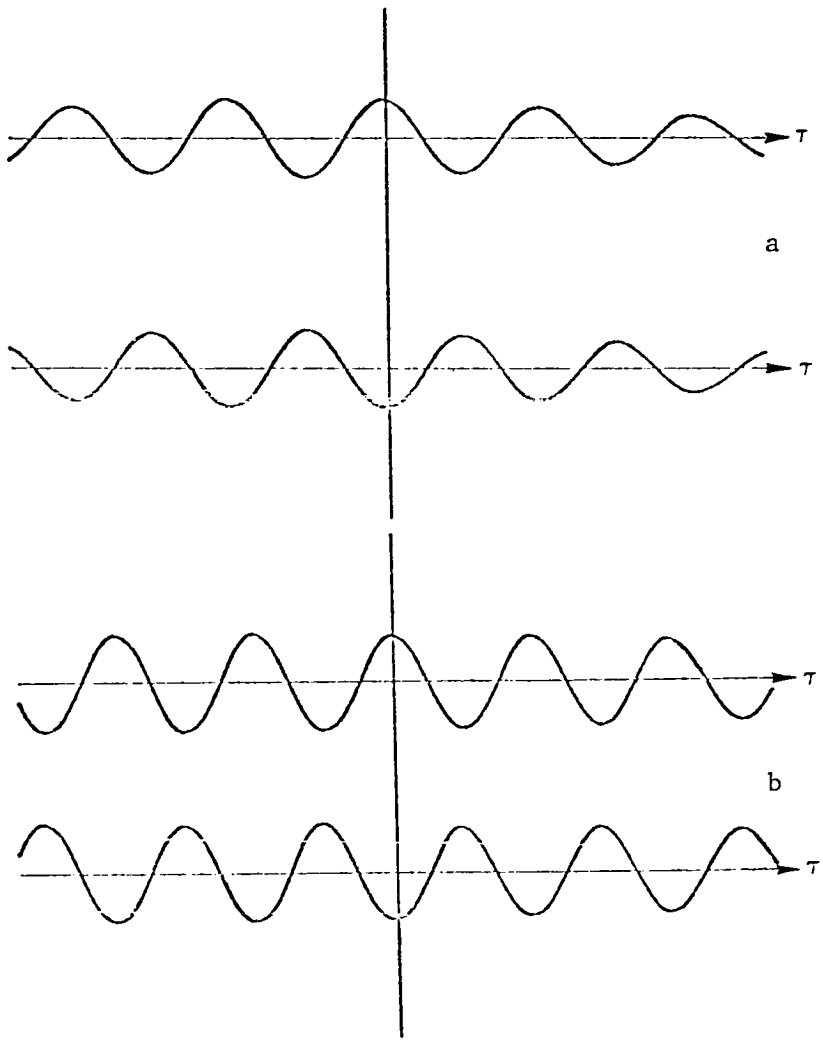

Figure (3-37) Cross-correlations between two hot-wire signals with (a) reference probe placed at x/D = 0.10, y/D = 1.0, z/D = 4.0, and traversing probe at x/D = 0.97, y/D = $\pm$ 1.0, z/D = 5.5 (signals filtered between 550 and 700 Hz), (b) reference probe placed at x/D = 0.10, y/D = -1.0, z/D = 10.0, and traversing probe at x/D = 0.97, y/D = $\pm$ 1.0, z/D = 12.0 (signals filtered between 600 and 750 Hz). Re = 9955.

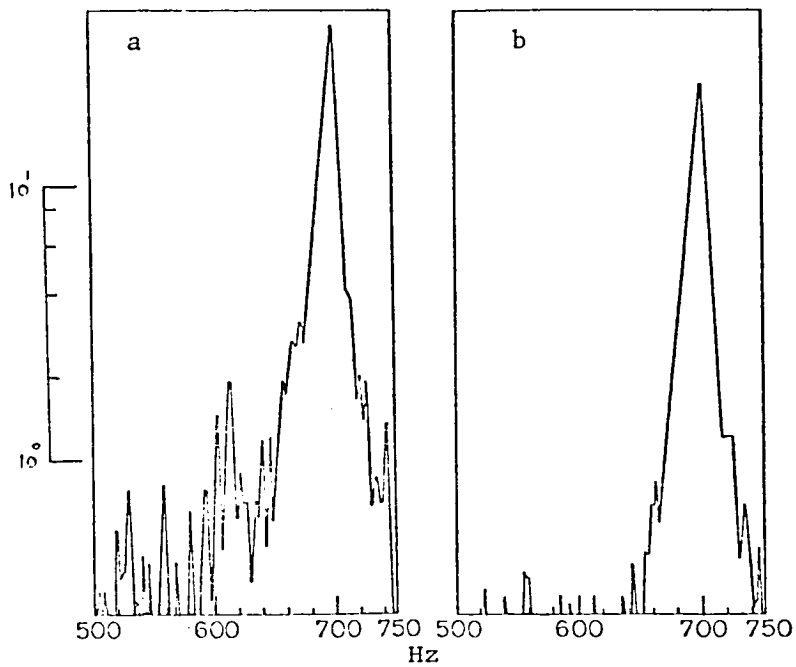

Figure (3-38) Frequency spectra of hot-wire signals at x/D = 0.97, y/D = 1.0, and (a) z/D = 14, (b) z/D = 26. Re = 9955.

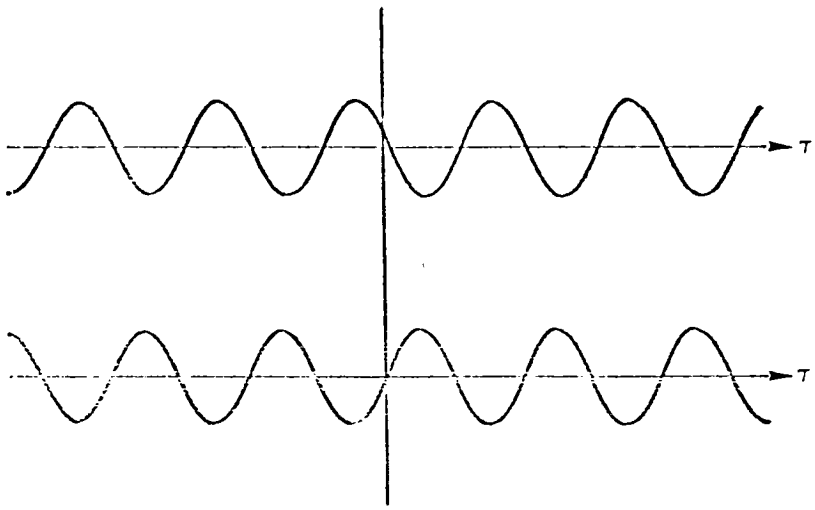

Figure (3-39) Cross-correlations between two hot-wire signals (filtered between 600 and 750 Hz) with reference probe at x/D = 0.10, y/D = -1.0, z/D = 24, and traversing at x/D = 0.97, y/D = $\pm$ 1.0, z/D = 26. Re = 9955.

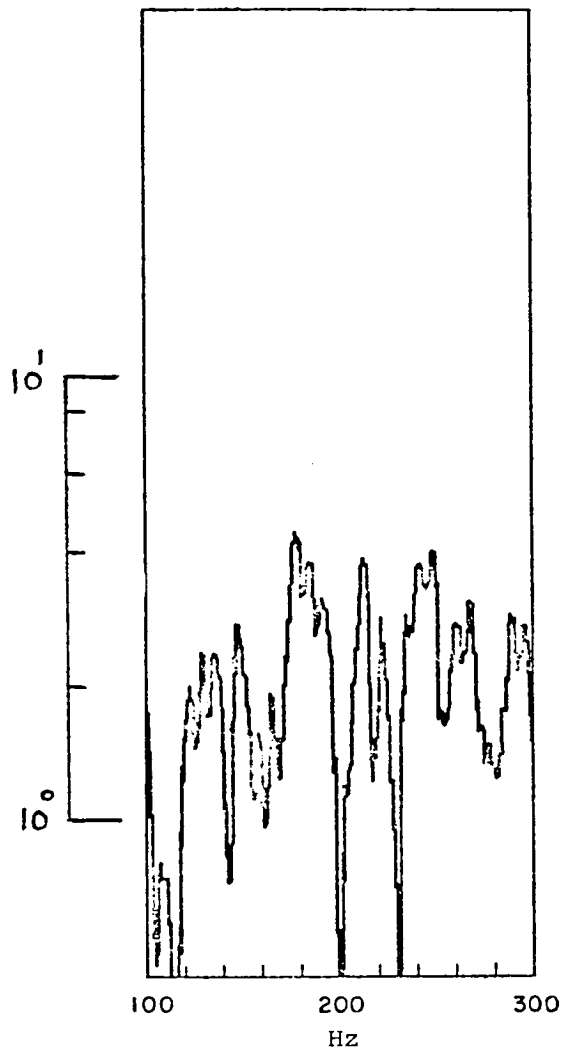

Figure (3-40) Frequency spectrum of hot-wire signal at x/D = 3.44, y/D = 2.0, z/D = 0.25. Re = 9955.

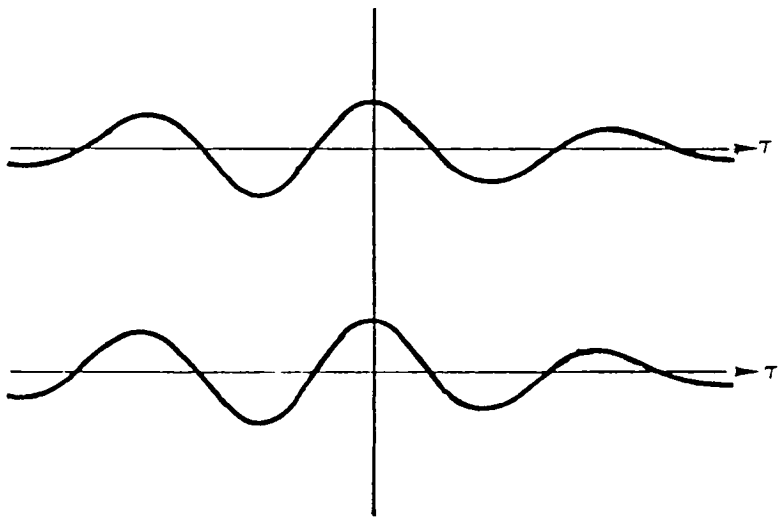

Figure (3-41) Cross-correlations between two hot-wire signals (filtered between 100 and 200 Hz) with reference probe at x/D = 0.10, y/D =-0.70, z/D = 2.25, and traversing at x/D = 3.44, y/D = $\pm$ 2.0, z/D = 0.25. Re = 9955.

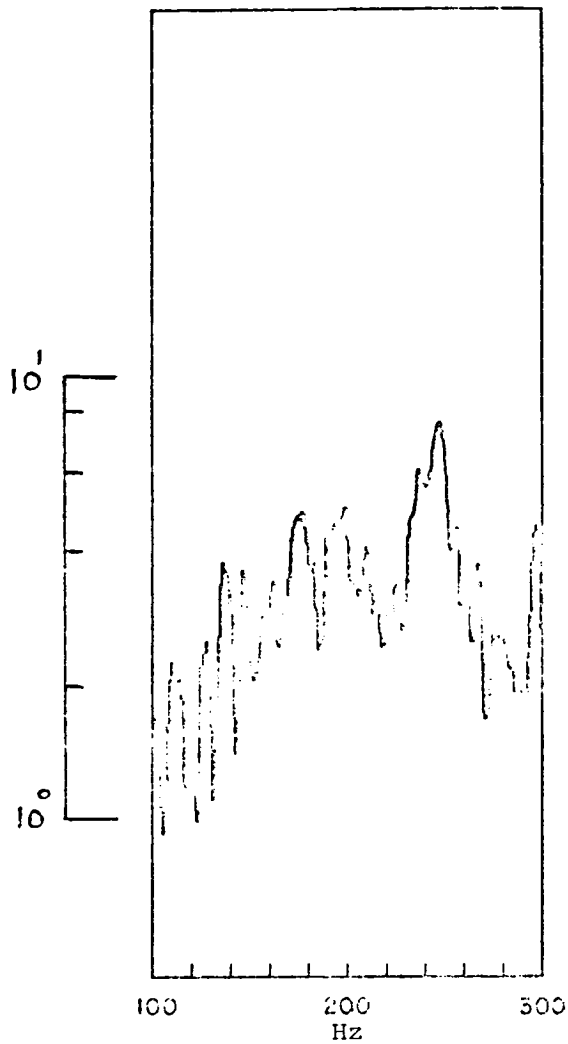

Figure (3-42) Frequency spectrum of hot-wire signal at x/D = 3.44, y/D = 2.0, z/D = 0.75. Re = 9955.

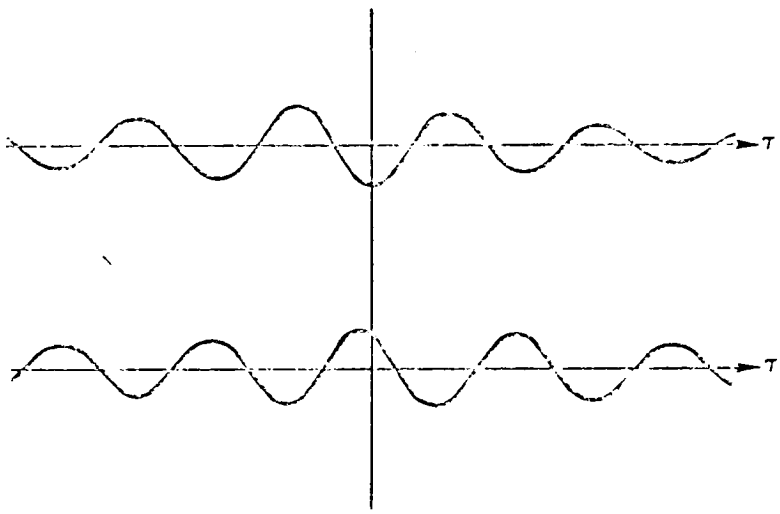

Figure (3-43) Cross-correlations between two hot-wire signals (filtered between 200 and 300 Hz) with reference probe at x/D = 0.10, y/D = -1.0, z/D = 0.0, and traversing probe at x/D = 3.44, y/D = $\pm$ 2.0, z/D = 2.0. Re = 9955.

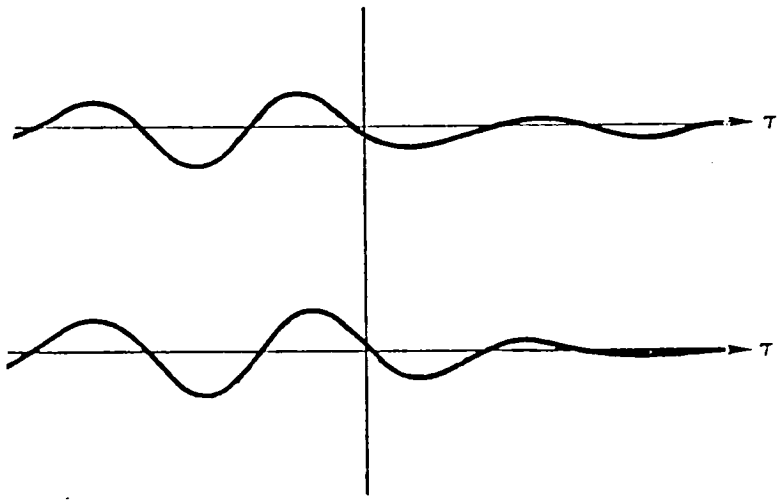

Figure (3-44) Cross-correlations between two hot-wire signals (filtered between 100 and 200 Hz) with reference probe at x/D = 0.10, y/D =-1.0, z/D = 2.25, and traversing at x/D = 8.53, y/D = $\pm$ 3.0, z/D = 1.25.Re = 9955.

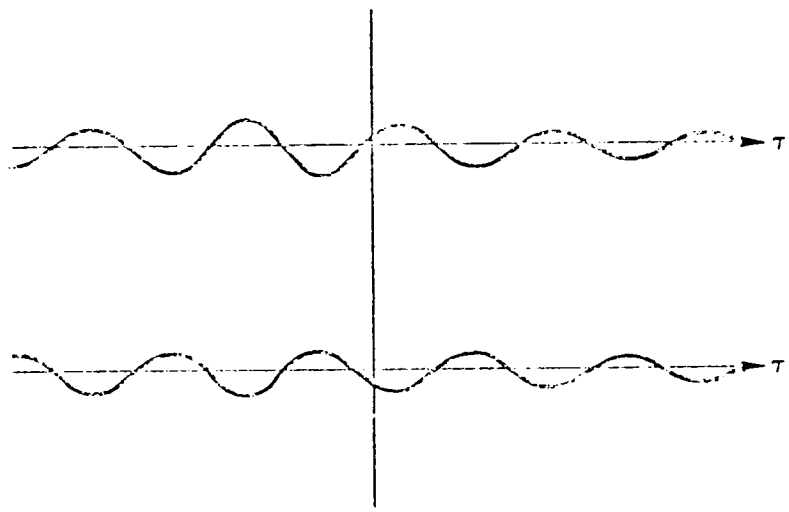

Figure (3-45) Cross-correlations between two hot-wire signals (filtered between 200 and 300 Hz) with reference probe at $x/D = 0.10$, $y/D = -1.0$ $z/D = 0.0$, and traversing at $x/D = 8.53$, $y/D = \pm 3.0$, $z/D = 4.0$. $Re = 9955$.

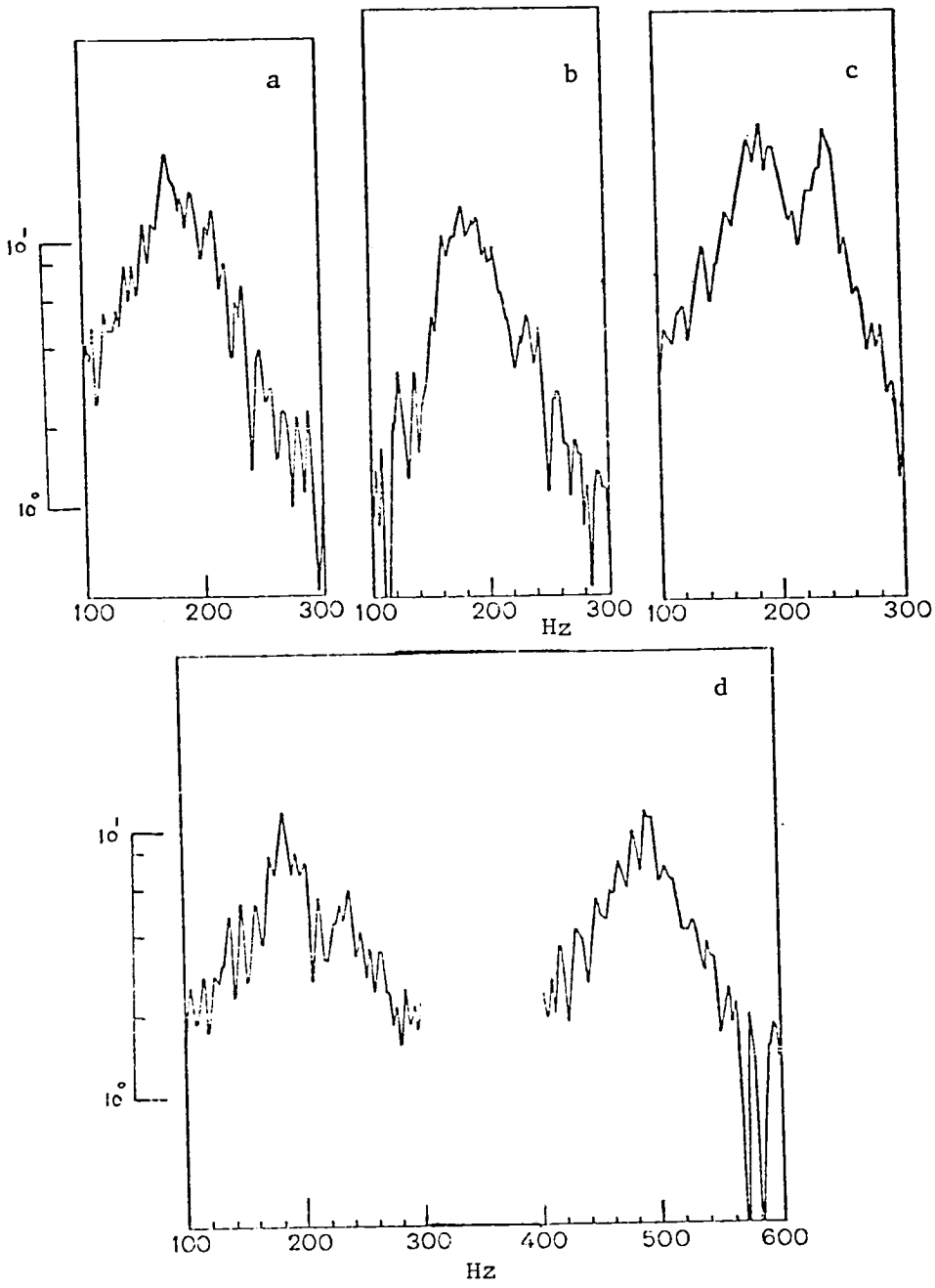

Figure (3-46) Frequency spectra of hot-wire signals at x/D = 0.97, y/D = 0.0, and (a) z/D = 0.0, (b) z/D = 0.25, (c) z/D = 0.50, (d) z/D = 0.75. Re = 9955.

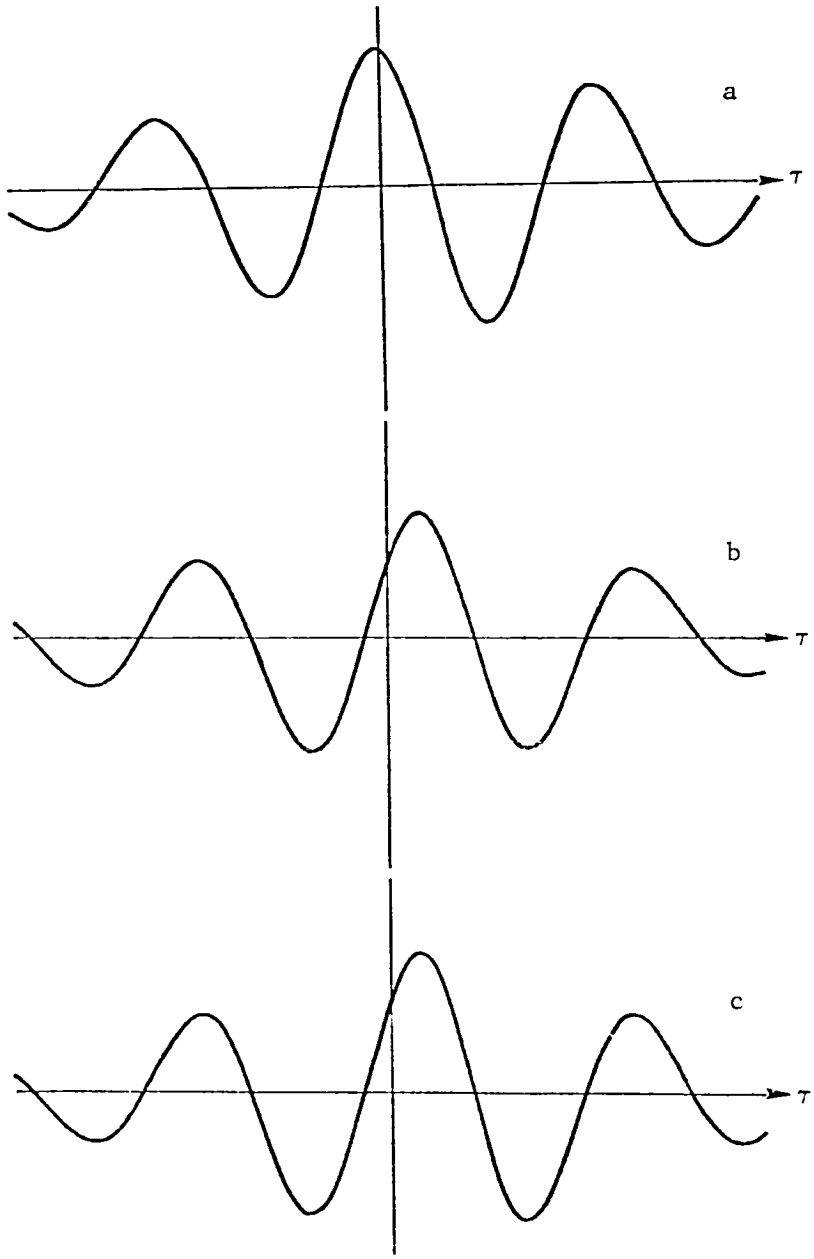

Figure (3-47) Cross-correlations between two hot-wire signals (filtered between 100 and 200 Hz) with reference probe at x/D = 0.10, y/D = -1.0, z/D = 3.0, and traversing one at x/D = 0.97, y/D = 0.0, and (a) z/D = 0.0, (b) z/D = 0.50, (c) z/D = 0.75, traversing probe's signal delayed. Re = 9955.

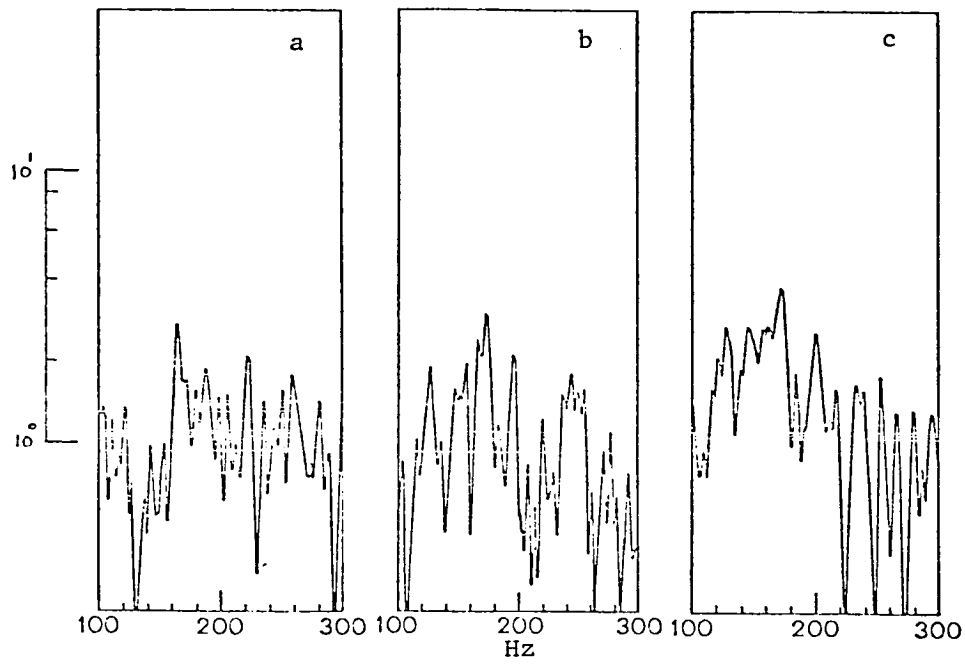

Figure (3-48) Frequency spectra of hot-wire signals at x/D = 3.44, y/D = 0.0, and (a) z/D = 0.0, (b) z/D = 1.0, (c) z/D = 2.0. Re = 9955.

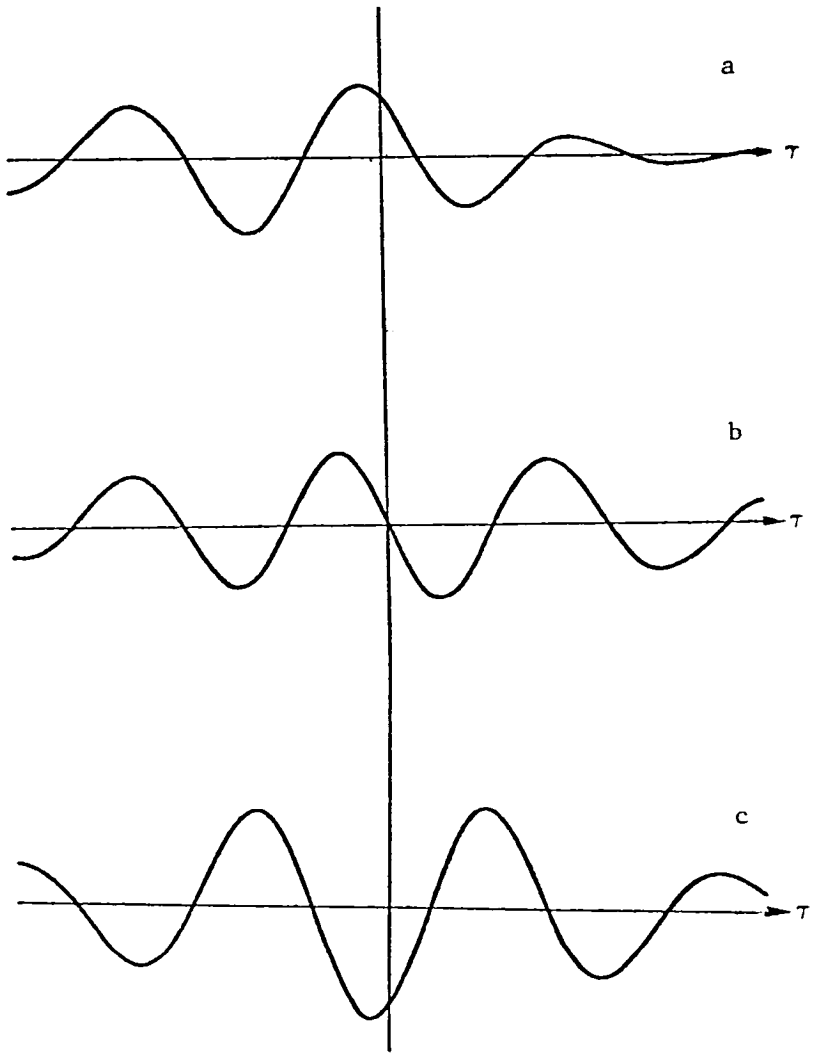

Figure (3-49) Cross-correlations between two hot-wire signals (filtered between 100 and 200 Hz) with reference probe at x/D = 0.10, y/D = -1.0, z/D = 3.0, and traversing probe at x/D = 3.44, y/D = 0.0, and (a) z/D = 0.0, (b) z/D = 1.0, (c) z/D = 2 traversing probe's signal delayed. Re = 9955.

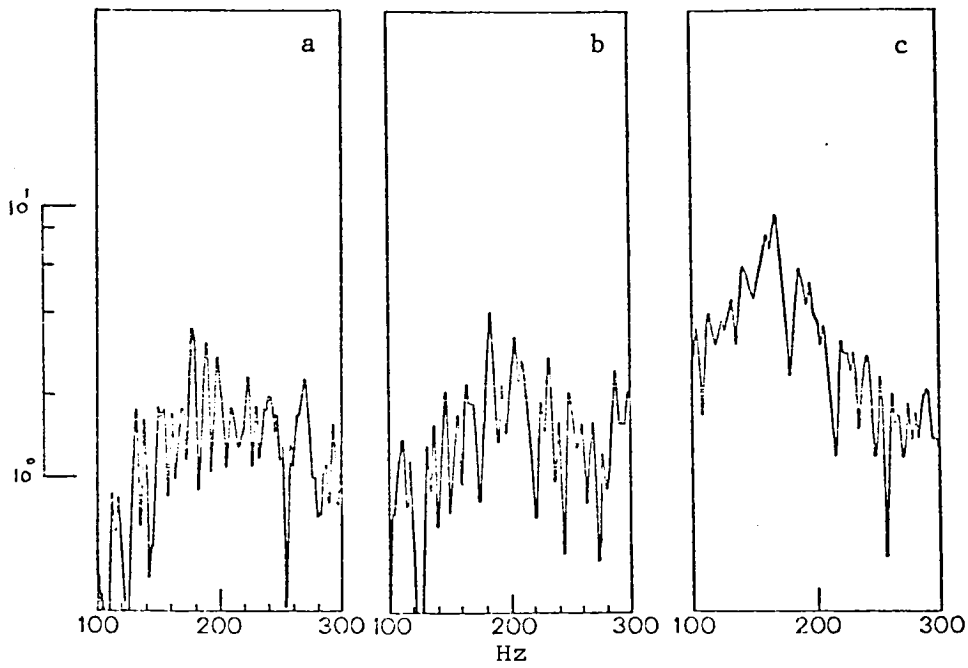

Figure (3-50) Frequency spectra of hot-wire signals at x/D = 6.03, y/D = 0.0, and (a) z/D = 0.0, (b) z/D = 1.0, (c) z/D = 3.0. Re = 9955.

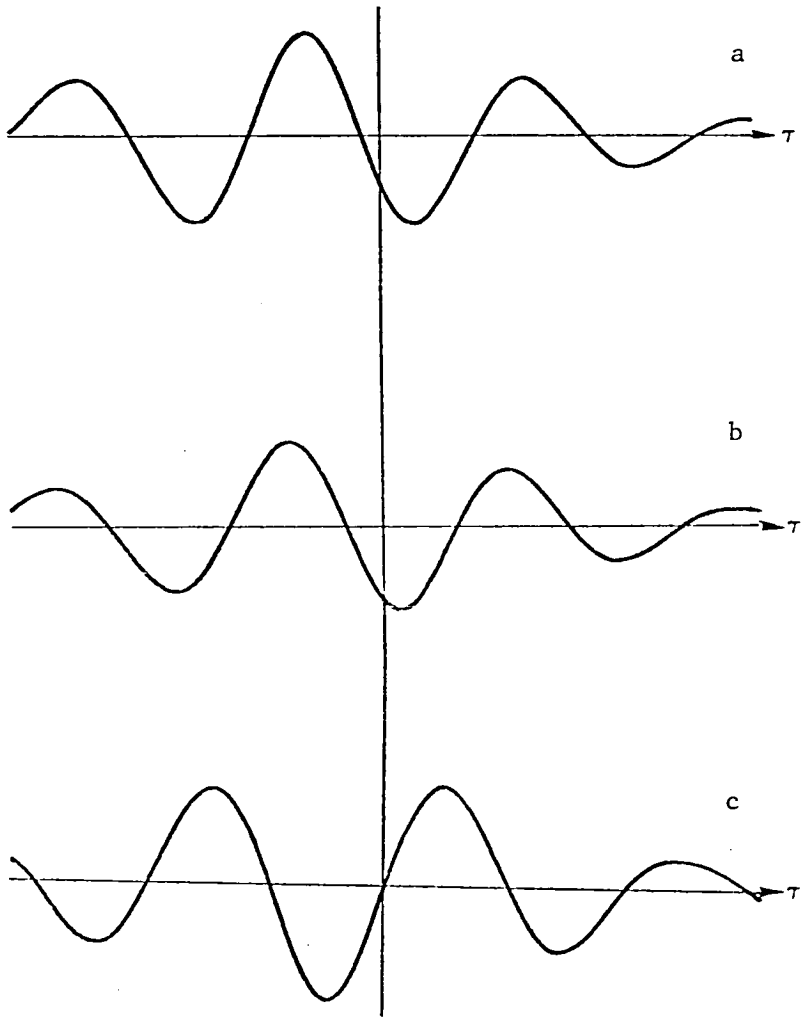

Figure (3-51) Cross-correlations between two hot-wire signals (filtered between 100 and 200 Hz) with reference probe at x/D = 0.10, y/D = -1.0, z/D = 3.0, and traversing probe at x/D = 6.03, y/D = 0.0, and (a) z/D = 0.0, (b) z/D = 1.0, (c) z/D = 3.0, traversing probe's signal delayed. Re = 9955.

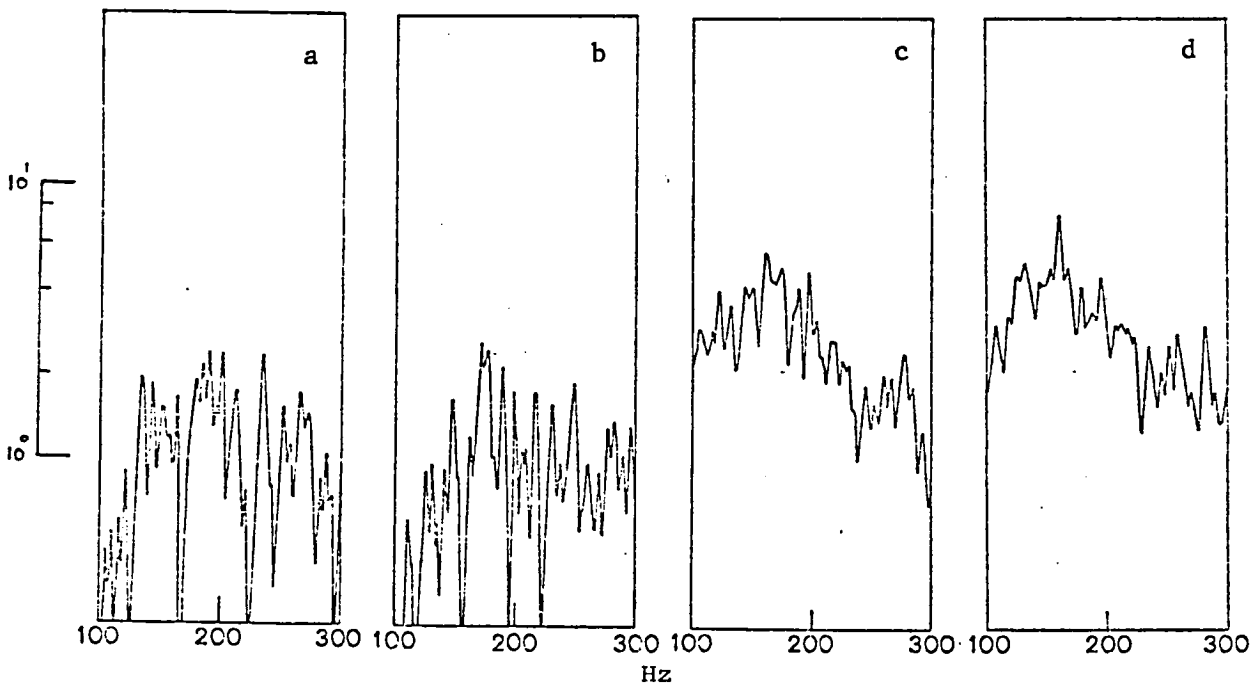

Figure (3-52) Frequency spectra of hot-wire signals at x/D = 8.53, y/D = 0.0, and (a) z/D = 0.0, (b) z/D 1.0, (c) z/D = 3.0, (d) z/D = 3.50. Re = 9955.

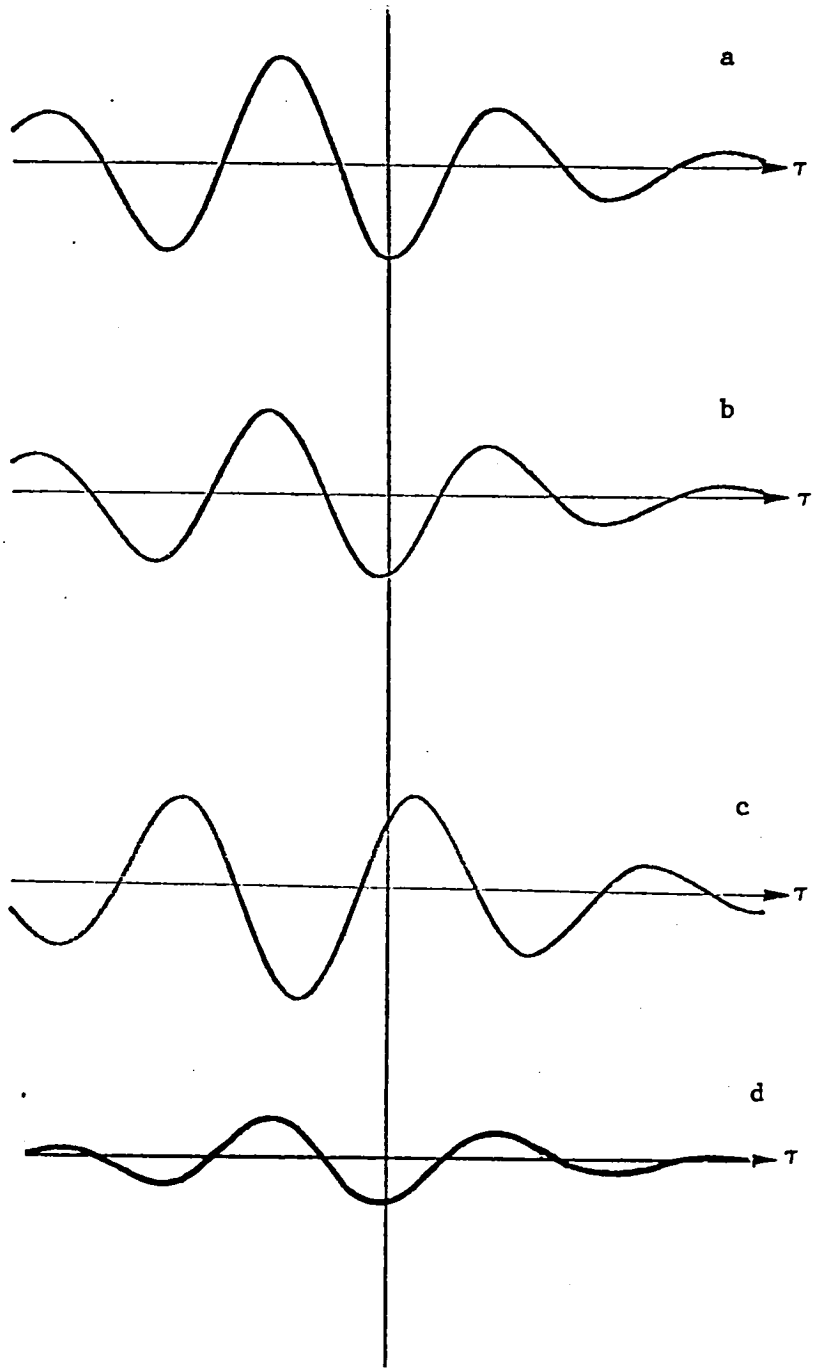

Figure (3-53) Cross-correlations between two hot-wire signals (filtered between 100 and 200 Hz) with reference probe at x/D = 0.10, y/D = -1.0, z/D = 3.0, and traversing probe at x/D = 8.53, y/D = 0.0, and (a) z/D = 0.0, (b) z/D = 1.0, (c) z/D = 3.5, (d) z/D = 4.5, traversing probes signal delayed. Re = 9955.

REFERENCES

Ayoub, A. and Karamcheti, K., "An Experiment on the Flow Past a Finite Circular Cylinder at High Subcritical and Supercritical Reynolds Numbers," to appear in the Journal of Fluid Mechanics.

Ayoub, A. and Karamcheti, K. 1976, "Pressure Fluctuations on the Surface of a Cylinder in Uniform Flow," Joint Institute for Aeronautics and Acoustics, Report TR-3, Stanford University.

Bearman, P. W. 1967, "On Vortex Street Wakes," J. Fluid Mechanics 28,625.

Bearman, P. W. 1969, "On Vortex Shedding from a Circular Cylinder in the Critical Reynolds Number Regime," J. Fluid Mechanics 37, 577.

Bloor, M. S. and Gerrard, J. H. 1966, "Measurements on Turbulent Vortices in a Cylindrical Wake," Proc. Roy. Soc., Ser. A, 294, 319

Bendat, J. S. and Piersol, A. G. 1966, "Measurement and Analysis of Random Data," John Wiley, New York.

Berger, E. and Wille, R. 1972, "Periodic Flow Phenomena," Ann. Rev. Fluid Mech. 4, 313.

Bishop, R. E. D. and Hassan, A. Y. 1963, "The Lift and Drag Forces on a Circular Cylinder in a Flowing Fluid," Proc. Roy. Soc., Ser. A, Vol. 277.

Bradshaw, P. 1971, "An Introduction to Turbulence and its Measurement," Pergamon Press.

Dryden, H. L. and Hill, G. C. 1930, Bur. Stand, J. Res., Vol.5, RP 221.

Etzold, F. and Fieldler, H. 1976, "The Near-Wake Structure of a Cantilevered Cylinder in a Cross-Flow," Z. Flugwiss. 24, 77.

Fage, A. and Johansen, F. C. 1927, "On the Flow of Air Behind an Inclined Flat Plate of Infinite Span," Proc. Roy. Soc., Ser. A, 116.

Fage, A. and Johansen, F. C. 1928, "The Structure of Vortex Sheets," Phil. Mag., Vol. 5.

Fiedler, H. E. and Wille, R. 1970, "Some Observations in the Near Wake of Blunt Bodies," AIAA Journal, Vol. 8, 1140.

Gerrard, J. H. 1961, "An Experimental Investigation of the Oscillating Lift and Drag of a Circular Cylinder Shedding Turbulent Vortices," J. Fluid Mech., 11, 244.

Gerrard, J. H. 1966, "The Mechanics of the Formation Region of Vortices Behind Bluff Bodies," J. Fluid Mech., 25, 401.

Goldburg, A., Washburn, W. K., Florsheim, B. H. 1965, "Strouhal Numbers for the Hypersonic Wakes of Spheres and Cones," AIAA Journal, Vol. 3, 1332.

Goldburg, A., Florsheim, B. H. 1966, "Transition and Strouhal Number for the Incompressible Wake of Various Bodies," Phys. Fluids, 9, 45.

Goldstein, S., ed. 1965, "Modern Developments in Fluid Dynamics," Vol. 2, Dover Publications, Inc.

Gould, R. W. F., Raymer, W. G. & Ponsford, P. J. 1968, "Wind Tunnel Tests on Chimneys of Circular Section at High Reynolds Numbers," Proc. Symp., "Wind Effects on Buildings and Structures," Laughborough Univ.

Gowda, B. H. L. 1975, "Some Measurements of the Phenomena of Vortex Shedding and Induced Vibrations of Circular Cylinders," Technische Universität Berlin Report DLR-FB 75-01.

Keefe, R. T. 1961, "An Investigation of the Fluctuating Forces Acting on a Stationary Circular Cylinder in a Subsonic Stream and of the Associated Sound Field," University of Toronto Institute of Aerophysics, Report No. 76.

Kovasznay, L. S. G. 1949, "Hot-Wire Investigation of the Wake Behind Cylinders at Low Reynolds Numbers," Proc. Roy. Soc. Ser. A, 198.

King, R. 1977, "A Review of Vortex Shedding Research and Its Application," Ocean Engng. Vol. 4, 141.

Marris, A. W. 1964, "A Review on Vortex Streets, Periodic Wakes, and Induced Vibration Phenomena," Trans. ASME, J. Basic Eng. 86, 185.

Maskell, E. C. 1963, "A Theory of the Blockage Effects on Bluff Bodies and Stalled Wings in a Closed Wind Tunnel," Aeronautical Research Council, R & M No. 3400.

Maull, D. F. & Young, R. A. 1972, "Vortex Shedding from a Bluff Body in a Shear Flow," Proc. IUTAM/IAHR Symp. Flow-Induced Structural Vibrations, Karlsruhe, W. Germany.

McCroskey, W. J. 1977, "Some Current Research in Unsteady Fluid Dynamics - The 1976 Freeman Scholar Lecture, "Journal of Fluids Engineering, Trans. ASME Vol. 99, Ser. 1, No. 1, 8.

Morkovin, M. V. 1964, "Flow Around Circular Cylinder - A Kaleidoscope of Challenging Fluid Phenomena, "A.S.M.E. Symp. on Fully Seperated Flows, Philadelphia, 102.

Okamoto, T. & Yagita, M. 1973, "The Experimental Investigation on the Flow Past a Circular Cylinder of Finite Length Placed Normal to the Surface in a Univorm Stream," Bull. JSME, 16, 805.

Ramamurthy, A. S. and Lee, P. M. 1973, "Wall Effects on Flow Past Bluff Bodies, " J. Sound and Vibration, 31, 443.

Roshko, A. 1954a, "On the Drag and Shedding Frequency of Two-Dimensional Bluff Bodies," NACA TN NO. 3169.

Roshko, A. 1954b, "On the Development of Turbulent Wakes from Vortex Streets," NACA Rep. 1191.

Smith, C. A., Varzaly, A., and Baganoff, D., "Initial Operating Characteristics of the Stanford University Aero/Astro Dept. Subsonic Wind Tunnel," Aero/Astro Dept. Rep., to be Published.

Smith, C. A. 1978, "Features of a Wake Tone Flow Field," Ph.D. Thesis, Stanford University.

Taneda, S. 1952, "Studies on Wake Vortices," Rep. Res. Institute Applied Mech., Kyushu Univ., 1, 131.

Wieselsberger, C., Ergebn, D. A. V. A. 1932 zu Gottingen, Lief. II, 24.